İSTANBUL TEKNİK ÜNİVERSİTESİ ★ FEN BİLİMLERİ ENSTİTÜSÜ

AKIM AYRILMASI

YÜKSEK LİSANS TEZİ

Müh. Hayri ACAR

Bölüm   : UÇAK MÜHENDİSLİĞİ
Program   : UÇAK

TEMMUZ 1991

ISTANBUL TECHNICAL UNIVERSITY ★ INSTITUTE OF TECHNOLOGY AND SCIENCE

FLOW SEPARATION

M.Sc. THESIS

Hayri ACAR, B.Sc.

Date of Submission : June 10, 1991

Date of Approval   : July 08, 1991

Examination Committee

Supervisor : Assoc. Prof. Dr. Veysel ATLI

Member   : Assoc. Prof. Dr. C. Ruhi KAYKAYOGLU

Member   : Assoc. Prof. Dr. M. Fevzi UNAL

JULY 1991

ACKNOWLEDGEMENTS

CONTENTS

NOMENCLATURE

A_m	: Maximum cross section area of the models
A_t	: Cross section area of the test section
A_m/A_t	: Blockage ratio
C_p	: Pressure coefficient $(C_p = \frac{P_i - P_\infty}{q_\infty})$
d	: Diameter of the cylindrical model
δ	: Boundary layer thickness
δ_s	: Boundary layer at separation
ϕ	: Stream function
L/d	: Fineness ratio
P_i	: Static pressure of the tap placed on the model surface
P_∞	: Static pressure of the mean flow
q_∞	: Dynamic pressure
Re_d	: Reynolds number based on the model diameter
τ_ω	: The wall shear stress
U_∞	: Free stream velocity
U_{ref}	: Reference velocity $(U_{ref} = .5U_\infty)$
y_{ref}	: Locus of the reference velocity

ABSTRACT

FLOW SEPARATION

One of the important characteristics of viscous flow past a solid body is the separation phenomenon. Quite a number of important references is available on the subject of the separation bubble in two-dimensional incompressible flow. However a fully satisfactory engineering method for the prediction of the characteristics of these bubbles does not yet exist. Despite two-dimensional case, literature on the circular flow separation around the nose of a circular blunt body are quite rare. Therefore, it is quite necessary to carry out more experimental works especially circular separation.

The present study tries to increase our knowledge about circular separation bubble. The effect of Reynolds number on the flow field around circular cylinder with blunt nose (which is parallel to uniform flow), have been investigated experimentally.

This study consists of five main sections (Chapter 1-5) and 1 appendix (Appendix A).

In Chapter 1, the importance of the subject was explained. The purpose and contents of this work were also given.

In Chapter 2, a general brief about flow separation was given.

Chapter 3, consists of the experimental investigation performed in this study.

The results obtained in this work and the discussions of these results were presented in Chapter 4.

In the last chapter -Chapter 5- the conclusions and the originality of this work were given.

In Appendix A, the results of the mean velocity and turbulence intensity measurements for Model-1 were given.

ÖZET

AKIM AYRILMASI

Akım ayrılması akışkanlar mekaniği ve aerodinamiğin en karmaşık ve dolayısı ile incelenmesi en zor olaylarından biridir. Buna karşılık mühendislikteki birçok uygulamada akım ayrılması oluşmaktadır. Bu nedenle akım ayrılmasının incelenmesi ayrı bir öneme sahiptir.

Olayın fiziksel olarak açıklanması genellikle deneysel çalışmalardan elde edilmektedir. Ayrıca hesaplama metodlarının ve teorinin geliştirilmesi ve desteklenmesi açısından da deneysel çalışmalar gerekmektedir. Akım ayrılması incelemelerinde deney şartlarına göre uygun deney tekniği seçilmelidir.

Akım alanının hareketli olarak görüntülenebilmesi akım ayrılmasının anlaşılması açısından önemlidir. Ayrıca akım görünürlüğü deneyleri kalitatif olarak en çabuk ve en etkili deney tekniğidir.

Akım ayrılmasının yeri ve ayrılmış akımın karakteristikleri kantitatif olarak hız profili, yüzey sürükleme katsayısı ve ısı transferi ölçümleri ile bulunabilir. Fakat kayma tabakası çok küçük ve ince olduğu için ölçme aletlerinin de ona göre akımı bozmayacak şekilde küçük olması gerekmektedir. Kayma tabakası hız profilleri genellikle sıcak-tel anemometresi ile ölçülmektedir.

Aerodinamik elemanların maksimum performansını genellikle akım ayrılması olayının belirlemesi nedeniyle, akışkanlar mekaniği çalışmalarının esas amacı sınır tabaka ayrılmasının tamamen belirlenebilmesi olmalıdır. Yani akım karakteristikleri ve geometri, Reynolds ve Mach sayısı gibi önemli parametrelerin etkisi incelenmelidir. Bu amaçla bu çalışmada küt burunlu eksenel simetrik silindir etrafındaki akım ayrılması deneysel olarak incelenmiştir. Narinlik oranı ve Reynolds sayısı (model çapına bağlı) parametre olarak seçilmiştir.

Akım ayrılmasını meydana getiren nedenler geometrik süreksizlik ve ters basınç

gradyantıdır. Bu etkilerin meydana gelişine bağlı olarak değişik akım ayrılması hallerine rastlanabilir. Küt burunlu bir silindir etrafındaki akım ayrılması halinde ayrılma yeri sabit ve burun kısmında olmasına karşılık akım genel olarak eksenel simetriktir ve yapısı küt burunlu levha üzerindeki iki boyutlu akım ayrılmasına nisbeten daha karışıktır. Fakat küt burunlu levha haline kıyasla daha çok uygulama alanı olan küt burunlu silindir hali için çalışmalar daha azdır.

Deneyler, İTÜ 50x50x200cm deney odası kesitli açık devreli Subsonik Hava Tüneli'nde yapılmıştır. Serbest akım hızı 10 m/s'dir. Bu hıza karşılık gelen türbülans şiddeti .3%'tür.

Narinlik oranının akım alanına etkisinin incelendiği deneylerde akım görünürlüğü ve basınç ölçümü teknikleri kullanılmıştır. Akım görünürlüğü deneylerinde yağ-filmi methodu seçilmiştir. Bu teknik hava akımına maruz cisim yüzeyi üzerindeki akım çizgilerinin çabuk ve kolay olarak resimlenebilmesini sağlar. Sürtünme kuvvetine bağlı olarak hava akımı katı yüzey üzerine sürülen yağı beraberinde götürür. Geride kalan boya maddesi ise akım ayrılması ve yapışması gibi fiziksel olaylar hakkında kualitatif olarak bilgi verir. Eğer yüzey sürükleme çizgileri bir çizgi etrafında birleşiyorsa yüzey üzerindeki yağlar bu çizgi etrafında toplanır. Bu çizgiye "Ayrılma çizgisi" denir. Eğer yüzey sürükleme çizgileri bir çizgi üzerinden uzaklaşıyorsa bu çizgiye de "Tekrar yapışma hattı" denir. Bu çalışmada 10 numaralı makina yağı, gaz yağı ve karbon tozunun uygun bir şekilde karıştırılmasıyla elde edilen sıvı, beyaz renkli modeller üzerine sürülüp (d=50mm, L/d=3.1,4.0,5.0,9.2), hava akımına maruz bırakıldıktan sonra, akım çizgilerinin fotoğrafları çekilmiştir. Fotoğraflardan elde edilen sonuçlara göre narinlik oranı azaldıkça tekrar yapışma hattının model burnundan olan uzaklığının azaldığı ve narinlik oranı (L/d) 5, değerine kadar küt burunlu silindir etrafındaki akımı etkilediği, bu değerden sonra ise narinlik oranının etkisinin ortadan kalktığı görülmüştür.

Basınç ölçümü deneylerinde ise 9 ayrı model kullanılmıştır (d=50mm, L/d= 3.1, 4.0, 5.0, 5.94, 6.92, 7.5, 7.92, 8.28, 9.2). Basınç pirizleri model yüzeyi üzerinde ve simetri ekseni doğrultusunda burundan itibaren 4d uzaklığa kadar 18 adet yerleştirilmiştir. Deneylerde 2 adet mikromanometre kullanılmıştır. Bunlardan biri dinamik basınç ölçümünde, diğeri ise model yüzeyi üzerindeki pirizlerden alınan basınç ile serbest akım statik basıncı arasındaki farkın ölçümünde kullanılmıştır. Simetri ekseni boyunca model yüzeyi üzerindeki basınç katsayısı dağılımının

$$C_p = \frac{P_i - P_\infty}{q_\infty}$$

eşitliği ile bulunduğu bu deneylerde narinlik oranının küt burunlu silindir etrafındaki akım alanına etkisi hakkında akım görünürlüğü deneylerinde elde edilen sonuç doğrulanmıştır. Narinlik oranı azaldıkça modelin arka yüzeyindeki akımın hızlandığı ve basınç katsayısı "0" değerine daha küçük x/d değerinde ulaştığı ve L/d'nin 5'ten büyük olması halinde narinlik oranındaki değişimler akım alanını etkilemediği görülmüştür.

Reynolds sayısının akım alanına etkisinin incelendiği deneylerde ise sıcak-tel anemometresi kullanılmıştır. Sıcak-tel anemometresinin ölçü ucu, elektrikle ısıtılan bir telden ibarettir. Akışkan akımı telin soğumasına, dolayısı ile direncinin azalmasına neden olur. Telin sıcaklığını sabit tutabilmek için gerekli akım ölçülerek hava hızı tayin edilebilir.

Sıcak-tel anemometresi şu ünitelerden oluşmuştur: 1- Güç Ünitesi. 2- Filtre. 3- Dijital Voltmetre. 4- RMS Ünitesi. 5- Lineerleştirme Ünitesi. 6- Sıcak-tel probu 7- Hareket Mekanizması. 8- Hareketi sağlayan motor. 9- Hareket Kontrol Ünitesi 10- Data Acquasition Ünitesi. 11- Bilgisayar.

Anemometrenin voltaj çıktısı (E) ile hava akım hızı (U) arasındaki bağıntı:

$$E^2 = E_0^2 + BxU^{1/m}$$

şeklindedir. Burada B ve m sıcak-tel probu ve sıcak-tel ile hava akımı arasındaki sıcaklık farkı ile ilgili sabitlerdir. E_0 ise hava akım hızı sıfır olduğu zaman anemometrenin gösterdiği voltaj değeridir.

Eğer sistemde bir lineerleştirme ünitesi kullanılırsa lineerleştirme ünitesinin voltaj çıktısı (E_l) ile hava hızı (U) arasında lineer bir bağıntı vardır:

$$U = KxE_l$$

Burada E, E_0 ve E_l volt, U ise m/sn cinsindendir. K bir sabittir ve K=10 olacak şekilde lineerleştirme ünitesi ayarlanabilir.

Akım görünürlüğü ve basınç ölçümü deneylerinin sonuçlarına göre narinlik oranının değeri yaklaşık olarak 5'ten büyük alınırsa, narinlik oranındaki değişimlerin akım alanını etkilemediği bulunmuştu. Bunun için Reynolds sayısının parametre olarak seçildiği deneylerde, modellerin narinlik oranı 7.5 olarak seçilmiştir. Bu deneylerde kullanılan modellere ait çapa bağlı Reynolds sayıları ise sırasıyla şöyledir: $3.45x10^4$, $5.18x10^4$, $7.59x10^4$.

Sıcak-tel anemometresi akımın yönünü belirleyemez. Anemometrenin çıktısı her zaman pozitiftir. Fakat akım ayrılması sonucunda oluşan hava habbeciği içinde ters akım bölgesi vardır. Bu bölge anemometre çıktılarında, yüzeye yakın bölgede bir artış ve tekrar azalma ile ayırt edilebilir. Hız profillrinde, bu bölge bulunarak ve bu bölgedeki hız değerlerinin direkt negatif değeri alınarak düzeltme yapılmıştır.

Hız ve türbülans profillerinden faydalanarak akımın tekrar yapışma hattı, akım habbeciği boyutları ve sınır tabaka kalınlıkları bulunmuştur. Limit akım çizgisi akım fonksiyonunun ($\phi = 0$) sıfır olduğu noktalar bulunarak çizilmiştir. Akım küt burunlu silindirin burun kısmında kopuyor ve belli bir uzaklıkta yüzeye tekrar yapışıyor, bunun sonucunda da akım habbeciği oluşuyor. Akım habbeciğinin model yüzeyinden olan dik uzaklığı model burnundan itibaren artıp, bir maksimum değerden sonra tekrar azalmaktadır. Akım habbeciği içinde bir dönme bölgesi ve dolayısı ile ters akım oluşmaktadır. Akım habbeciğinin içinde bulunan istasyonlarda ki akım hızı, y doğrultusunda gidildikçe, serbest akım hızından büyük bir değere ulaşmaktadır ve daha sonra serbest akım hızı değerine kadar azalmaktadır. Akım habbeciğinden sonra sınır tabaka kalınlığı model yüzeyi boyunca kalınlaşmaktadır.

Türbülansın maksimum olduğu noktalar akım habbeciği yüksekliği ile benzer bir davranış göstermektedir ve bu noktalar hız gradyantının büyük olduğu noktalara tekabül etmektedir. Akım habbeciği içindeki istasyonlarda türbülans küçük bir maksimum değere sahiptir. Akım habbeciğinin üst kısmında kayma tabakası olduğu için buradaki türbülans dağılımı sınır tabaka türbülans dağılımına benzemektedir.

Model yüzeyi üzerindeki Türbülans profillerinde, türbülans şiddetinin maksimum değerlerinin x/d'ye göre çizilen değişimi oldukça karışık bir yapıya sahiptir.

Reynolds sayısının $3.45x10^4$ değeri için hız ve basınç dağılımları karşılaştırılırsa, hız dağılımından elde edilen tekrar yapışma noktası basınç dağılımında, basınç katsayısının maksimum olduğu noktadan daha önceki bir noktaya tekabül etmektedir. Basınç katsayısının minimum olduğu nokta ise akım habbeciği yüksekliğinin yaklaşık olarak en büyük değerine karşılık gelmektedir.

Reynolds sayısı arttırıldığında akım habbeciğinin boyu ve yüksekliği büyümektedir. Fakat akım habbeciğinin boyutları d çapı ile boyutsuzlaştırılırsa tekrar yapışma noktasının yeri artan Reynolds sayısı ile sabit kalmaktadır. Habbecik yüksekliği ise d çapı arttırıldıkça boyutsuz olarak küçülmektedir.

Akım habbeciğinin içinde bulunan istasyonlardaki hız profillerinde, akım hızının $1.01\ U_\infty$ olduğu, akım habbeciği dışında ise akım hızının $.99\ U_\infty$ olduğu noktaların grafiği çizilirse, bu noktaların dağılımı akım habbeciği yüksekliğinin yapısını verdiği görülmüştür. Ortak bir dağılım elde etmek için logaritmik eksen takımı kullanılmıştır.

Boyutsuz eksen eksen takımı kullanılarak hız profilleri için üniversal bir eğri elde etmek amacıyla oluşturulan grafiklerde, U_{ref} serbest hava akımı hızının yarısıdır. y_{ref} ise hız profilinde akım hızının referans hıza ulaştığı noktanın model yüzeyinden olan dik uzaklığıdır. Akım habbeciği içindeki istasyonlarda hız dağılımının düzeltme yapılmış bölgelerinde karışıklık olmasından dolayı inceleme yapılırken hız profilleri tekrar yapışma noktasından önce ve sonra olmak üzere iki gruba ayrılmıştır.

3 ayrı Reynolds sayısı için çizilen boyutsuz hız grafiği göstermiştir ki ters akımın oluştuğu bölge hariç hız profilleri için üniversal bir eğri elde edilebilir. Özellikle tekrar yapışma noktasından sonraki boyutsuz hız profilleri çok iyi bir uyum göstermiştir.

Elde edilen sonuçlar sırasıyla şu şekilde genelleştirilebilir:

1- Küt burunlu silindir halinde narinlik oranı (L/d) akım alanı için önemli bir parametredir. Narinlik oranının etkisini kaldırmak için (L/d) değeri, 5'ten büyük alınmalıdır.

2- Çapa bağlı Reynolds sayısı arttıkça küt burunlu silindirin burun kısmında oluşan akım habbeciğinin boyutları da büyümektedir. Fakat akım habbeciğinin boy ve yüksek-

liği d çapı ile boyutsuzlaştırılırsa, artan Reynolds sayısı ile, tekrar yapışma noktasının yeri değişmemektedir ve boyutsuz habbecik yüksekliği küçülmektedir.

3- Ters akım bölgesi içindeki hız değeri 35% U_∞ değerine kadar ulaşmaktadır. Akım habbeciği içindeki istasyonlarda türbülansın maksimum olduğu noktalar yaklaşık olarak akım habbeciği yüksekliğine karşılık gelmektedir.

4- Özellikle tekrar yapışma noktasından sonraki hız profilleri için, boyutsuz eksen takımı kullanılarak, bir üniversal eğri elde edilebilir.

CHAPTER 1

INTRODUCTION

Boundary-layer separation from a surface is an important problem because it is usually responsible for setting an upper limit to the performance of aerodynamic divices. Because of flow separation, energy is lost. As maximum performance usually occurs very close to the separation condition and the subject is relevant to a wide range of engineering and environmental applications, an ability to predict boundary-layer separation has been, and remains, a major aim of fluid mechanics research. So the objective must be to develop understanding of the flow characteristics and of the influence of important parameters including geometry, Reynolds and Mach numbers, and to make use of this understanding to improve design procedures.

Considerable theoretical, experimental, and computational work has been undertaken in last years in an effort to understand the nature of three-dimensional flow separation.

In most cases calculations have not been able to identify separation lines mainly because the numerical methods used in three-dimensional boundary-layer flows have not been sufficiently accurate to represent zones of influence and dependence governing the three-dimensional boundary-layer development along the surface. The difficulty of solving the Navier-Stokes equation for separated flows has led to do solution of simplified problems.

Physical understanding is usually obtained from experimental investigations and experimental results are essential to the developement and evalution of calculation methods, and it is useful to review them and the understanding which they provide.

The interpretation of flow phenomena associated with separation is not always straightforward and requires both skill and experience. Therefore, it is necessary to examine in detail the various experimental techniques available in order to make right choice for the given conditions of the experiment as well as for the particular problem of flow separation that is to be studied.

The actual observance of flow may lead to an understanding of an obscure flow phenomenon. Therefore, flow visualization based solely on observation and needing to tedious data reduction is a very effective and satisfactory technique for obtaining qualitative information. Flow visualization techniques are often grouped in two categories; those applicable to wind tunnels and those applicable to liquid channels. In this study the oil-film technique was used. The surface streamline or flow direction on the surface may be visualized by coating a surface with oil film. Since a separation line is generally an envelope of surface streamline, the separation line is detected by this technique.

The position of separation and characteristics of separated flow may be determined by quantitative measurements, e.g., of the velocity profile, skin friction, and heat transfer in neighbourhood of separation and within the separated region. These physical measurements are generally tedious, expensive, and require considerable amount of data. Furthermore, since the shear layer of attached flow is usually thin, the measuring devices must be accordingly small, and special techniques for

their manufacture are reqired.

In this study pressure distribution along the model symmetry axis is obtained by measuring the pressures in various points. An adverse pressure gradient is a necessary condition for flow separation on a continuous body surface. Hence, the position of separation may be estimated for some cases by surveying the pressure distribution, for example, in the case of laminar flow over a surface where a sufficiently strong adverse pressure gradient prevails. In this case, laminar flow separation may be expected to occur downstream of the pressure minimum. As separation as approached, the shear layer grows rapidly. Therfore, an estimate of separation point generally survey and measurement of the shear layer growth.

The velocity profiles of shear flows are commonly measured with a hot-wire anemometer. The standard hot-wire anemometer consist essentially of a short length of very fine wire supported between two metal prongs and heated electrically. The air velocity is deduced from the cooling produced by the airflow. Method is satisfactory for studying separation air speeds less then 30 m/s.

In the present work a blunt nose circular cylinder is used. Due to the missile aerodynamics, the flow separation on the blunt nose of a circular cylinder has a practical importance in addition to its fundamentel importance. The blunt nose separation depends on the geometry of the body, Reynolds and Mach numbers, and angle of attack. In this study first the effect of the fineness ratio and then the effect of Reynolds number on the flow field around the circular cylinder was examined. In examining the effect of the fineness ratio, flow visualization and pressure measuring techniques were used. In examining the effect of Reynolds number, hot-wire anemometer was employed.

All the tests were carried out in ITU subsonic open-circuit wind tunnel with a test section 50x50x200 cm. Separation and reattachment lines and critical points on the body have been identified from the flow visualization, pressure, and hot-wire measurements.

The results of the experiments and the discussion are given in Chapter 4.

CHAPTER 2

GENERAL CHARACTERISTICS OF FLOW SEPARATION

2.1 INTRODUCTION

This chapter attempts to outline the flow separation and describe the characteristics and effects of parameters on this phenomenon. Because the phenomenon is complicated, it is necessary to understand its physical aspects before making experiments. So after giving a general brief about flow separation, the original present studies and their results were examined.

2.2 GENERAL STRUCTURE OF FLOW SEPARATION

Under certain conditions, fluid flowing over bodies separates from wall surfaces, causing pressure, velocity and temperature conditions to change drastically from conditions of flow attached along the wall. The subject of fluid flow separation is one of the many aspects of viscous flow, which is very important but complicated. Because of flow separation, energy is lost. In case of external flow at subsonic speeds, such as in airborne vehicles, drag increases , lift decreases, and reverse flow and stalling occur. Because of complexity of the problem, a rigorous definition of flow separation should be made. The classical concept of flow separation is due to viscosity [1]. When a fluid flow past a fixed body, because of the effect of the viscosity, no matter how small, the layer of fluid immediately adjacent to the surface is at rest. Away from the wall the fluid is in motion with certain velocity. This means that as the solid surface is approached, fluid layers are retarded. The retardation arises out of the action of the viscous forces. It is observed that for fluid with small

viscosity, such as water and air, the retardation effects are confined only to a very thin region close to the body.

In such a region the velocity rises rapidly from zero at the wall to its value in the main stream. In that region the spatial rate of change of velocity in a direction normal to the body is large, and consequently the viscous forces would not be negligible even if the viscosity were small. Outside that region the velocity gradients are small and the viscous forces there would be negligible. The thin region close to the body in which the viscosity effects are confined is called the boundary layer [2]. Further features are that the boundary layer thickness grows generally rapidly at and downstream of the separation line and the interaction between viscous and inviscid flow becomes large [3].

When flow separations occurs near the front of a body, there is often the possibility that the separated shear layer will reattach on a downstream portion of the body surface. This depends on the body shape and on the ratio of its streamwise to transverse dimensions [4].

In adition, a necassary condition for flow separation is the adverse pressure gradient. The flow esparation is not only caused by a gradual process, but also by a severe discontinuity of the tangent to the surface [1].

If the body surface is of finite dimension, then flow separation is inevitable because the flow expands over the downstream edge and flows away from the wall. Thus, flow separates at the trailing edge of a wing, around a corner of a rearward-facing step, at a cavity; see Fig.2.1.
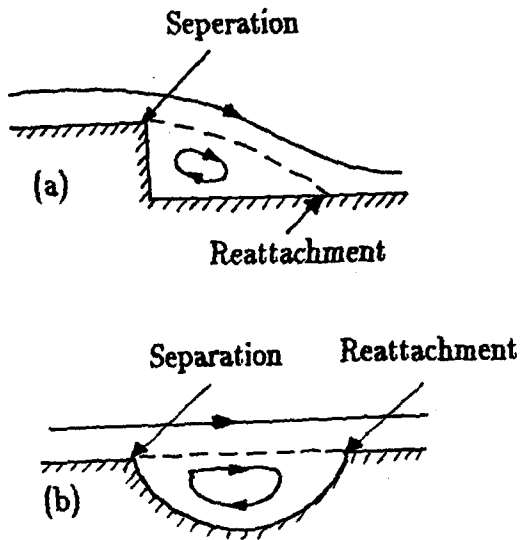
Figure 2.1 Downstream separation
a) backward facing step;
b) cavity [5].
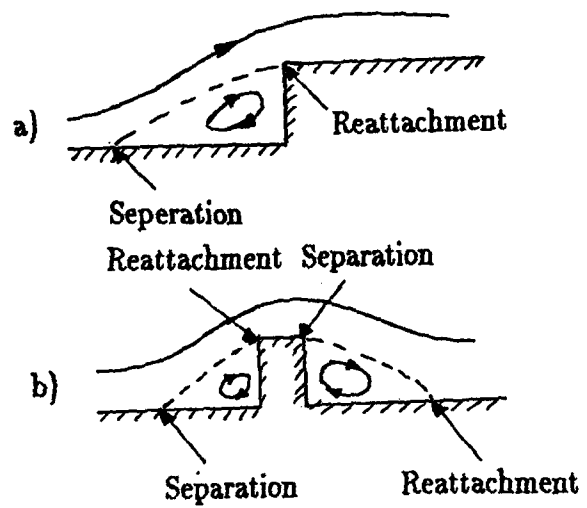
Figure 2.2 Upstream separation
a) forward facing step;
b) spoiler [5].
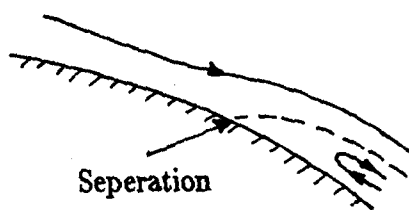
Figure 2.3 Flow separation from
smooth surface [5].
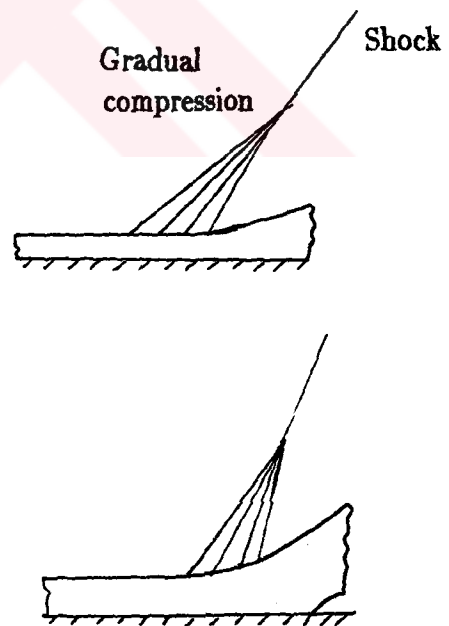
Figure 2.4 Shock waves softened by
the boundary layer.

Furthermore, flow also separates upstream of obstacles, such as a forward-facing step, a spoiler, and so on. Because the fluid is not capable of reaching an infinitely large velocity at the sharp corner, as the streamline along the wall approaches the obstacle, it leaves the wall. Fig.2.2 [5]. On sharp-edged, separation is fixed at the salient edges, whereas on rounded bodies, the location of the separation depends on the shape of the body and the state of the boundary layer [4].

The flow along a curved surface separates only if the streamwise pressure gradient is positive (or adverse); this is shown in Fig.2.3 for subsonic flow. Thus the separation point is located on the portion of the surface where the flow decelerates. Downstream of separation, reverse flow may occur [5].

As shown in Fig.2.4, separation may occur at supersonic speeds if a shock wave strongly interacts with the boundary layer and creates a sufficiently large rise in pressure downstream from the shock interaction.

It is clear from these illustrations that the governing factors that causing separation for both subsonic and supersonic flow are the finite dimension of the body surface, the abrupt change of the geometrical shape of the body surface, the viscosity, and either a continuous or discontinuous adverse pressure gradient which reduces the streamwise kinetic enrgy of flow is used to overcome the pressure rise. The first two items (the finite dimension of the body surface and abrupt change of the geometrical surface configuration) are associated purely with the body configuration. However, the flow that confronts the abrupt change of surface configuration may also be associated with the adverse pressure gradient caused: (1) by the pressure of existing wall surface upstream of a corner (Fig.2.2.a), or (2) by a pressure gradient due to the formation of shock at a corner. In relation to fluid mechanics, these last

two factors (adverse pressure gradient and viscosity) are essential for flow separation. If one of these factors is missing, then flow can not separate

Figures 2.1 and 2.3 indicated that the vortices in the separated region are formed in such a way that the direction of the surface streamline of the vortices is toward the separation point and opposite to the surface streamline upstream from it. Hence, the separation streamline may be regarded as the line that divides all the surface streamlines into those coming from the separated and unseparated portions of the flow. Two sets of surface streamlines of opposite flow direction meet at the separation point. This phenomenon is the same for laminar as for turbulent flow [5].

In a two-dimensional steady flow, it is generally recognised that separation occurs when the wall shear-stress vanishes at a certain point which is called separation point. Beyond the point, the wall shear-stress τ_w is negative which corresponds to a velocity distribution along the direction normal to the surface having a portion close to the wall where the streamwise component U streams oppsite to that of the outer main flow.

In most three-dimensional flows, such a definition becomes insufficient and useless. Legendre [6] has shown that nearly all the observed surface flow patterns belonging to what are called separated flows can be interpreted in a rational and simple way by introducing a very limited number of elementary singularities into the family of skin-friction lines of an isolated obstacle.

Singular points are classifiable into two main types: nodes and saddle points. Nodes may be further subdivided into two subclasses: nodal points and foci (of attachment and separation)

A nodal point (Fig.2.5.a) is the point common to an infinite number of skin-friction lines. At this point, all of the skin-friction lines except one (labelled AA in Fig.2.5.a) are tangential to a single line BB. At a nodal point of attachment, all of the skin-friction lines are directed outward away from the node. At a nodal point of separation, all of the skin-friction lines are directed inward towards to node.

A spiral node (Fig.2.5.b) differs from a nodal point in Fig2.5.a, in that it has no common tangent line. An infinite number of skin-friction lines spiral around the singular point, either away from it (i.e., a focus of attachment) or into it (i.e., a focus of separation).

At a saddle point (Fig.2.5.c), there are only two particular lines, CC and DD, that pass through the singular point. The directions on either side of the singular point are inward on one particular line and outward on the other particular line. All of the other skin-friction lines miss the singular point and take directions consistent with the directions of the adjacent particular lines. These particular lines are barriers in the field of skin-friction lines, making one set of skin-friction lines inaccessible to an adjacent set.

Above-mentioned singular points, acting either in isolation or in combination, fulfil certain characteristic fuctions which largely determine the distribution of skin-friction lines on the surface. The nodal point of attachment is typically a stagnation point on a forward facing surface, such as the nose of a body, where the external flow from the upstream thereby acts as a source of skin-friction lines thet emerge from the point and spread out over the surface. Conversely, the nodal point of separation is typically a point on a rearward-facing surface, and acts as a sink where the skin-friction lines that have circumscribed the body surface may vanish. The

(a) Node.

VORTEX LINE

SKIN-FRICTION LINE

(b) Spiral node (Focus)
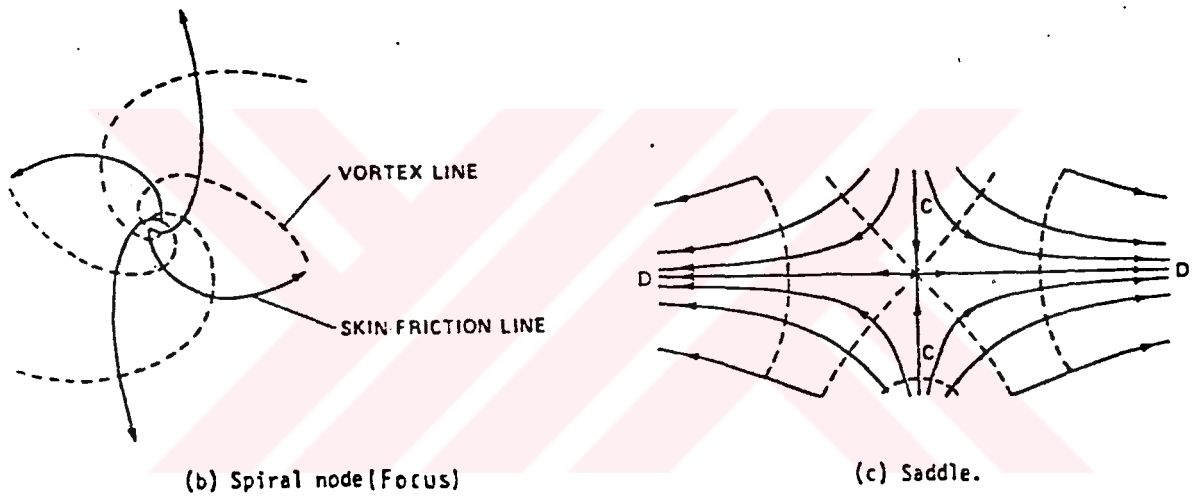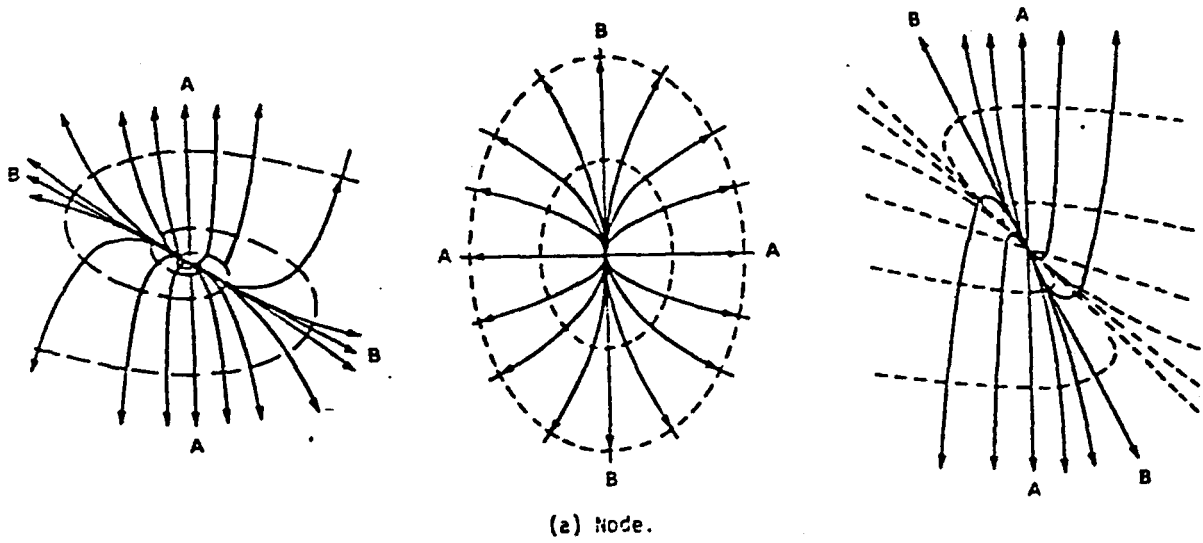
(c) Saddle.

Figure 2.5 Singular point [6].

SADDLE

SEPARATION LINE
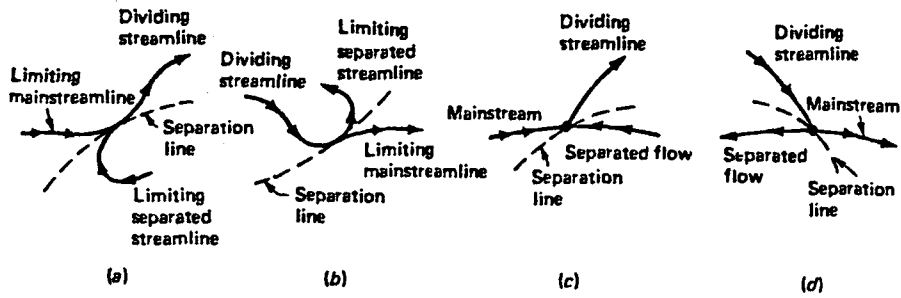
NODE

ATTACHMENT LINE
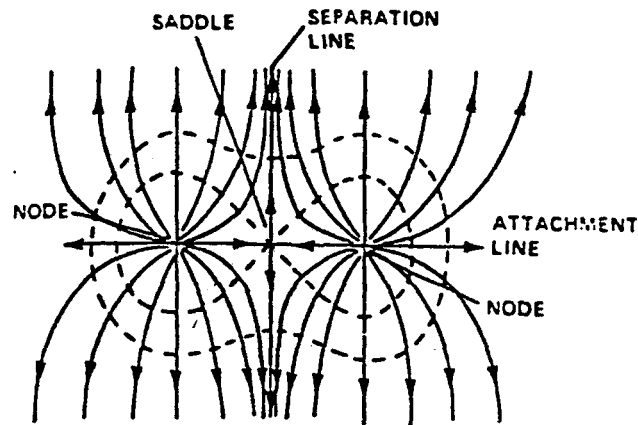
NODE

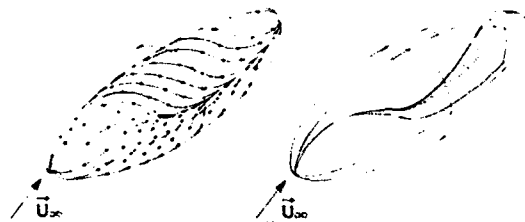Figure 2.6 Example of adjecent node and a saddle point [6].

saddle point acts typically to separate the skin-friction lines issuing from adjacent nodes. An example of the saddle point is illustrated in Fig.2.6. Skin-friction lines emerging from the nodal points of attachment are prevented from crossing by the presence of a particular skin-friction line emerging from the saddle point. The particular skin-friction line is called a line of separation. Skin-friction lines from either side lend to converge on the line of separation.

As shown by analysis of three-dimensional shear-layer, the necessary condition for separation of three-dimensional flow is that the derivative of a velocity component normal to the separation line at the wall must vanish. But this is not a sufficient condition for separation; the velocity of three-dimensional flows must be described by more then a single component. If the derivative of one of the velocity components vanishes, it may merily cause a change in the direction of the surface flow. The sufficient conditions are illustrated by the examples:

Maskell has clarified the matter conceptually by distinguishing between two types of three-dimensional behaviour: (1) ordinary separation, resulting in a shear layer, and (2) singular separation resulting in a bubble formation. In either case, Maskell notes that separation is characterised by the meeting and combining of two limiting streamlines on the surface, one from the main stream and one from the separated region. The two streamlines join together in one dividing stream-line which lies between the separated mainstream regions. If the two streamlines meet tangentally, the dividing streamline may gradually bend away from the surface (Fig.2.7.a-b). Maskell terms this ordinary three-dimensional separation. If the two surface streamlines meet head on, the dividing streamline breaks away abruptly, as in two-dimensional separation; Maskell terms this singular separation (Fig.2.7.c-d).

Figure 2.7 The concept of ordinary and singular separation
in three dimensional boundary layer flow:
a) ordinary separation,   e) horse-shoe type
b) ordinary reattachment,   separation.
c) singular separation,   f) crossflow sepa-
d) singular reattachment [7]   ration [8].

If the flow is truly three-dimensional, singular separation will only occur at isolated points, typically in a plane of symmetry or along a stagnation streamline in the surface [7].

The topological approach used by Tobak and Peake and the phenomenological approach used by Wang have led to the definition of two classes of three-dimensional flow separation. The first class of separation, called global separation by Tobak and Peake and closed separation by Wang, has a saddle point associated with the flow separation, and the separation line is defined as one of the lines that pass through the saddle point Fig.2.7. Chapman subdivide this class of separation: (1) Horse-shoe type separation, (2) crossflow separation.

The second class of separation, called local separation by Tobak and Peake, open separation by Wang, and crossflow separation by Chapman, developes gradually and results when the limitting streamlines squeeze together and fluid is forced away from the surface (Fig.2.7). There are no sudden changes when crossflow separation begins, and its onset is not easily defined. Furthermore, since no saddle points are associated with crossflow separation, the separation line can not be defined as a line that passes through a saddle point. Instead, the separation line generally is defined to be a line on which skin-friction lines converge [8].

Prandtl, founder of the boundary layer, explained the physical phenomenon of separation in this way: Consider the velocity profile of a two-dimensional or axially symmetric boundary layer upstream from separation where the pressure gradient is continuous and adverse (Fig.2.8). Within the thin boundary layer of thickness δ, the effect of viscosity is such that a strong velocity gradient $\delta u/\delta y$ prevails near the wall. The flow velocity at the wall is zero, and with increasing distance y,u grows

rapidly and gradually approaches the magnitude of U_∞, the inviscid flow velocity at the outer edge of the boundary layer. Compared to the main stream, the retarded flow in the boundary layer suffers a relatively greater deceleration, and, since the momentum of the flow near the wall is small, the ability of the fluid to move forward against the pressure rise is also limited. This small amount of momentum and energy along the body surface is eventually used up downstream in order to overcome the pressure rise and friction. Hence, the fluid particles are finally brought to rest. Because the main stream itself is decelerating, it is unable to energise the fluid in the boundary layer and accelerate. Thus, when the surface streamline reaches the point on the wall where $(\delta u/\delta y)_{y=0}$ (or zero stress position), it begins to break away from the wall and separates the flow from the surface. The zero stress condition also implies that τ_w changes at this point from a positive to a negative value. If τ_w is negative, then $\delta u/\delta y$ is negative at the wall, or u is negative near the wall. Thus reverse flow occurs downstream from the separation point.

As seen from Fig.2.8, the velocity profile downstream at the separation point of inflection. Upstream of separation $\delta u/\delta y > 0$ at the wall. At the edge of the boundary layer where the viscosity effect vanishes and $\delta u/\delta y = 0$, the magnitude of $\delta u/\delta y$ decreases and $\delta^2 u/\delta y^2$ becomes negative. Hence, at a certain normal distance from the wall, $\delta^2 u/\delta y^2$ becomes equal to zero and the velocity profile will have a point of inflection. When the velocity profile has a point of inflection, then flow is unstable and tends to become turbulent. The line which starts at the point of separation and connects the point of zero velocity within the viscous layer apart from the wall may be defined as the zero velocity line, as shown in Fig.2.8. By finding the zero velocity line, a measure of deviation of stream lines due to separation and a boundary of a region of vortices can be obtained. Because of the deviation of potential flow stream lines due to separation and formation of vortices in the separated region, the flow separation causes loss of energy. If a mixing of the slower fluid near the wall with
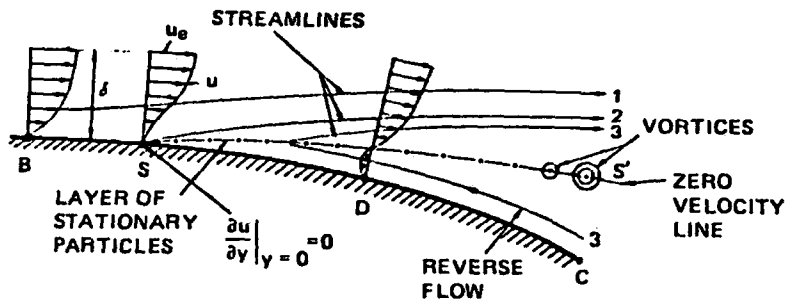
Figure 2.8 Velocity profile near a separation point [1].
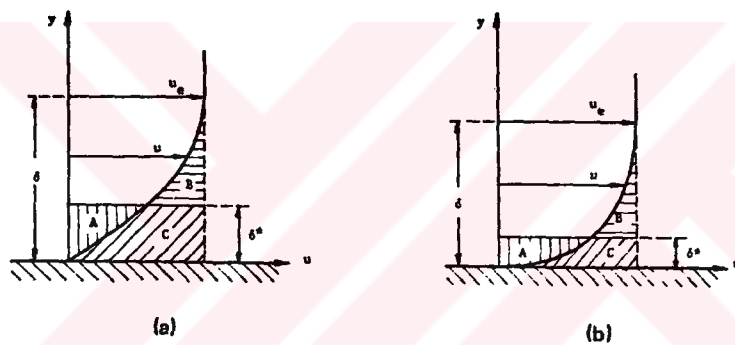
Figure 2.9 Boundary layer velocity profiles:
   a) laminar boundary layer,
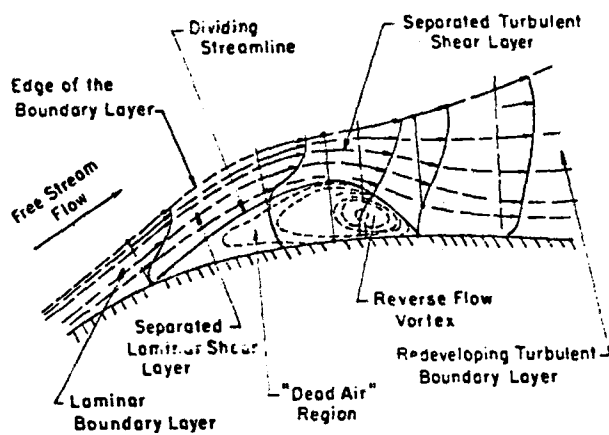   b) turbulent boumdary layer [1].

Figure 2.10 Flowfield in the vicinity of a transitional separation bubble [9].

faster fluid further out will take place, then the forward movement of fluid against the pressure rise and friction will be facilitated because of the increased momentum and energy of the fluid near the wall.

The viscous mixing of the fluid can increase the momentum near the wall. By its nature, turbulent flow provides such mixing of the slower fluid near the wall (the faster fluid is farther out). This increases momentum near the wall and results in a change in the velocity profile. Compare Fig.2.9.b to the laminar velocity profile shown in Fig.2.9.a. These figures also indicate that the velocity is steeper in a turbulent than in a laminar boundary layer [1].

Hence, turbulent flow facilitates the streamwise movement of the fluid against the pressure rise and friction. Therefore, turbulent flow separates farther downstream then does laminar flow.

The separated flow region is often called the "dead water" region, but dead does not necessarily mean the zero velocity. Actually, even though flow separation takes place over or behind the two-dimensional surfaces, this region consists of a complex vertical, unsteady three-dimensional flow that often has considerable velocity.

The major features of flow in the vicinity of transitional separation bubbles are shown in Fig.2.10. Downstream of the laminar separation point, a wedge of recirculating fluid developes that is bounded by the airfoil surface and the separated shear layer. This fluid wedge makes up the laminar portion of the separation bubble. The magnitude of reverse flow velocities in this region is typically very small, on the order of a few percent of that at the edge of the shear layer. The displacement effect

of this wedge of fluid on the external flow causes a reduction in the adverse pressure gradient that would exist if the bubble were absent. In many cases, the gradient in surface pressure in this region is reduced approximately to zero. Once transition of the separated shear layer has occured momentum exchange across this layer by the turbulent mixing process reduces the vertical extent of the reverse-flow layer and also the displacement effect of the bubble. A deceleration of the external flow over the bubble's turbulent portion results with an accompanying adverse pressure gradient. The magnitude of the reverse-flow velocities are much larger in this region., on the order of 20 % of U_∞. If the bubble is small relative to the airfoils' chord, the external velocities at the separation and reattachment point are nearly equal to those that would be present at those locations if no bubble had formed. This type of separation bubble is generally referred to as a "short bubble". If the local Reynolds number is low enough and the pressure gradient is sufficiently steep, the turbulent mixing process is unable to produce flow reattachment. Under these conditions, the bubble "bursts": separated flow extends over much of the airfoil, which causes the airfoil's pressure distribution to collapse. Since this also a reduction in the adverse pressure gradient, reattachment eventually may take place. The length of the resulting "long bubble" can be in the order of airfoil's chord [9].

The separation bubble may be divided into three parts, namely viscous flow inside, the turbulent mixing region of reattachment, and the inviscid external flow.

It is assumed that the bubble is closed so that a "zero" stream line leaves the surface at S and reattaches at A. The boundary layer is of finite thickness at S, and since there is no longer a boundary condition requiring zero tangential velocity along the zero streamline (as there is no solid surface), the shear layer must be diffuse and extend inside the zero stream line. The fluid is thus set into motion inside the bubble and there circulatory flow exists satisfaying the continuity requirement for

closed bubble. As Fig.2.10 shows, at the rear end of the bubble, the stream line widens considerably. It may be assumed that there is transition to turbulent flow near station (1) or slightly farther upstream. Because the transition from laminar to turbulent flow in the boundary layer becomes most clearly discernible by a sudden and large increase in the boundary-layer thickness and in the shearing stress near the wall [10]. The velocity profile at station (2) will show the vertical tangent characteristics of a separation profile. The pressure between S and P1 is nearly constant, but between P1 and A a large pressure change exists [1].

Prandtl showed that separation is caused by excessive momentum loss near the wall in a boundary layer trying to move downstream against in increasing pressure, $\delta p/\delta x > 0$, which is called an adverse pressure gradient. The opposite case of decreasing pressure, $\delta p/\delta x$, is called a favourable gradient, where flow separation can never occur.

Fig.2.11 illustrates the general shapes of velocity profiles with separation and without separation [11].

Fig.2.12 shows some experimental profiles of u/U_∞ vs y/δ for various pressure gradients, in turbulent flow.

The profile shape a distinctive look about them that seems to spell analytic trouble: they are about as laminar as they can possibly be. They seem to smash up against the wall as if there were velocity slip at the wall; actually, they drop linearly to zero within a thickness to small to be seen. For the uppermost profile, for example, the linear (viscous) drop-off in the region $0 < y/\delta < .002$. The profiles also seem to have a characteristic concavity near $y/\delta = .2$. This is the beginning of
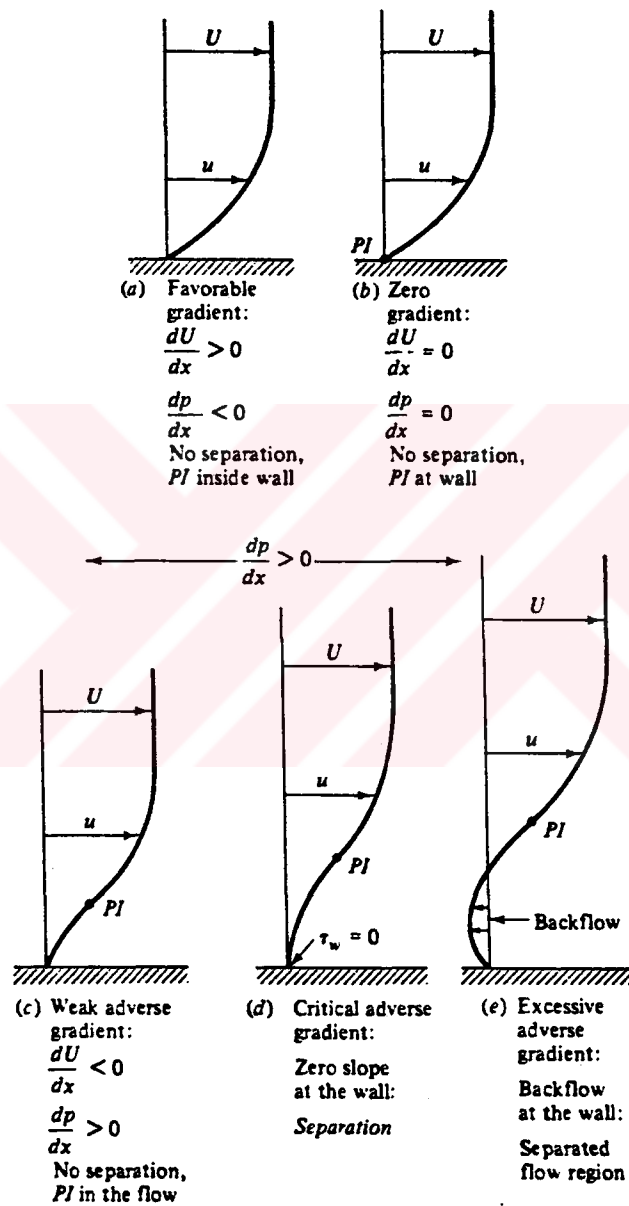
Figure 2.11 Effect of the pressure gradient on boundary layer profiles, PI:profile point of inflection.
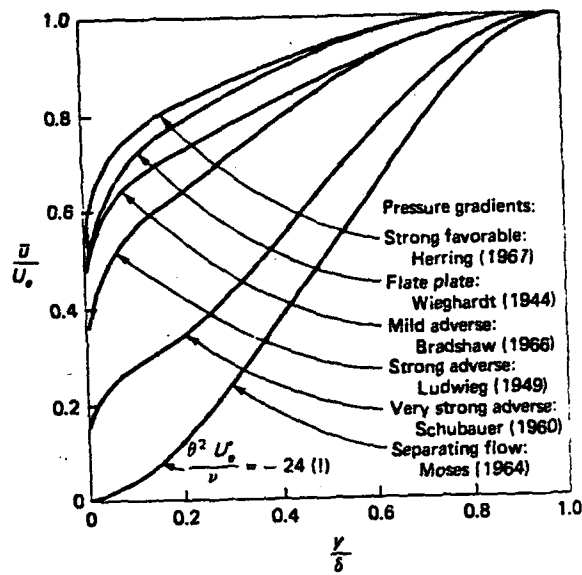
Figure 2.12 Experimental turbulent-boundary-layer velocity profiles for various pressure gradients [7].
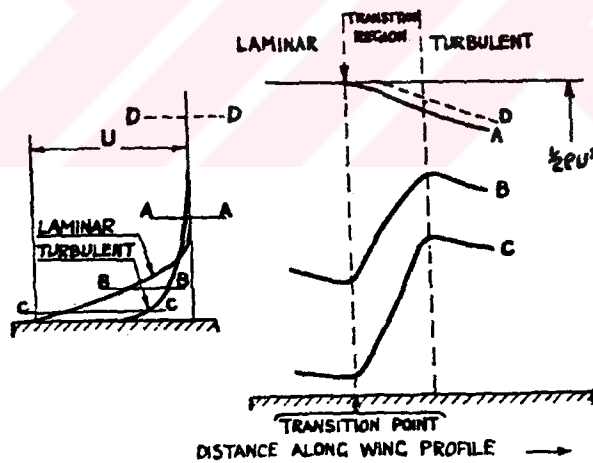
Figure 2.13 Diagrams for explaining the methods used for locating the region of transition to turbulent flow [12].

the outer (fully turbulent) layer [7].

Fig.2.13 shows the region of transition to turbulent flow. The left-hand figure shows typical distribution of mean velocity in the boundary layer just before and just after the onset of turbulence. The right-hand figure shows the variation of pressure in a pitot tube moved through the transition region along lines prallel to the wing surface at various distance from it [12].

Very little is still known of details of the flow structure in the reattaching zone where the separated shear layer reattaches onto a solid surface. The behaviour of large-scale vortices in the reattaching zone play a decisive role in determining flow properties not only in the separation bubble but in the developing region downstream of the bubble. Fig.2.14 gives a sketch of turbulent separation bubble.

The reattachment of a mixing layer at the end of a separation bubble is an example of a flow in which shear layer changes its species (i.e. its name); after reattachment to the surface, the mixing layer is called a boundary layer, although it is clear that relaxation from the turbulence structure typical of mixing to that typical of a boundary layer will not be instantaneous [14].

Free stream turbulence is the name given to the background level of random, three-dimensional velocity fluctuations present in every fluid stream. The turbulence intensity is usually defined as the ratio of the r.m.s. velocity fluctuation of the streamwise component, u', to the mean flow velocity. It is customary to describe the magnitude of the intensity in relative terms such as: "high", meaning more than 10 % or so and found, for example, in the natural wind; "low", meaning less than about 5 % ; or "very low", usually meaning less then 1 % which corresponds to the
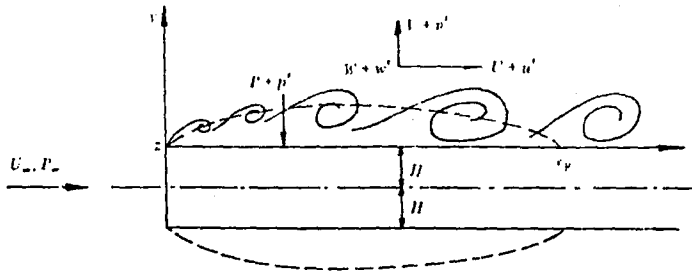
Figure 2.14 Configuration of flow on the blunt plate [13].
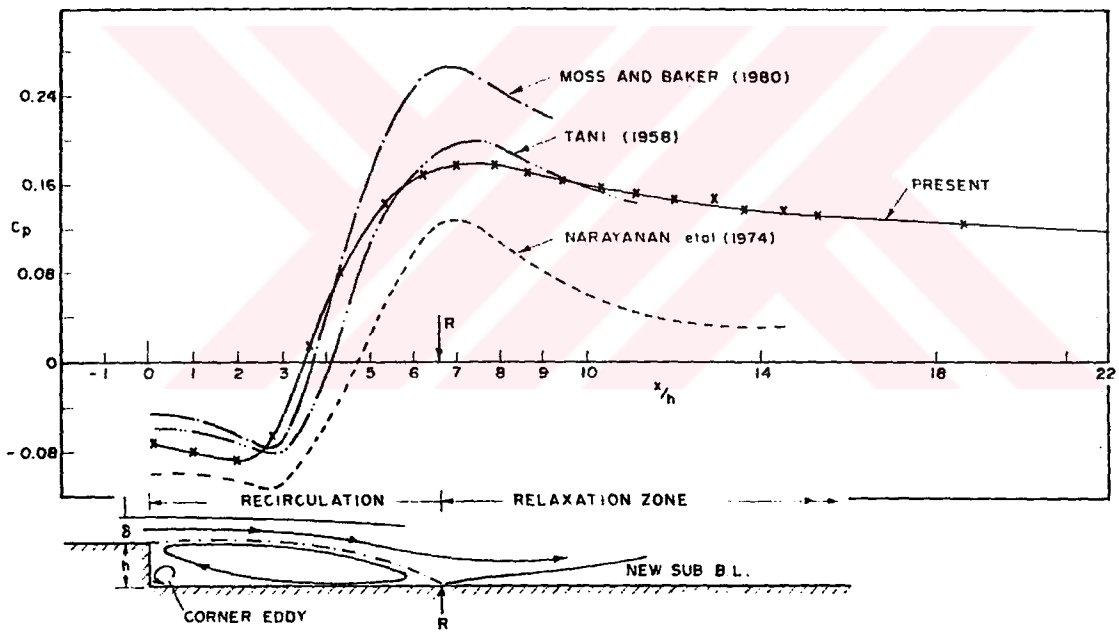
Figure 2.15 Pressure distribution behind a plain back step [15].

levels found in low-turbulence wind tunnels.

The presence of turbulence in the free stream tends to increase skin friction. Two basic mechanisms are responsible: one is that boundary undergoes transition to turbulence earlier, with an attendant increase in skin-friction coefficient from laminar values to turbulent ones. The other mechanism is the increased mixing and momentum transfer under the influence of free stream turbulence [4].

The back step flow configuration, investigated by Gai and Sharma [15] provides a simplest example of the phenomenon of separation, recirculation, reattachment and subsequent relaxation of the shear layer. Fig.2.15 shows the pressure distribution for the plain rearward facing steps where $h/\delta s = 0$ (1) (δs: boundary layer at separation) and for different blockage ratios. It is noted that the decrease in pressure in the relaxation region is quite slow.

The flow over a delta wing at incidence separates at the leading edge and reattaches on the upper surface. As the flow moves spanwise from the reattachment line, a secondary separation line forms near the leading edge and both lines lie on conical rays through the vortex of the wing.

When the leading edge of a delta wing is sharp, the flow separates at the leading edge and a spiral vortex sheet occurs like that in Fig.2.16.
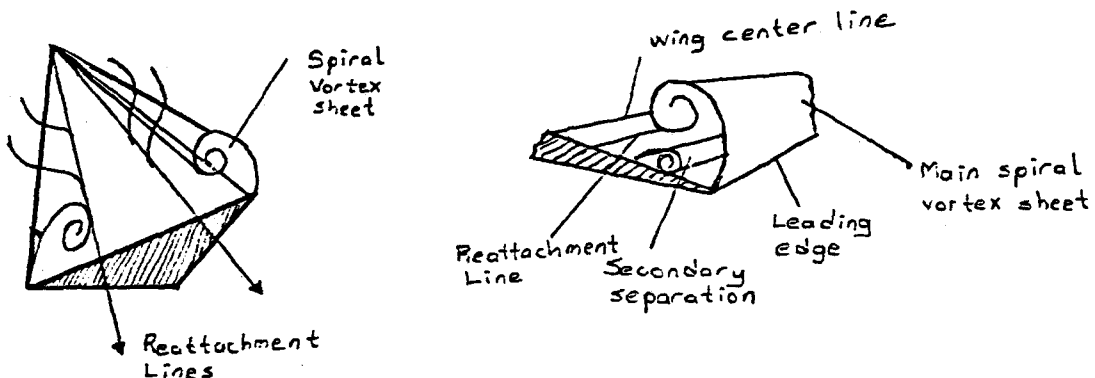
Figure 2.16 a) inviscid vortex flow over delta wing, b) upper surface flow geometry [16].

However the theoretical pressures on the upper surface were found to drop below the experimental data near the leading edge. Horvey and Hummel show that this difference is due to a secondary separation on the upper surface that produce a secondary vortex in the opposite direction of the primary vortex (see Fig.2.16).

The secondary vortex increases the surface pressures in the region below it. The reattachment line is the line where the stream surface moves over the top of the primary vortex and reattaches to the upper surface [16].

In order to obtain such information directly, Dianat and Castro [17] had made quantitative measurements of the mean and fluctuating skin-friction field on the top surface of various three-dimensional bodies in a thick turbulent boundary layer, and the results were given in Fig.2.17.

Fig.2.17 shows the centerline (y=0) mean flow streamlines suggested in Ref.[17] near the leading edge. Fig.2.17.c entails a high curvature of the separating shear layer since this is almost certainly laminar initially, it could be argued that such a high curvature is inherently unlikely. The flow in Fig.2.17.d with fluid being ejected spanwise near the free nodes, circumvents the difficulty. It must be emphasised, however, that the physical scale of this region is exceedingly small, and neither the mean nor the fluctuating surface shear stress data can be used confidently to deduce the leading edge behaviour with any certainty.

The effect of turbulence and shear on the flow around square cylinders has been investigated by Adatia [18] for models with and without free end. It has been found that end plates are necessary to simulate a two-dimensional flow condition. According the experiment results the sketch of the flow separation around square
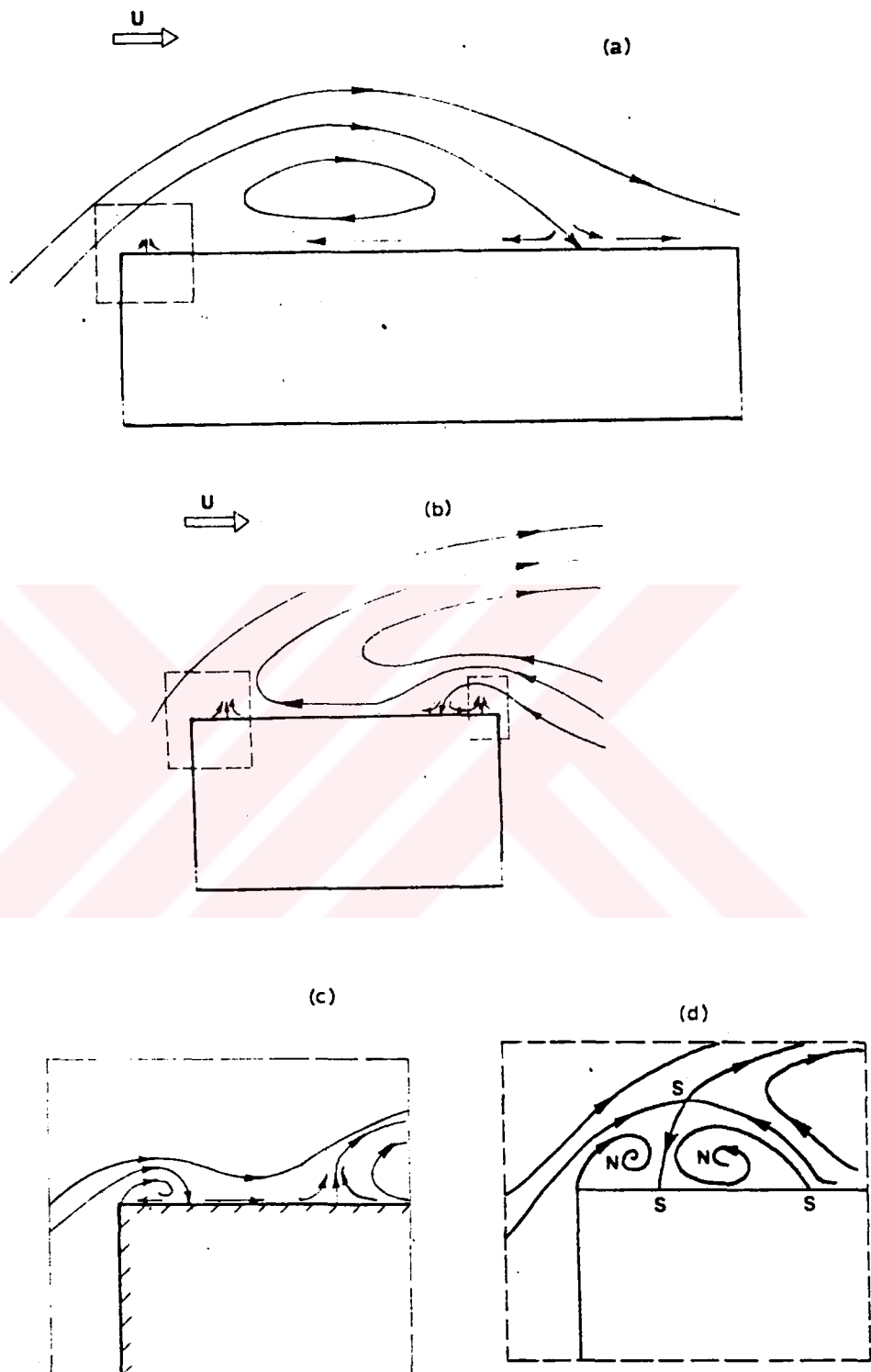
Figure 2.17 Mean streamlines on centre plane [17].

cylinders were given in Fig.2.18 and Fig.2.19.

Cherry, Hillier and Latour [19] has investigated the unsteady separated and reattaching flow formed by two-dimensional rectangular leading-edge geometry. This geometry was selected because of two important simplifying features: the geometrically fixed separation positions, and the highly favourable pressure gradient on the front face which means that the separating shear layer is extremely thin compared with the overall bubble scale. A schematic view of mean-flow field and mean-pressure distribution is given in Fig.2.20.

Experiments which were performed by Ruderich and Fernholz [20] in the highly turbulent and disturbed flow over a bluff plate with a long splitter in its plane of symmetry. The flow separates at the sharp bevelled edge of the bluff plate, forms a free shear layer on top of the reverse-flow region which is bounded on its other side by the splitter plate, and reattaches on the splitter plate over a narrow region curved in spanwise direction. The schematic diagram of the mean flow and the corresponding pressure distribution is given in Fig.2.21.

Fig.2.22 shows a sequence of mean-velocity profiles through the reverse-flow and reattachment region into the attached shear layer. The most obvious features are velocity maxima and minima of the profiles in the reverse-flow region, and their rather fast disappearance in the attached flow. The maximum velocity remains every where higher than the upstream velocity U_∞, which is indicative of the blockage effect of the flow.

U_{ref} and $(y - y_{ref})/x$ are the dimensionless length scale for the present flow.

SHEAR LAYER MEAN
CENTRE LINE
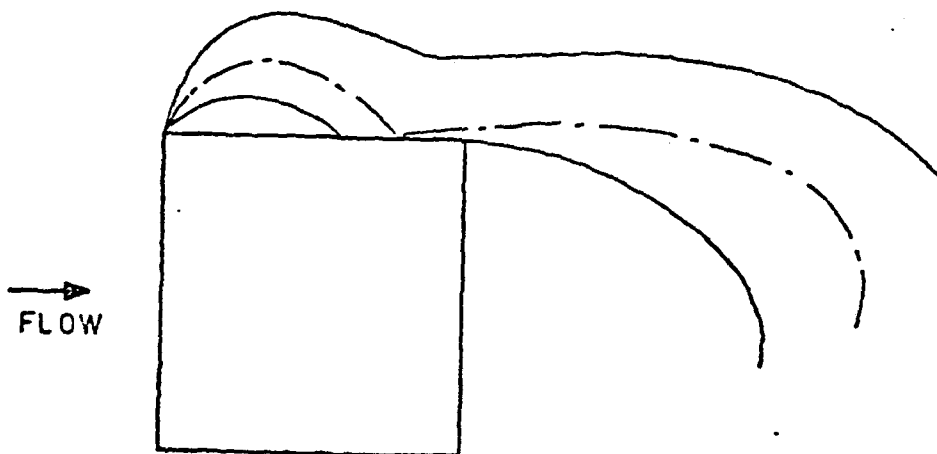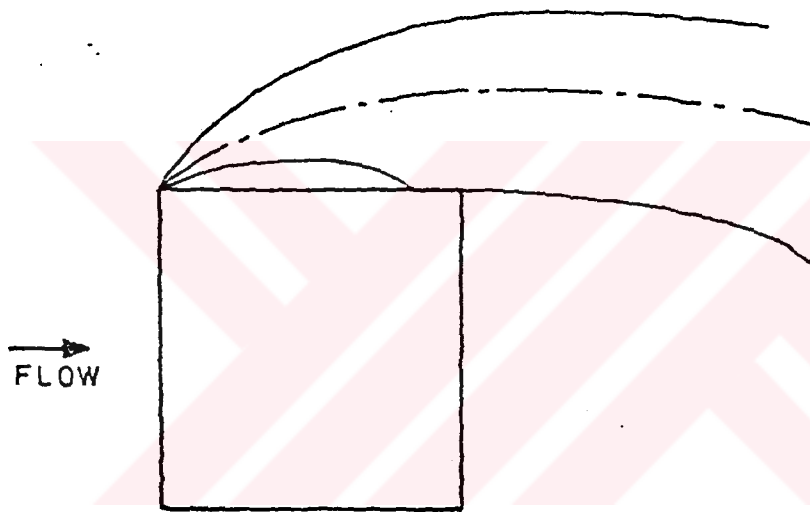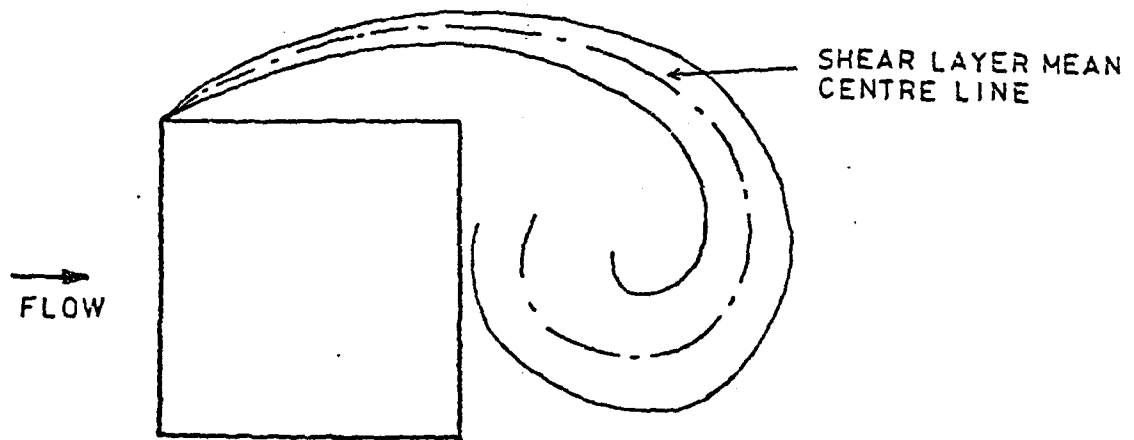
FLOW

FLOW

FLOW

Figure 2.18 a) Uniform flow, b) turbulent flow, c) turbulent flow with path
distorsion [18].
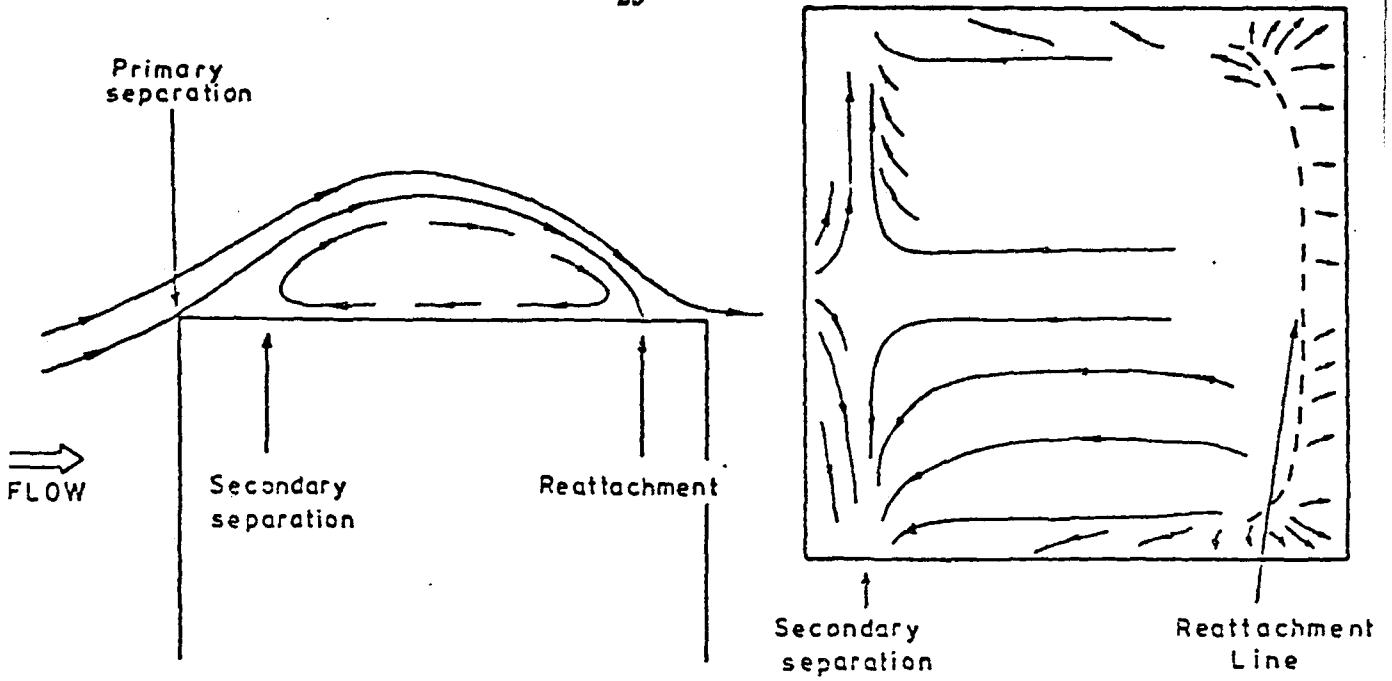
Figure 2.19 a) Flow streamlines over top surface in turbulent flow,

b)flow pattern on top surface in turbulent flow [18].
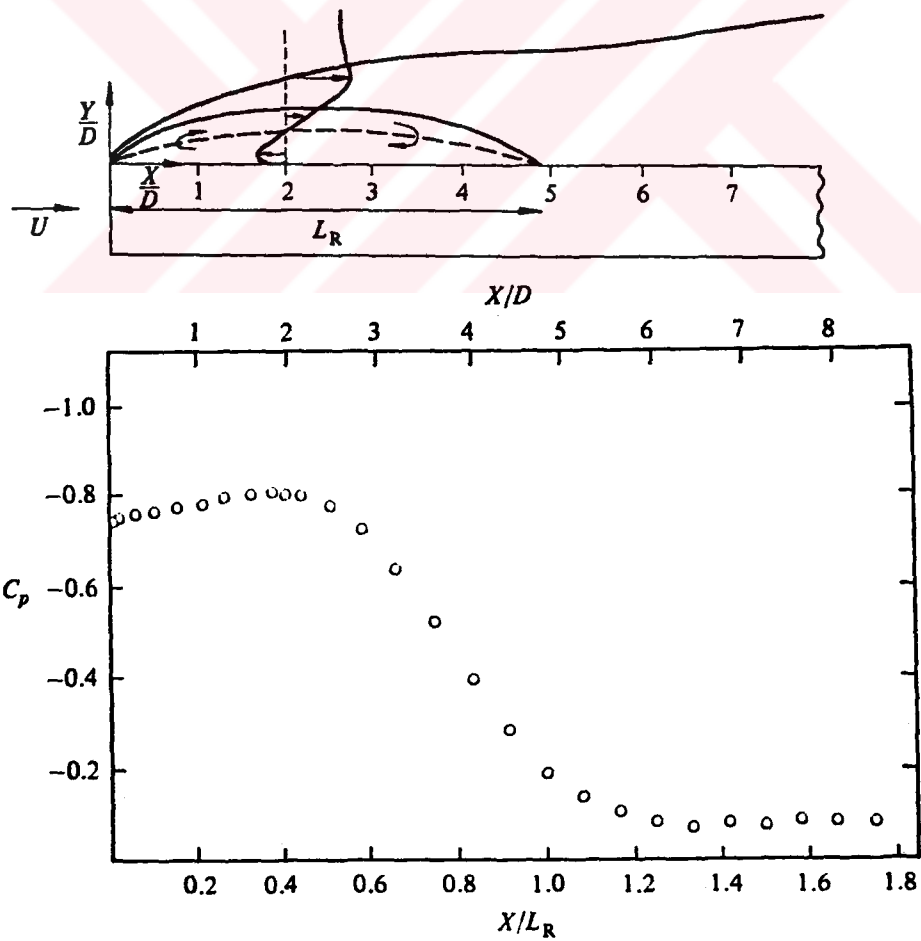
Figure 2.20 a) Schematic of mean-flow field,

b) mean-pressure distribution [19].
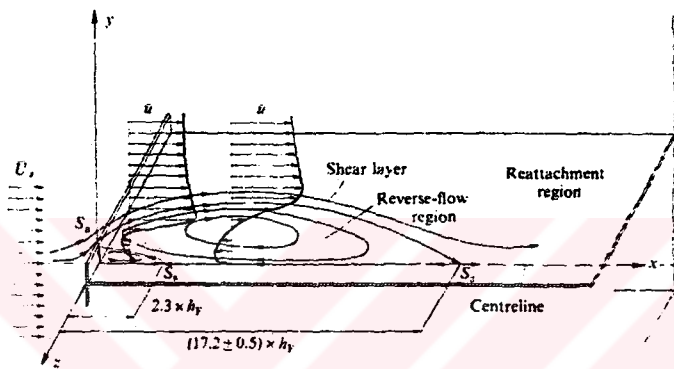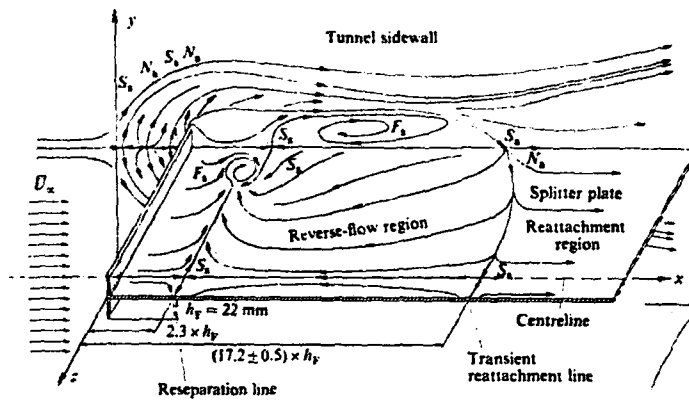
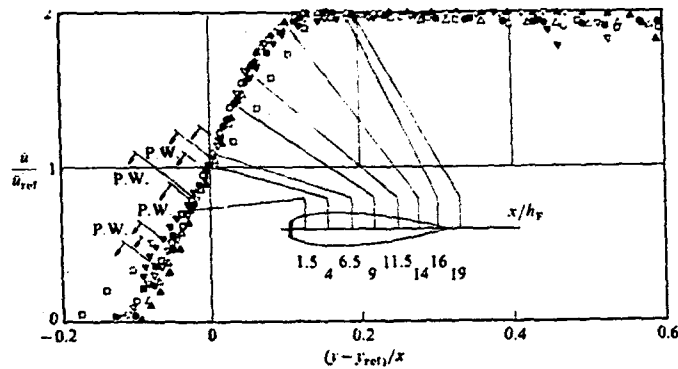Figure 2.21 Schematic diagram of the mean flow downstream of a normal plate   [20].

Figure 2.22 Developement of the mean-velocity profiles in a curved shear layer   [20].

Hear U_{ref}, which is U_{max} or $.5U_{max}$ and easier to determine downstream from reattachment, would be appropriate reference velocity. y_{ref} denotes the locus of U_{ref}. If one is prepared to accept a less general similarity concept than self-similarity, that of "profile similarity" may be used instead. Profile families are defined as showing profile similarity if individual profiles collapse on a single curve. This is achieved by making the profile data dimensionless by the respective maximum value and by plotting them against $(y - y_{max})/x$, where y_{max} is the locus of the maximum velocity.

An experimental investigation of spontaneous and forced transition on a secant-ogive-nose axisymmetric body was conducted for Reynolds number based on the model length by Kegelman and Mueller [21]. In Fig.2.23 the velocity and turbulence intensity profiles that they had measured were given.
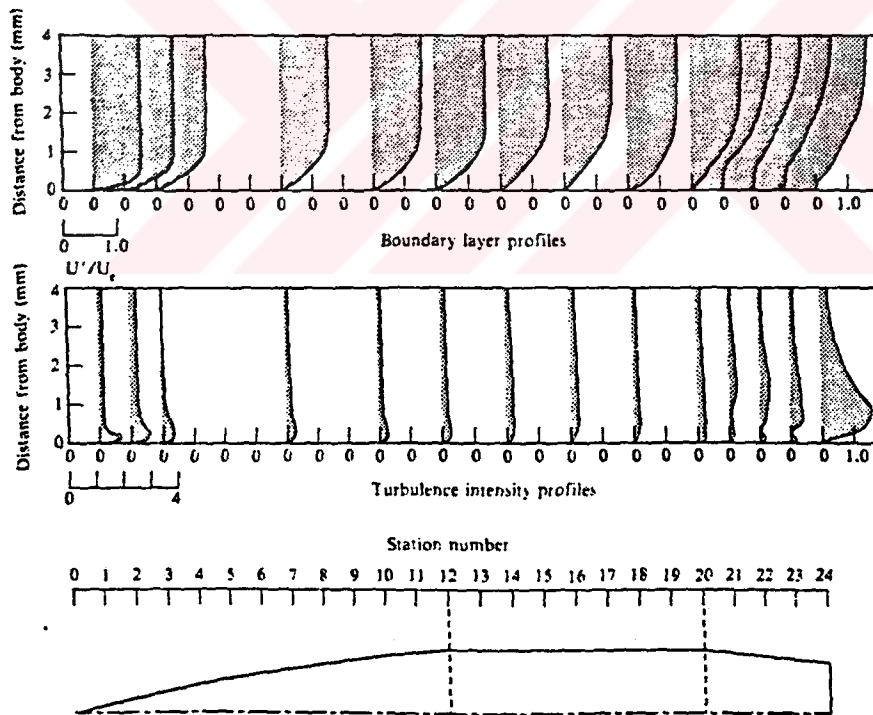
Figure 2.23 Boundary layer and turbulence intensity profiles for ogive nose axisymmetric body [21].

CHAPTER 3

INSTRUMENTATION AND EXPERIMENTAL TECHNIQUES.

3.1 INTRODUCTION

This chapter, consists of the experimental investigation performed in the present work. The wind tunnel where the experiments were carried out, the models, and the experimental techniques used in these experiments were explained.

3.2 WIND TUNNEL

The experimental study were carried out in ITU's open-circuit wind tunnel with a test section of 50x50x200cm. This tunnel has a variable speed up to 30 m/s. A schematic view of the tunnel is given in Fig.3.1. In the experiments the uniform air flow velocity was 10 m/s at the test section of the tunnel and in this velocity the turbulence intensity was about .3

The velocity and turbulence profiles of the boundary layer on the test section wall at a certain station are given in Fig.3.2. By using the velocity profile, the boundary layer thickness was obtained as 2.6 cm.

In order to find the flow quality in the test section, pressure distribution along the test room, founded without and with model, are given in Fig.3.3. As it can be seen from the figure, after mid point of the test section air flow begins to decelerate which means that the cross-sectional area of the test section becomes larger. But
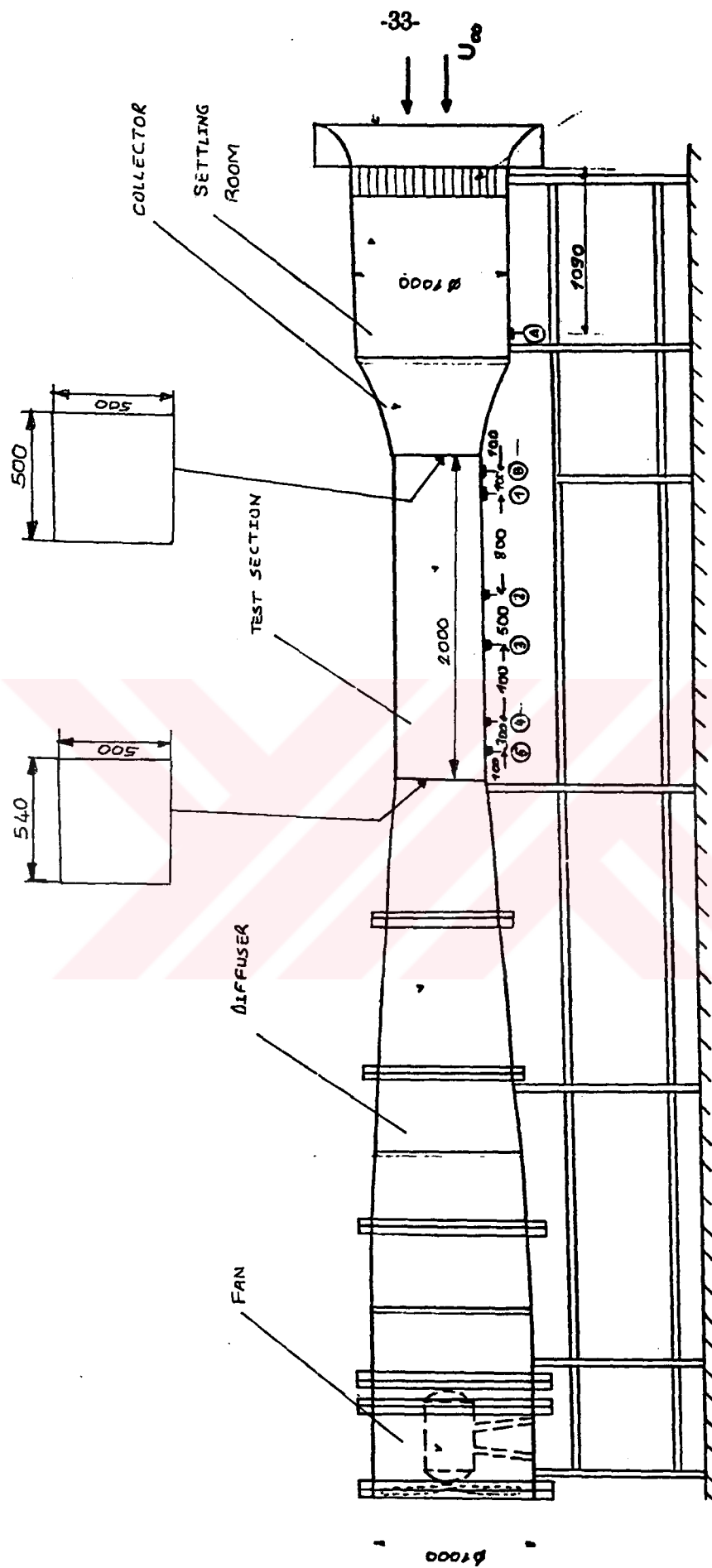
Figure 3.1 A schematic view of the wind tunnel
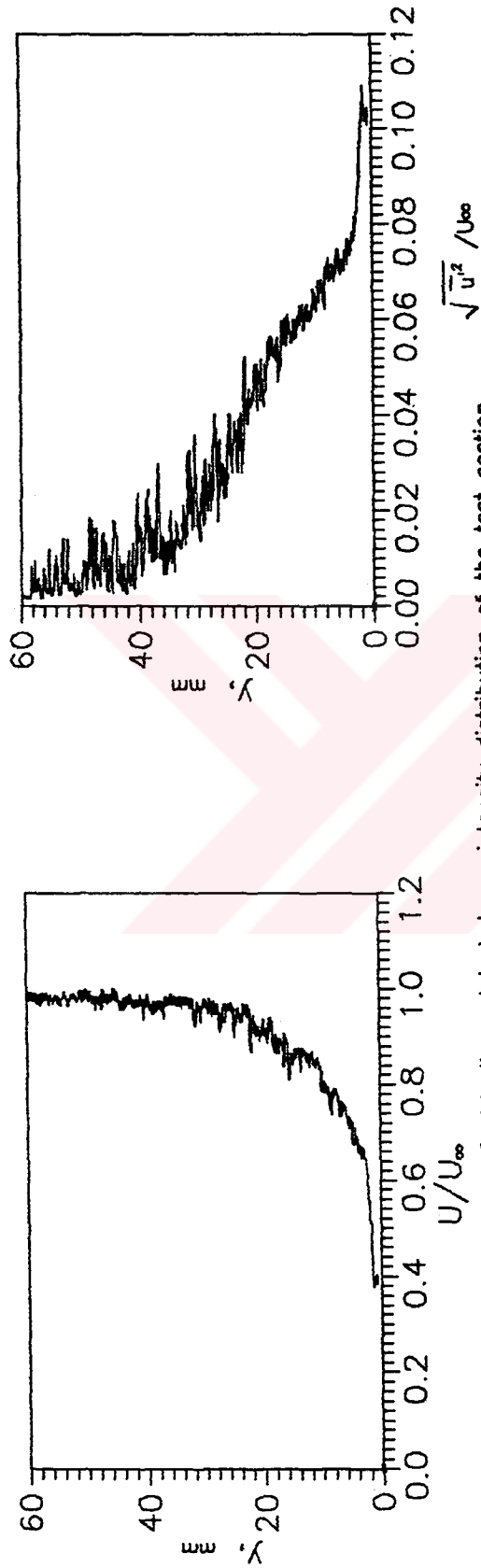
Figure 3.2 Velocity and turbulence intensity distribution of the test section.
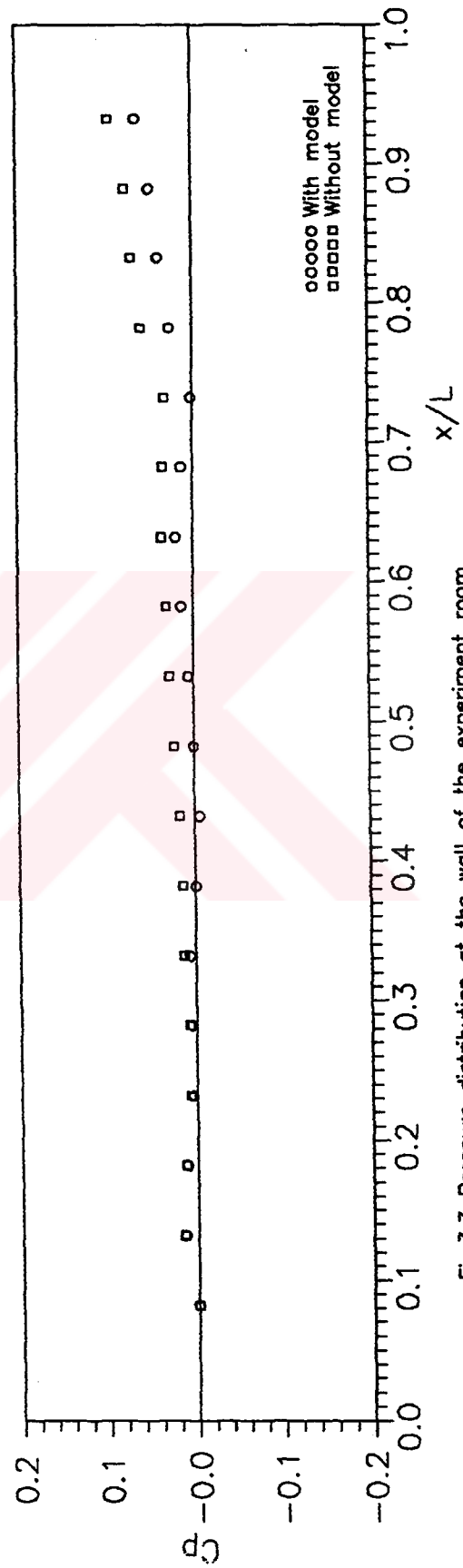
Fig.3.3 Pressure distribution at the wall of the experiment room.

when there is a model, the cross-sectional area of the test section reduces, so the air flow becomes more uniform relative to the conditions without model.

3.3 MODELS

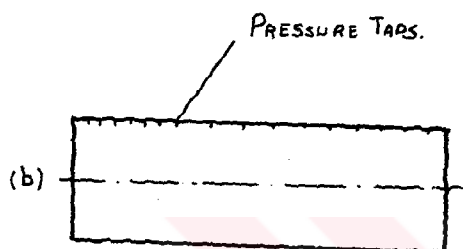In this study three groups of circular cylinders produced at the Trisonic Laboratory of ITU were used.

In the investigation of the flow field qualitatively by using flow visualization technique, with the oil-film method, four circular cylinder with different fineness ratios (d=50mm, L/d=3.1,4.0,5.0,9.2) were used. The geometric features of these models are shown in Fig.3.4.a.

In the investigation of the pressure distribution, to find the effect of the fineness ratio to flow field, 9 different circular cylinder with different fineness ratios (d=50mm, L/d=3.1,4.0,5.0,5.94,6.92,7.5,7.92,8.28,9.16) were used. In order to measure the static pressures on the surface of the models there were 18 holes opened on the model surface of each model along the symmetry-axis. Then metalic pipes with 1.1 mm outer diameter (injection pipes) were settled down in these holes. Plastic tubes with 1.1 mm inner diameter and 2.3m length were used in the connection between the pressure taps and the measurement instrument, micromanometer. The geometric features of these models and the place of the pressure taps are shown in Fig.3.4.b.

The velocity and turbulence intensity profiles were measured with hot-wire anemometer. In these experiments 3 circular cylinder with the same fineness ratio and with different Reynolds number based on the cylinder diameter ($Re_d = 3.45x10^4, 5.18x10^4, 7.59x10^4$) were used. The geometric features of these models are
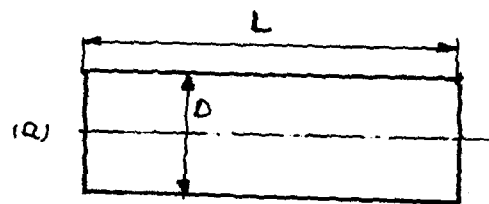
L

(a)   D

d=50mm L/d= 3.1, 4.0, 5.0, 9.2

PRESSURE TAPS.

(b)

d=50mm L/d= 3.1, 4.0, 5.0, 5.94, 6.92, 7.5, 7.92, 8.28, 9.2

(c)

$L/d=7.5$ $Re_d = 3.45x10^4$

$5.18x10^4$
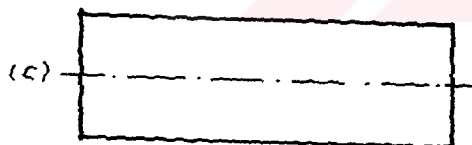
$7.59x10^4$

Figure 3.4 Geometric features of the models;

a) flow visualization models,
b) pressure measurements models,
c) hot-wire models.

shown in Fig.3.4.c.

3.4 EXPERIMENTAL TECHNIQUES

In this study three different experimental methods were used: Flow visualization and static pressure measurement techniques for investigating the effect of the fineness ratio on the flow field. Hot-wire anemometer was used for finding the velocity and turbulence intensity profiles

3.4.1 FLOW VISUALIZATION EXPERIMENTS

After many years of wind tunnel practice the surface oil flow technique is taken a standard technique for experimentation. This technique enables one to quickly and easily a picture of the flow pattern close to the surface of a solid body exposed to an airflow. The surface is coated with a specially prepared paint consisting of a suitable oil and a fine pigment that yields the colour to mixture. Due to the frictional forces, the air stream carries the oil with it, and the remaining streaky deposit of the pigment gives an information on the direction of flow and allows one to observe, in particular, the line of separation and reattachment [22]. The special physical and optical properties of oil permit flow to be observed at two or more conditions during a single test provided that sufficient time is allowed for each proceeding pattern to be obliterated and the next succeding one to be established [5]. The surface oil-flow technique can only be of a qualitative nature, and questions arise concerning the reliability of the indicated flow direction and presence of the oil sheet effects the original air flow. It is obvious that this technique is not able to show correctly the pattern of an unsteady flow [23].

In the present work oil used for surface flow visualization consists of a proper mixture of gasoline, carbon dust, and conventional motor oil with No:10. The surface

of the models were painted white so that the oil flow pattern could be visualized easily. If the oil film is thin and pure enough then it takes an identical form of the skin-friction lines. If the skin-friction lines converge to a particular line then oil accumulates on this line and this line is called the *separation line*. If the skin-friction lines diverge from a particular line, then this line is called the *reattachment line* [24].

The height of the oil accumulation line in a pattern is considerably less then 0.1 mm. Therefore it is expected that the interaction of oil with the separated flow and the displacement of the oil line from the separation line to be negligible [22].

In the present study, oil-film technique was used to find effect of the fineness ratio on the flow field around the circular cylinder with 4 different fineness ratios and at 10 m/s mean velocity conditions.

In the experiments after painting the model with proper mixture, the photographs were taken by camera while the tunnel was running. These photographs are given in Chapter 4. From the photographs limit flow patterns, separation and reattachment lines, can be easily obtained. The results are given in Chapter 4.

3.4.2 PRESSURE MEASUREMENTS

In the investigation of the effect of the fineness ratio on the flow field around circular cylinder, by using pressure measurement technique, 9 different models were used. Static pressure at the model surface were taken from the presure taps which were placed lying on the model surface from nose to 4d distance in the axis-symmetry direction.

One from the two micromanometers that were used in the experiments was

used to measure the dynamic pressure (q_∞) and the other was used to find the difference between the static pressure of each tap that was placed on the model surface (P_i) and the static pressure of mean flow (P_∞)

The experimental equipment is given in Fig.3.5. as it can be seen from this figure, the dynamic pressure of mean flow (q_∞) was measured as mmH_2O by using the wall pressure taps of the wind tunnel settling room and test section.

In order to measure the difference between the static pressure of the tap on the surface (P_i) and the static pressure of the mean flow (P_∞), one input of the micromanometer was connected with pressure tap that chosen and the other was connected with the test section static pressure tap. So the value of $(P_i - P_\infty)$ was measured as mmH_2O.

The pressure coefficient was calculated with the equation:

$$C_p = \frac{P_i - P_\infty}{q_\infty} \tag{3.1}$$

Experiments were made in the mean flow velocity of 10 m/s, so in a constant dynamic pressure. But in order to take care of the fluctuations in the mean flow velocity, dynamic pressure (q_∞) values were measured corresponding to each $(P_i - P_\infty)$ values.

In the measurements of the pressure the measurement errors and the standard deviation was calculated from the data. In the measurements of dynamic pressure the relative error is .23 mmH_2O and relative error is .009. The standard deviation these measurements is .26 mmH_2O. In the measurements of the difference of
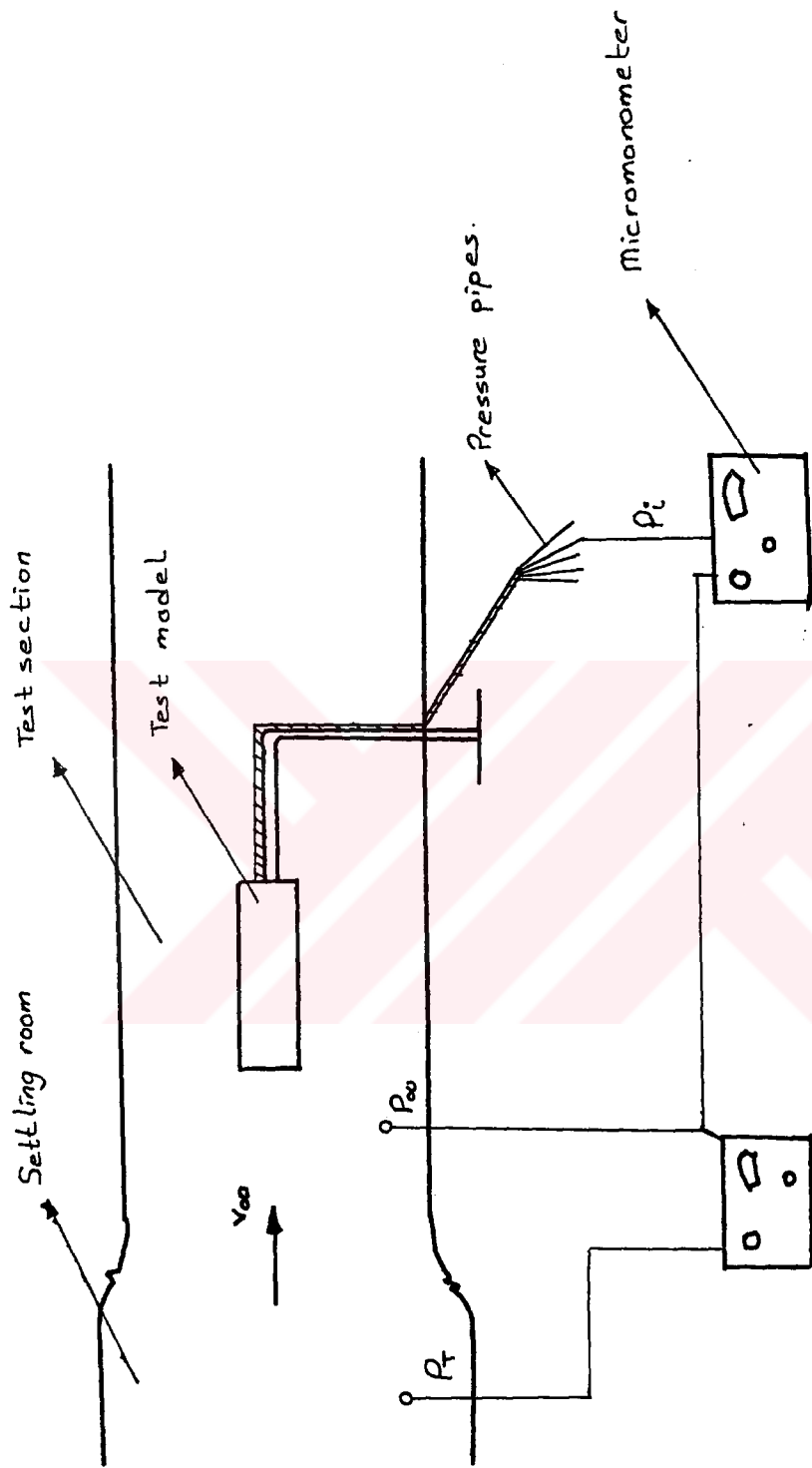
Figure 3.5 The experimental equipment where the pressure measurements were made.

of the static pressures the relative error is .08 and the standard deviation is .05 mmH_2O.

Tunnel blockage ratio is calculated from the division of the maximum cross section area (A_t) and it was founded as $(A_m/A_t)=.038$. As it was very little than .1, the effect of the blockage ratio is negligible.

3.4.3 HOT-WIRE ANEMOMETER

The hot-wire anemometer has been used for many years as a research tool in fluid mechanics. In spite of the introduction of new velocity measurement systems (i.e. the Laser Doppler Velocimeter), its applications are still expanding. The hot-wire anemometer is still the only instrument delivering at the output a truly analogue representataion of the velocity fluctuations.

A hot-wire anemometer has two main advantages over a pitot tube: 1) Its small size makes it possible to place the instrument very close to the wall, 2) Its extremely rapid response allows instantaneous velocity fluctuations, especially those of turbulent flow, to be measured.

The standard hot-wire anemometer probe consists essentially a short length of very fine wire supported between two metal prongs and heated electrically. The hot-wire is aligned normal to the air stream. The air velocity is deduced from the cooling produced by the airflow, either by recording the current needed to maintain a constant wire temperature or by measuring the potential difference across the wire with a constant current passing through it.

In this study, in the boundary-layer experiments, for the hot-wire measurements a constant temperature hot-wire anemometer (CTA) system of DISA components (55M10 constant Temperature Anemometer, 55D25 Auxiliary Unit, 55D31 Digital Voltmeter, 55D35 RMS Unit, 55D15 Linearizer, 52C01 External Stepper Motor, 52B01 Sweep Drive Unit, a standard type hot-wire probe DISA P11) was used. Mean velocity and RMS outputs of the anemometer were digitized by a data acquisition unit. During the hot-wire measurements, mean velocity and turbulence velocity outputs of the hot-wire anemometer were taken by a personal computer with 80386 micro-processor. The units and connection diagram of the system is given in Fig.3.6. The calibration of the hot-wire probe was made by using the wind tunnel.

There is a relation between the voltage output of the anemometer (E) in CTA-hot-wire system and airflow velocity (U):

$$E^2 = E_0^2 + BxU^{1/m} \qquad (3.2)$$

Here, B and m are the constants of hot-wire probe and the difference of the temperature between the hot-wire and fluid (air) circumstances. E_0 is the voltage output of the anemometer when air velocity is zero. If there is a linearizer in CTA-hot-wire system, there is a linear relation between the voltage output of the linearizer (E_l) and air velocity (U):

$$U = KxE_l \qquad (3.3)$$

In the equations the dimension of the E and E_l is volt and the dimension of the U is m/s. In the equation 3.3, K is a constant and in order to make the value of K as 10 the linearizer can be regulated [25].
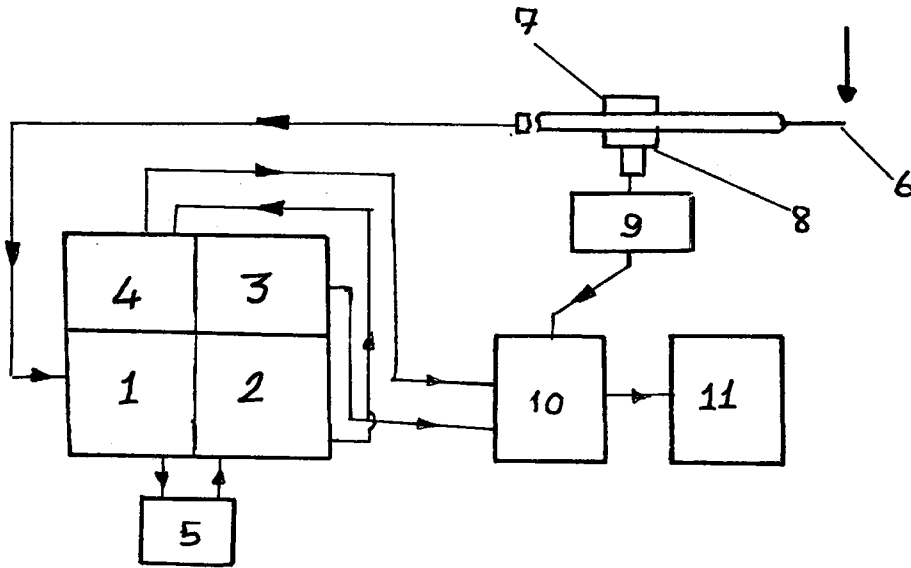
1 : DISA, 55M10 CTA (55M01 Main Unit, 55M05 Power Pack)

2 : DISA, 55D25 Auxiliary Unit (Filter)

3 : DISA, Digital Voltmeter (D.C)

4 : DISA, 55D35 RMS Unit

5 : DISA, 55D15 Linearizer and 52A40 Power Supply

6 : DISA, Hot-wire probe (i.e. A25, P01)

7 : DISA, Hatching Mechanism

8 : DISA, 52C01 External Stepper Motor

9 : DISA, 52B01 Sweep Drive Unit

10 : DISA, Data Acquasition System

11 : Personnel Competer

Figure 3.6 The unites and connection diagram of CTA Hot-wire system.

The outputs of a hot-wire anemometer do not indicate the flow direction; in other words, the mean velocity output of the hot-wire anemometer is always positive. However, the reverse flow in the recirculating region could be identified with an increase and then a decrease in the positive voltage as the probe approached the surface, as may be seen in Fig.3.17. It is also known that high turbulence, which exists in and near a recirculation region, makes a contribution to the mean velocity output of the hot-wire anemometer. Consequently, the mean velocity output of the anemometer for the zero mean velocity point in the recirculation region indicates a positive value instead of a zero value. Therfore, in Fig 3.7 [26], point A corresponds to the zero mean velocity point A'. The shift between the points A and A' is the contribution of turbulence to the mean velocity output of the anemometer. The mean velocity output of the anemometer for the points between point A and the surface corresponds to the reverse flow in the recirculation region and should be considered as negative although it is displayed as positive [26]. But in this study the mean velocity output of the anemometer for the recirculation regions were corrected like that: first the point A was shifted to the point A'' and then the signs of the outputs of the anemometer for the points between the beginning of the reverse flow and the surface shifted to negative, as seen again from Fig.3.7.

The error of the pressure measurements is given in Section3.4.2. The relative error in the measurements of the velocity with hot-wire anemometer is $\mp$ .1 m/s and in the measurements of the turbulence is $\mp$ .002 m/s.

The results of the hot-wire experiments are given in Chapter 4.
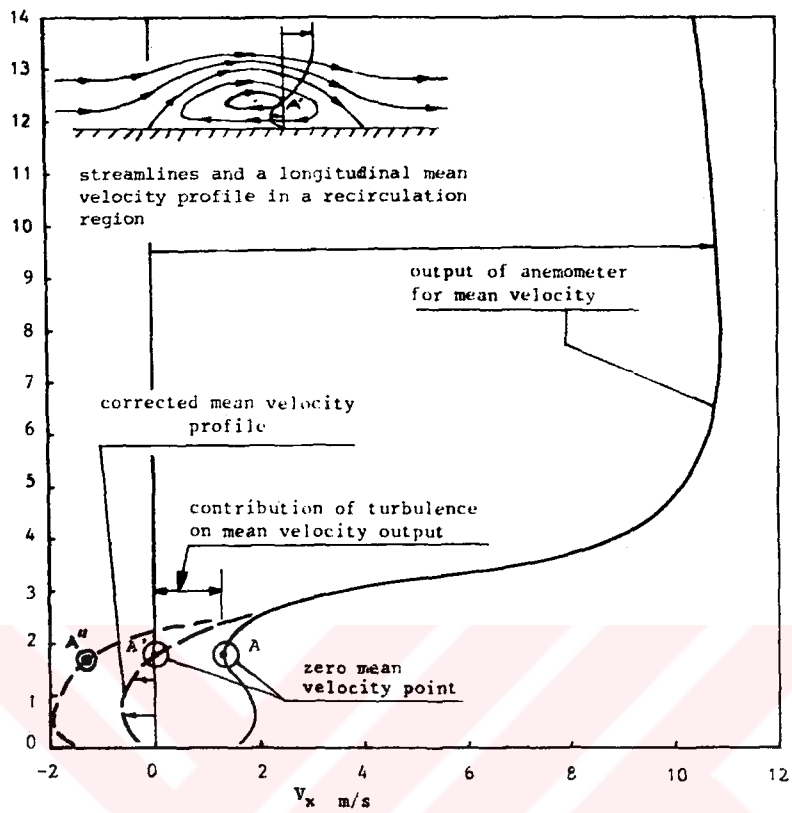
Figure 3.7 The correction of the velocity profiles.

CHAPTER 4

RESULTS AND DISCUSSION

4.1 INTRODUCTION

In this Chapter the results of the experiments are given including the photographs taken from oil-film technique, the pressure distributions and velocity and turbulence intensity profiles of the flow around the circular cylinders with different Reynolds number based on the model diameter. Then the discussion of the results are made.

4.2 RESULTS OF THE EXPERIMENTS

In examining the effect of the fineness ratio on the flow field around circular cylinder by using oil-film technique, four models were used. The fineness ratio (L/d, d=50mm) of these models are 3.1,4.0,5.0, and 9.2. The photographs which were taken by a camera is given in Fig.4.1.

In the investigation of the pressure distribution, to find the effect of the fineness ratio to flow field around circular cylinder, nine models were used. The fineness ratio (L/d, d=50mm) of these models are 3.1,4.0,5.0,5.94,6.92, 7.5,7.92,8.28,and 9.2. The results of the pressure measurements are given in Fig.4.2. In the graphic x-axis denotes the dimensionless change of the longitudinal distance of the point from the beginning of the model. Y-axis denotes the pressure coefficient C_p.

The mean velocity and turbulence intensity profiles were measured with hot-wire anemometer. In the experiments the measurements of mean velocity and turbulence were made in various stations. According to these measurements which were made perpendicular to the axis symmetry line, the velocity and turbulence outputs of the CTA-hot-wire system were taken and drawn by a personel computer with 80386 micro-processor.

In the hot-wire anemometer experiments to find the effect of the Reynolds number to the flow field around circular cylinder, three models were used. The fineness ratio of these models are constant (l/d=7.5) and the Reynolds numbers based on the model diameter are $3.45x10^4$, $5.18X10^4$, $7.59x10^4$.

Measurements of the velocity and turbulence intensity were made at 23 different stations in the longitudinal direction on each model. For an example the velocity and turbulence intensity graphics at each station for Model 1 is given one by one in Appendix A. In these graphics x-axis denotes a) dimensionless velocity (u/U_∞) and b) turbulence intensity. Y-axis denotes the distance of the measurement point from the model surface in perpendicular direction to the axis symmetry axis.

In order to compare the pressure measurements with hot-wire measurements, the longitudinal pressure coefficient distribution and the longitudinal mean velocity profiles measured at all stations aroun Model 1 are given in Fig.4.3. In the figure the limit streamlines ($\phi = 0$), around the recirculation region, obtained by using mean velocity profiles and the equation

$$\phi/(U_\infty.d) = \int_0^{y/d} (U_x/U_\infty)d(y/d) = 0 \qquad (4.1)$$

Here ϕ is stream function [25].

The longitudinal mean and turbulence velocity profiles measured at all stations around the Model 1,2, and 3 are given in the order with Fig.4.4, 4.5, and 4.6.

In order to see the effect of the Reynolds number on the flow field around circular cylinder, the velocity and turbulence profiles for three Reynolds number were drawn together. The velocity and turbulence profiles are given for y, distance between the point and the model surface, in Fig.4.7, and for y/δ, dimensionless distance, in Fig.4.8.

By using Fig.4.4, 4.5, and 4.6, the boundary layer thickness δ which corresponds to the distance of the point, where the mean air flow reaches 99 % of uniform flow velocity, from the surface were founded. The variation of the boundary layer thickness, δ, versus dimensionless longitudinal distance (x/d) is given in Fig.4.9.a and in logarithmic axis in Fig.4.9.b.

As it can be seen from the Fig.4.4, 4.5, and 4.6, on the recirculation region mean velocity values reach a value greater than 1 and then go to 1. So in this region it can not be defined that the boundary layer thickness as the distance of the point where air velocity reaches 99 % of U_∞, from the surface. In this region boundary layer thickness δ' was chosen as the distance of the point where air velocity reaches 101 % of U_∞, from the surface. Than the variation of the boundary layer thickness, δ', versus dimensionless longitudinal distance (x/d) is given in Fig.4.10.a and in logarithmic axes in Fig.4.10.b.

By using Fig.4.4, 4.5, and 4.6, the value of the maximum turbulent intensities and their y distance from the model surface for each turbulence profile were founded. The variation between maximum value of the turbulence and its y distance from the model surface, versus the dimensionless longitudinal distance (x/d) is given in Fig.4.11.

By using the dimensionless length scale suggested in Ref.[20], it is tried to have a similar velocity profile for all velocity profiles along the model surface. The method was used first for Model 1 and the result is given in Fig.4.12.a. Fig.4.12.b is drawn for only after reattachment velocity profiles. Finding of the y_{ref} and U_{ref} which were used in the graphics is explained in Chapter 2 or Ref.[20]. $(U_{ref} = .5U_\infty)$

The same method was used for Model 2, and 3 and the results are given in Fig.4.13.a and Fig.4.13.b.

In order to compare the results that were taken for each model, some group of stations before reattachment and after reattachment for each model were drawn and are shown in Fig.4.14.a and Fig.4.14.b.

Figure 4.1 The photographs which were taken by camera in the flow visualization experiments.
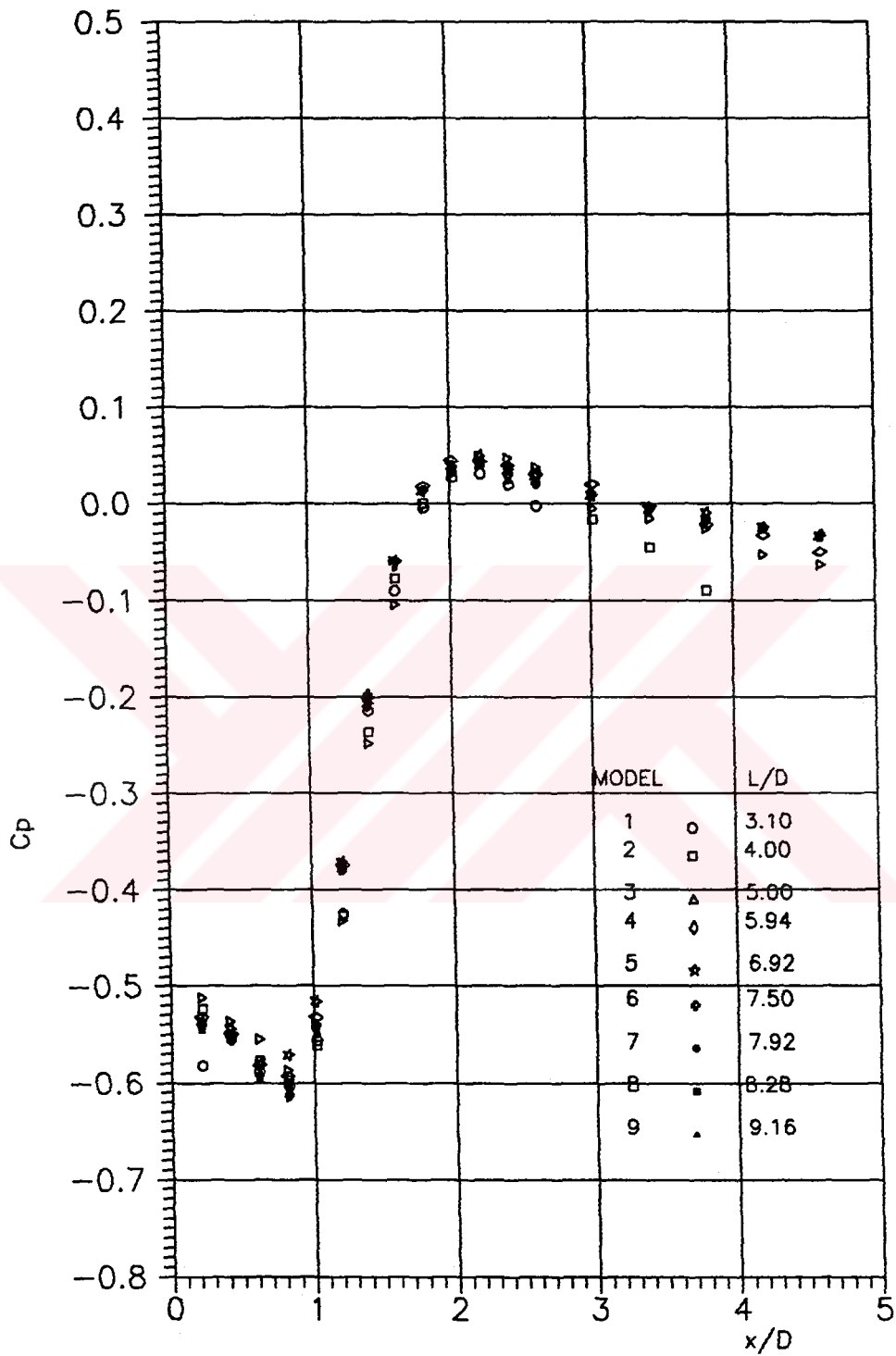
Figure 4.2 Development of the pressure coefficient along the centerline of the models.
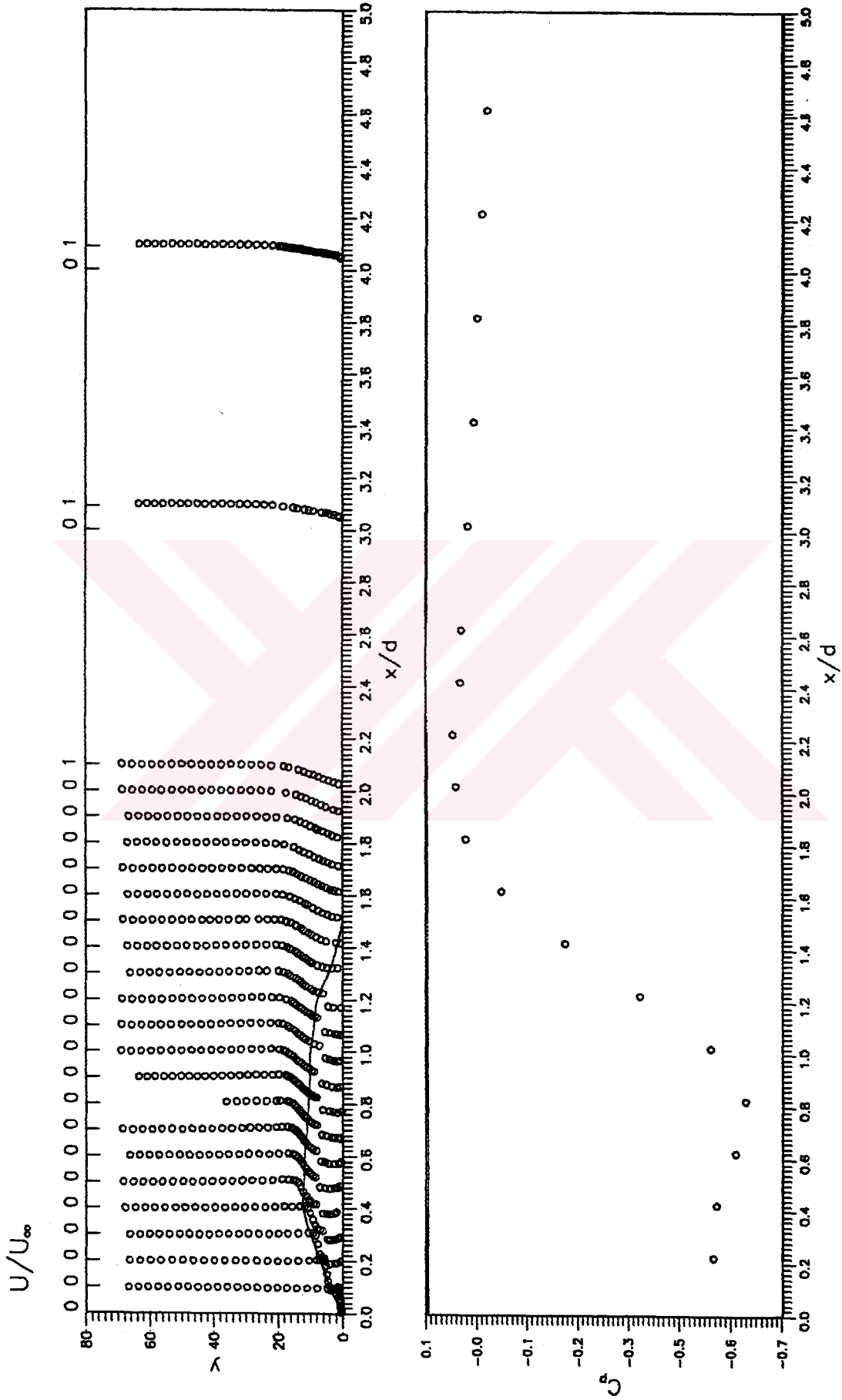
Figure 4.3 Comparison of velocity and pressure distributions for Model 1   Re_d=3.45x10^4
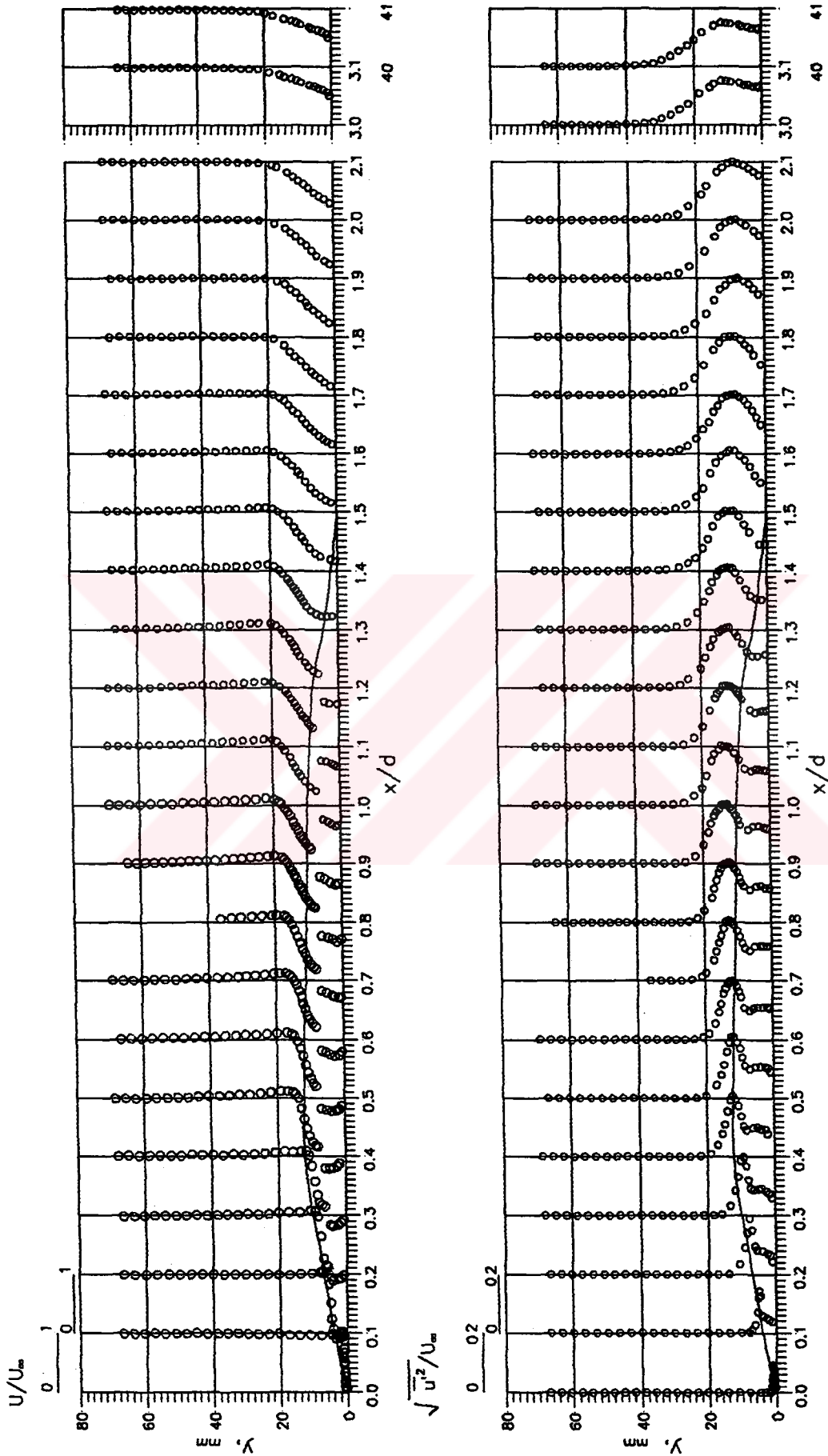
Figure 4.4 Mean velocity and turbulence velocity profiles around the model surface. $Re_d = 3.45 \times 10^4$
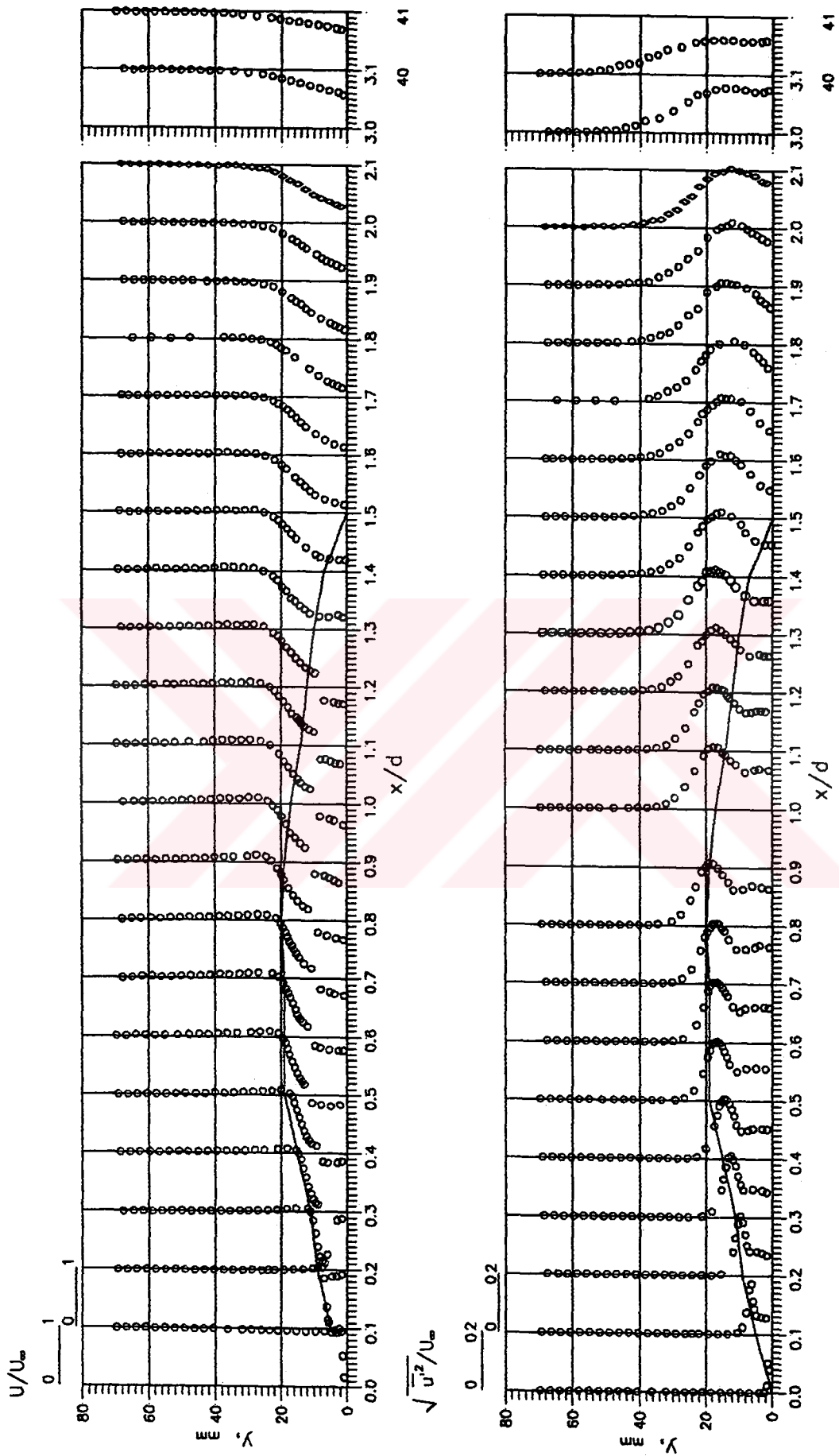
Figure 4.5 Mean velocity and turbulence velocity profiles around the model surface. $Re_d=5.18\times10^4$
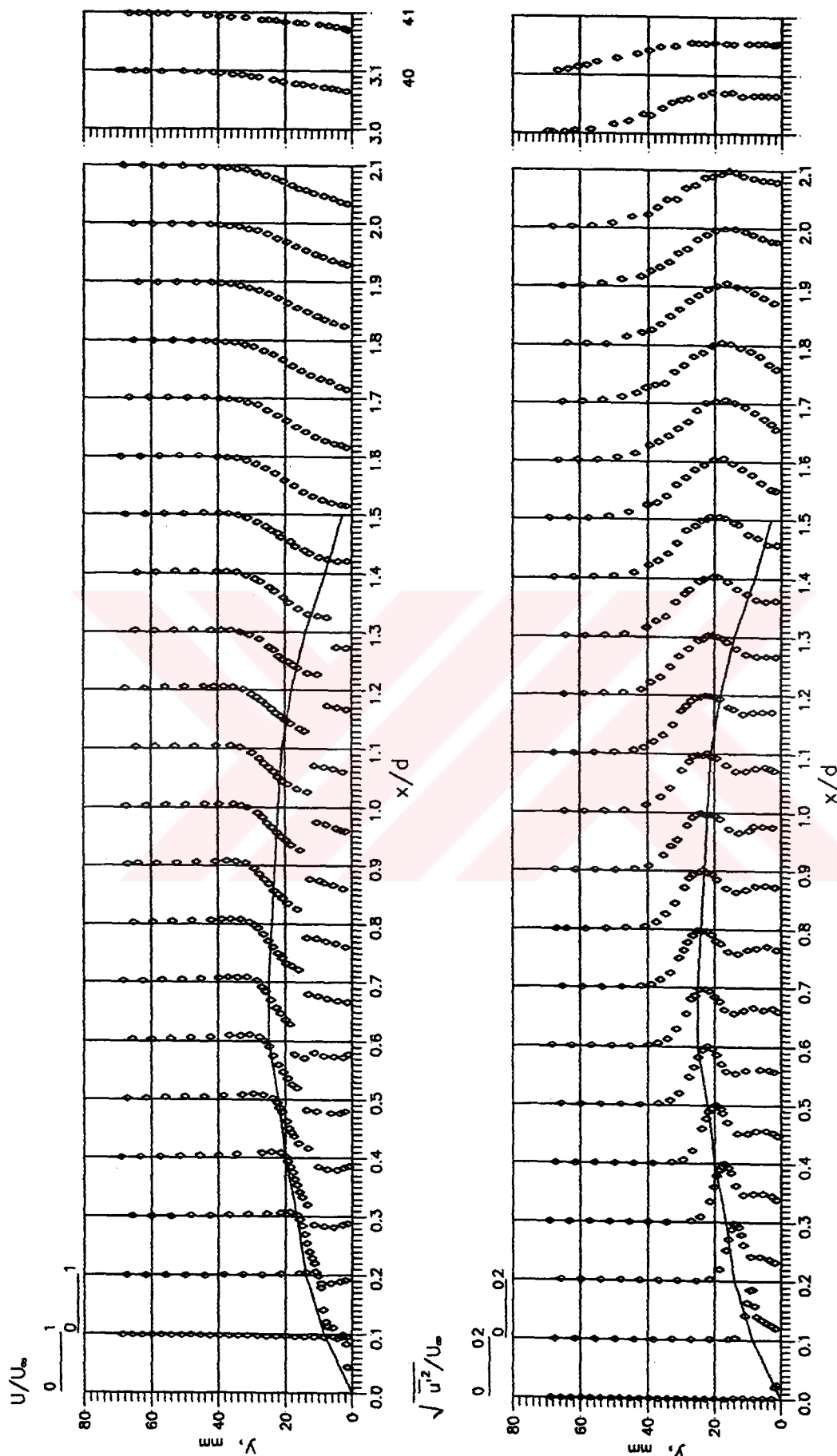
Figure 4.6 Mean velocity and turbulence velocity profiles around the model surface. $Re_d=7.59\times10^4$
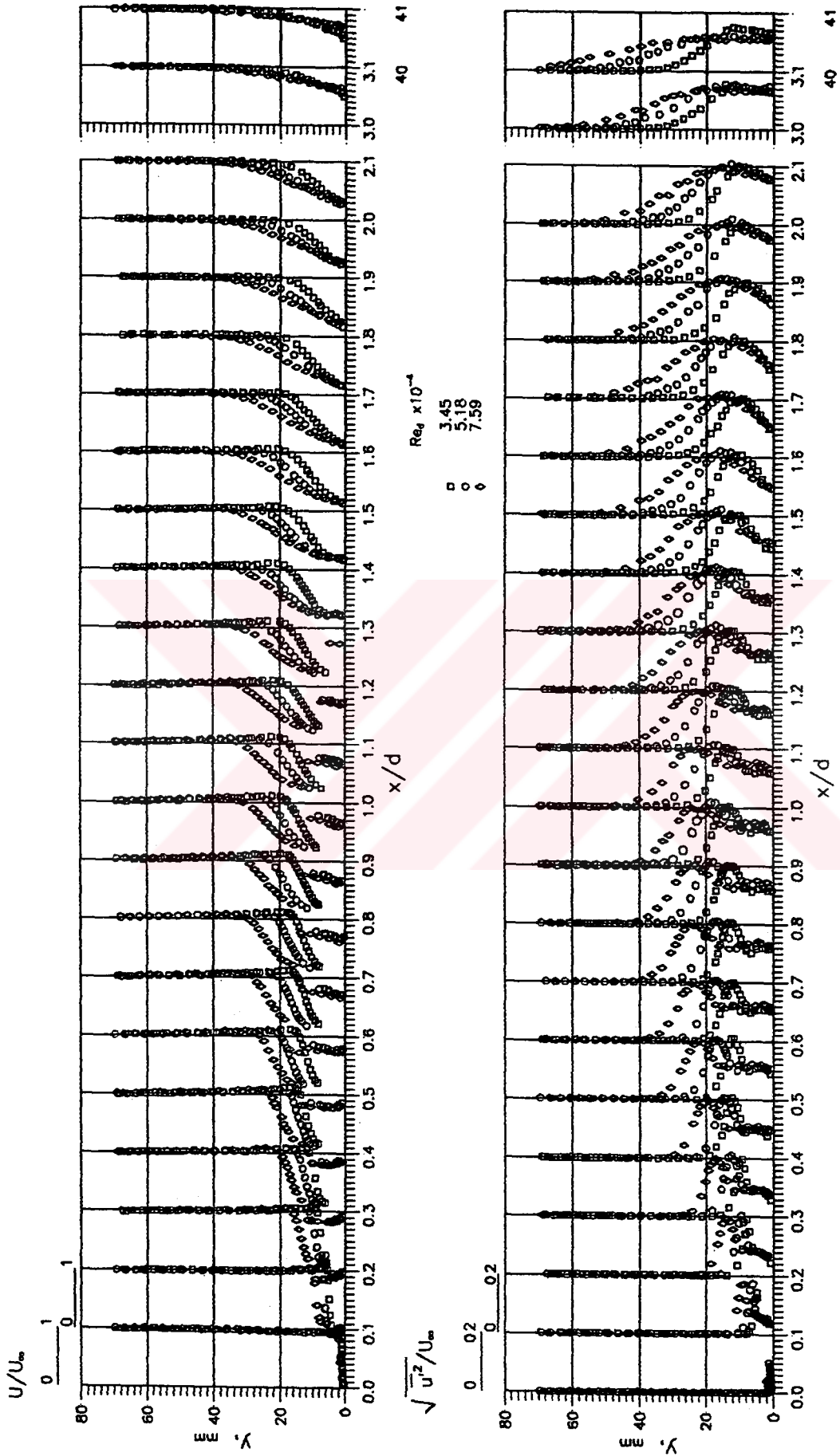
Figure 4.7 Mean velocity and turbulence velocity profiles around the models.
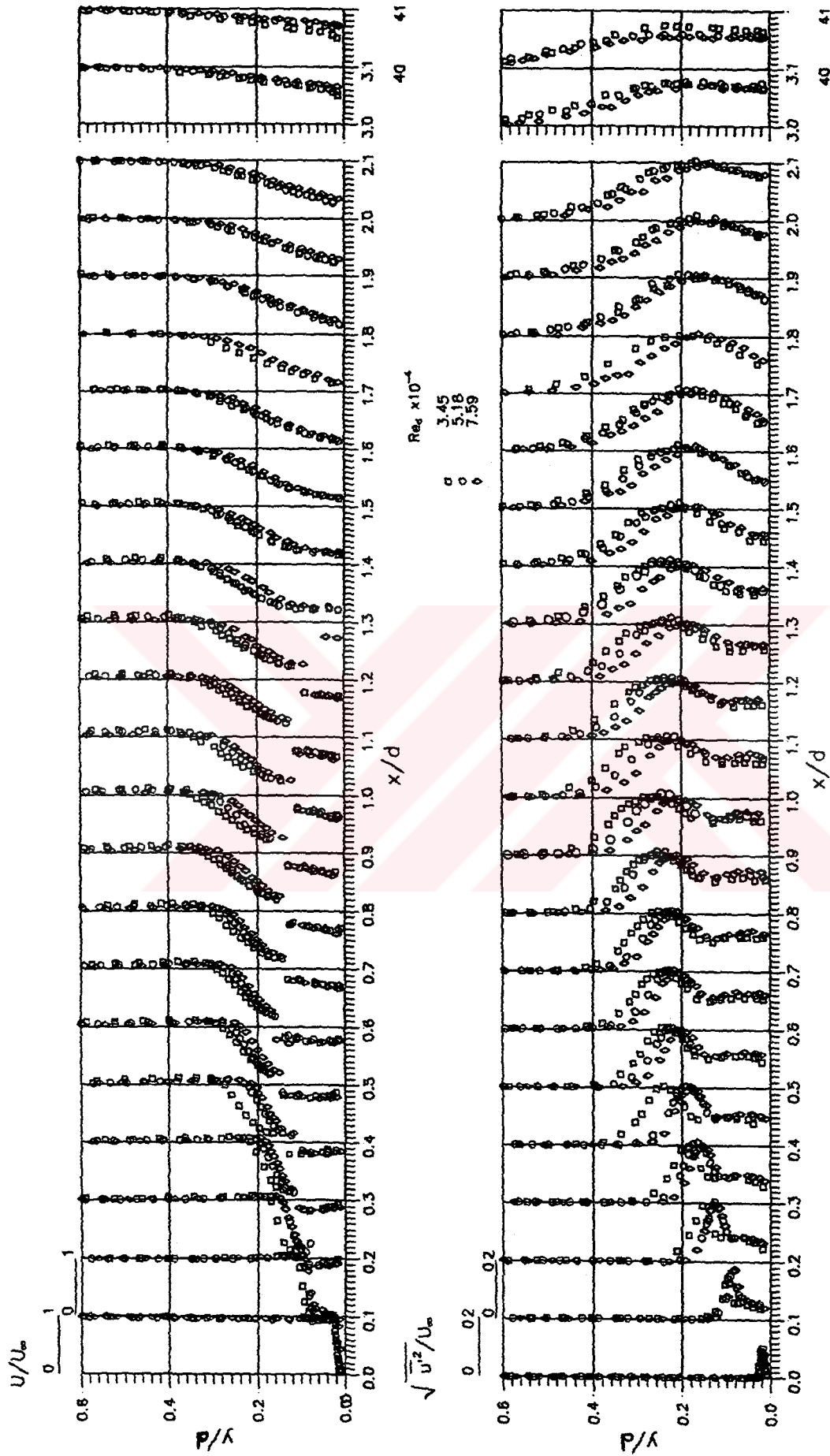
Figure 4.8 Mean velocity and turbulence velocity profiles around the models.
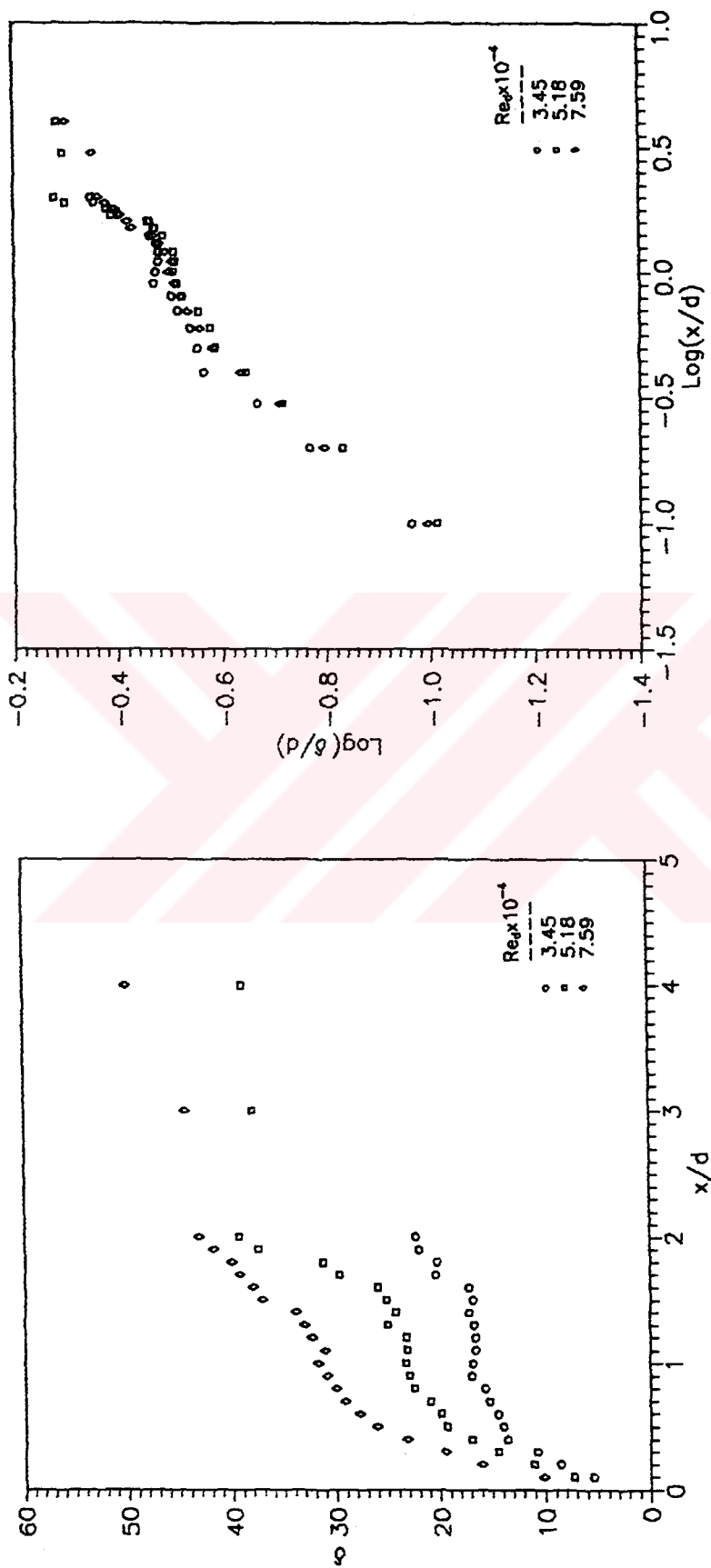
Figure 4.9   Distribution of the boundary layer thickness,δ,
along the surface of Model 1,2,and 3;
a) using δ-x/d,
b) using logarithmic axes.
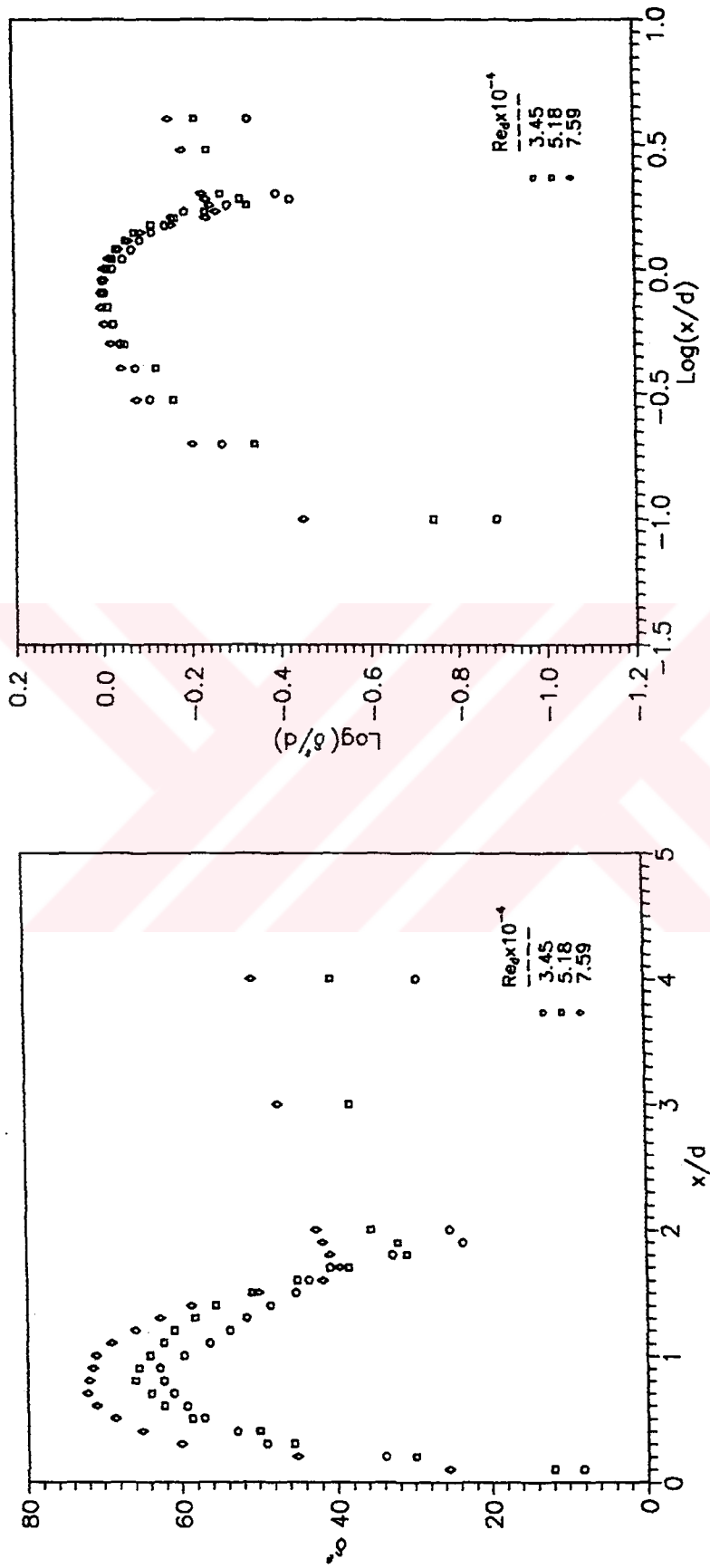
Figure 4.10 Distribution of the boundary layer thickness,δ', along the surface of Model 1,2,and 3;
a) using δ'-x/d,
b) using logarithmic axes.
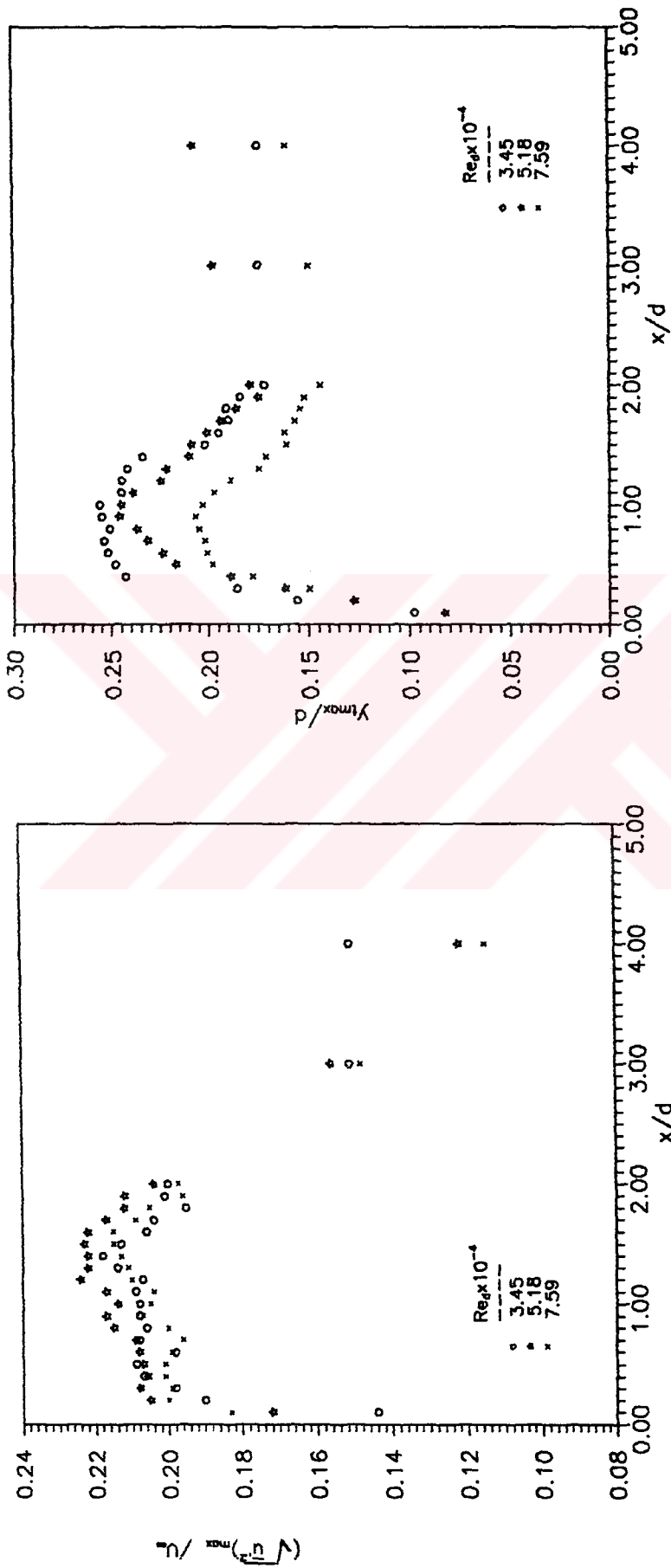
Figure 4.11 a) Maximum turbulence velocity, and
b) Location of maximum turbulence velocity.
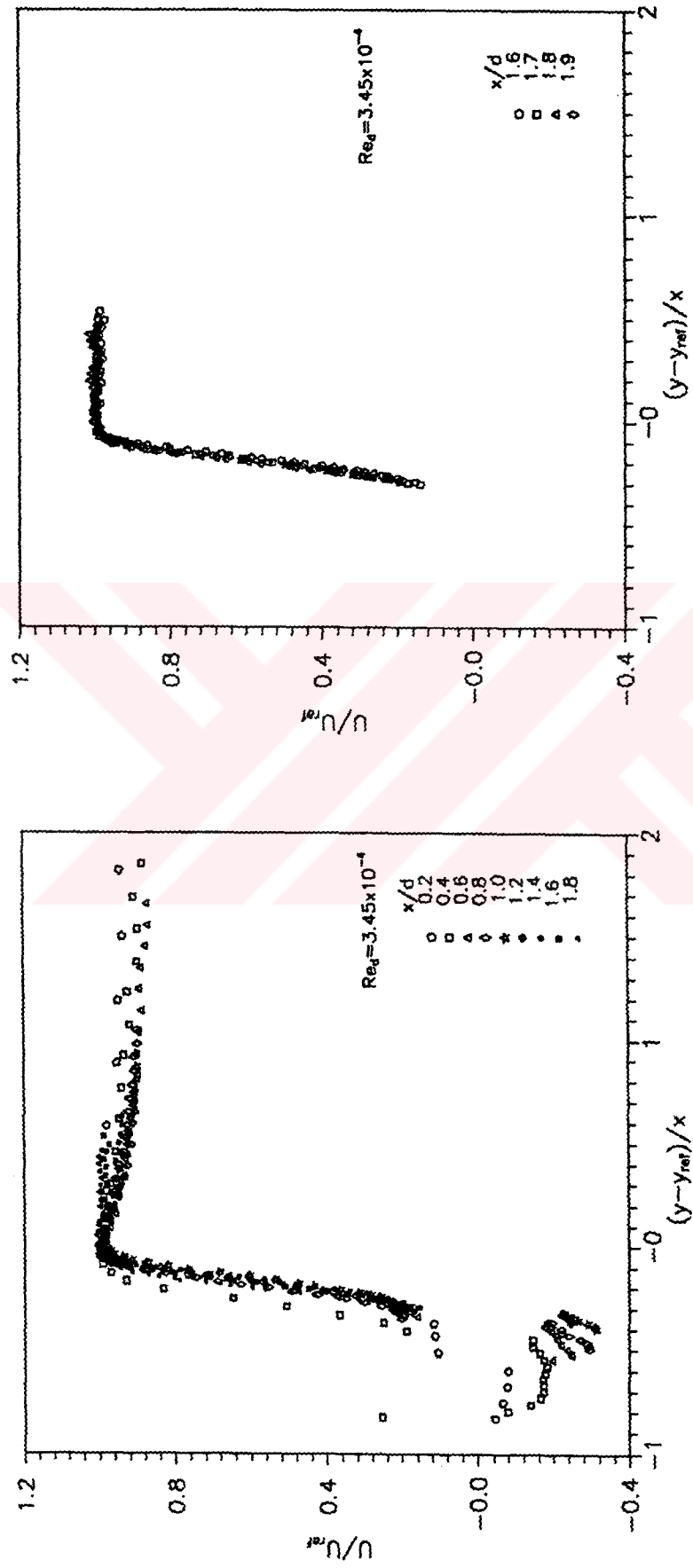
Figure 4.12 Development of the mean velocity profiles around the Model 1, with using dimensionless axes;
a) along the model surface,
b) after reattachment point.
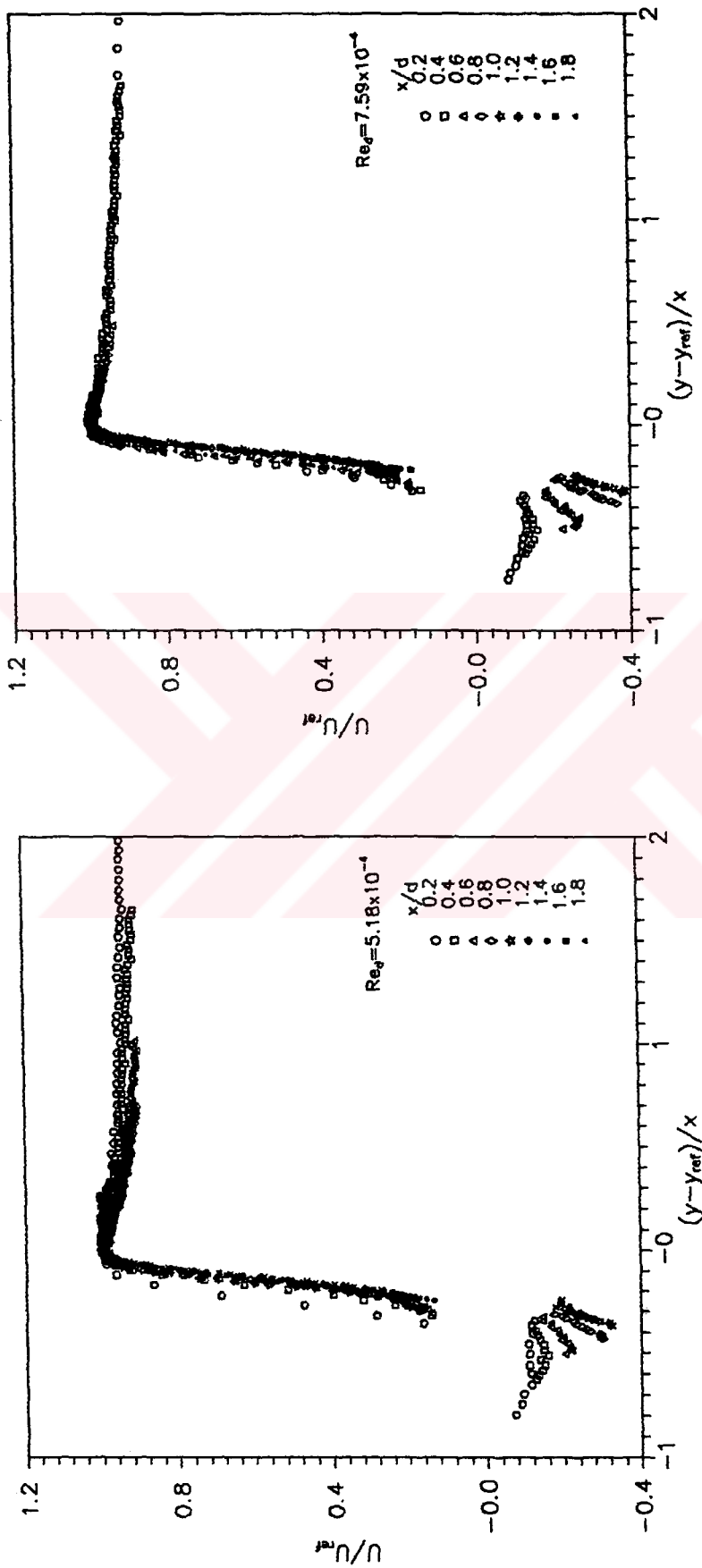
Figure 4.13 Development of the mean velocity profiles,
with using dimensionless axes;
a) for Model2,
b) for Model3.
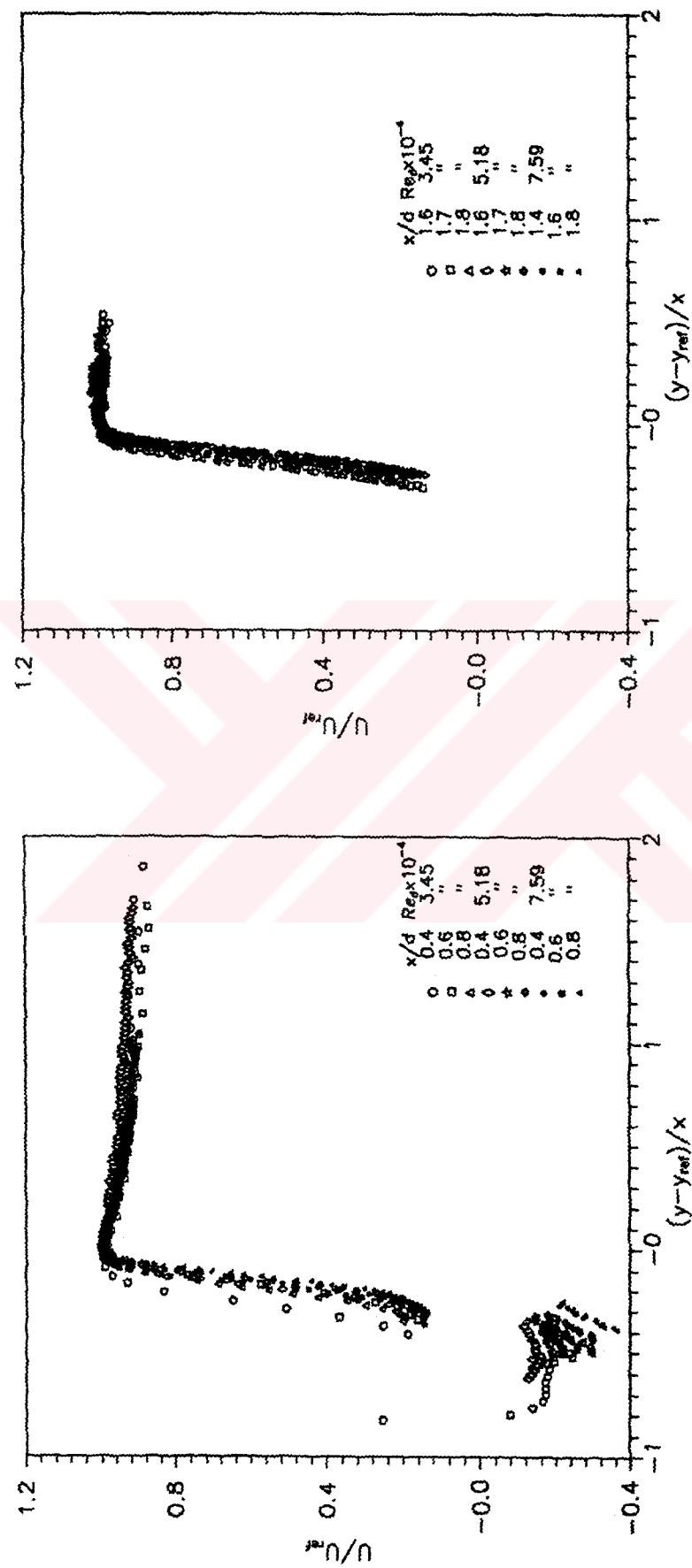
Figure 4.14 Development of the mean velocity profiles for
Model 1,2, and 3, with using dimensionless axes;
a) before reattachment point,
b) after reattachment point.

-64-

4.3 DISCUSSION

The photographs obtained from the flow visualization tests are given in Fig.4.1. The flow structure described by the flow visualization tests is sketched qualitatively in Fig.4.15.
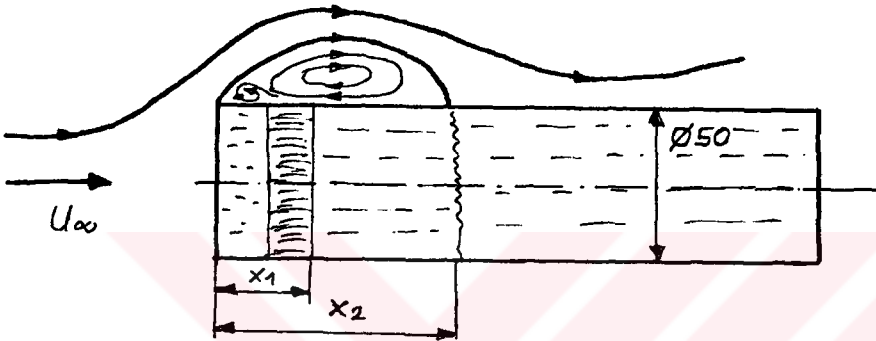
Fig.4.15. a sketch of the flow structure drawn from the flow visualization tests.

Here, X_1 is the distance of the secondary separation point from the beginning of the model nose and X_2 is the distance of the flow reattachment point again from the beginning of the model nose. Table 1 was prepared by measuring X_1 and X_2 values from the photographs.

Table 1 : The lengths of the recirculation regions obtain from flow visualization tests.

MODEL	L(mm)	L/d	X_1/d	X_2/d
1	37.5	3.1	.60	1.79
2	48.3	4.0	.58	1.83
3	61.0	5.0	.58	1.90
4	110.8	9.2	.58	1.91

As it can be seen from the Table 1 that the distance of the reattachment point from the model nose is increasing with increasing fineness ratio values till the value of 5.0. This means that the fineness ratio is an important parameter for flow field around the circular cylinder. If the fineness ratio increases from 5 to upper values, there is no change in the place of the reattachment point. So if the fineness ratios of the circular cylinders are taken as 7.5, the effect of fineness ratio is removed in the experiments in which the effects of the Reynolds number are investigated.

According to graphics taken from pressure measurements which are given in Fig.4.2, the same decisions which are determined in flow visualization tests, can be made for the effect of the fineness ratio. With increasing of the fineness ratio values the flow on the back part of the model surface begins to accelerate and reaches the zero value of the pressure coefficient earlier.

After examining the flow visualization photographs and pressure coefficient distribution, the fineness ratio were taken as 7.5 for the circular cylinders that were used in hot-wire measurements where the effect of the Reynolds number was investigated.

In Fig.4.3 where the velocity and pressure coefficient distribution are given together to make comparison, it can be seen that the reattachment point corresponds to a point before the maximum value of pressure coefficient C_p. This result is similar with the studies which are given in Ref.[15] and [20]. The point where the value of the pressure coefficient is minimum corresponds to a station in velocity profile where the value of the reverse flow velocity is maximum and maximum height of the bubble.

In Figs.4.4, 4.5, and 4.6 where the velocity and turbulence intensity profiles are given for three models with different Reynolds number based on the model diameter, it can be seen that as the circular cylinder has a blunt nose, the flow separation began at the nose, than bubble occured. The height of the bubble grown slowly and after a maximum value it began to decrease and finished at the reattachment point. In the separation bubble reverse flow occured but as the hot-wire anemometer can not show negative velocity values, the velocity data was corrected with a method which was explained in Section 3.4.3. After reattachment point velocity profiles seem to profiles of boundary layers without separation. According to the turbulence intensity profiles, separation bubble can be regarded as a solid surface.

As it can be seen from the Fig.4.7 that the dimensions of the separation bubble grown with Reynolds number increasements.

The boundary layer thickness δ grown along longitudinal direction and Reynolds number (Fig.4.9.a).

The alternative boundary layer thickness δ' showed an intersting development. Till reattachment point the boundary layer thickness δ' increase and then decreases like the bubble height. It reached the maximum value where the bubble

height was in maximum value. After reattachment point boundary layer thickness δ' grown slowly. According to the Fig.4.10.b which was drawn in logarithmic axes the distributions of δ' for each model collapsed approximately in one curve.

The graphic of the variation of the maximum value of the turbulence velocity with x/d (Fig.4.11.a) indicates that the maximum turbulence velocity increases with the Reynolds number increasements.

In order to have a universal curve for velocity profiles, the velocity u and the distance y are made dimensionless by the same reference velocity $(.5U_{max})$ and the same dimensionless lengthscale. By using that dimensionless axes, the velocity profiles collapsed in one curve especially at the locations after reattachment.

CHAPTER 5

CONCLUSIONS

An experimental investigation about the effect of the Reynolds number on the flow field around circular cylinder with blunt nose was made at 10 m/s air speed and at Reynolds numbers $3.35x10^4$, $5.18x10^4$, and $7.59x10^4$. In the experiments three different experimental methods were used: flow visualization and pressure measurements techniques for investigating the effect of the fineness ratio on the flow field around circular cylinder. Hot-wire anemometer was used for finding the velocity and turbulence intensity profiles.

According to flow visualization photographs, in order to eliminate the effect of the fineness ratio to the flow field, the fineness ratio must be greater than 5 or 6. The pressure coefficient distribution confirm this result. So in the experiments for investigating the effects of the Reynolds number, the model fineness ratios were taken as 7.5.

By using the photographs of oil-film technique, the distance of the reattachment point from the nose was fonded as 1.8d. By using the velocity profiles, it was founded as 1.6d. The results were close but not same. It is well known that in three-dimensional separation a reattachment region, instead of reattachment point, exists. According to the pressure coefficient distribution this results are available.

The pressure coefficient has a maximum value shortly after reattachment region, and has a minimum value at the separation bubble's maximum height. In this station maximum reverse flow close to the surface occurs.

Boundary layer thickness distribution along the surface shown the bubble's geometry. In reattachment region it falls down to its minimum value which corresponds to distance 1.7d from the model nose. The location of the maximum turbulence velocities at each station shown the same behaviour in the mixing region.

Velocity profiles drawn in dimensionless axes collapse in one curve shows that especially after reattachment region the velocity profiles became similar by using dimensionless axes.

The separation bubble dimensions grown with increasing model diameter (Reynolds number). But when y distance is divided with diameter of the cylinder to have dimensionless axis, the geometry of the bubble became smaller with increasing Reynolds number.

References

[1] Chang, P.K., "Separation of Flow", 1st Addition, Pergomon Press,1970

[2] Karamcheti, K., "Principles of Ideal Fluid Aerodynamics", John Wiley and Sons. Inc., 1966.

[3] von den Berg, B., "Topological Feature of Separated Flows", AGARD-AR-No.255, pp.4-7, May 1990.

[4] Bearman, P.W., and Morel, T., "Effect of Free Stream Turbulence on the Flow Around Bluff Bodies", Prog. Aerospace Sci., Vol.20, pp.97-123, 1983.

[5] Chang, P.K., "Control of Flow Separation", Hemisphere Publishing Corparation, 1976.

[6] Legendre, R., "R.Lignes de Courant d'un Écoulement Permanent, Décollement et Separation", La Recherche Aéero-spatiale, pp.327-335, 1977.

[7] White, F.M., "Viscous Fluid Flow", McGraw-Hill Book Co., 1974.

[8] Yates, L.A., and Chapman, G.T., "Numerical Investigation of Cross-flow Separation on a Three-Caliber Tangent Ogive Cylinder", AIAA Journal, Vol.26, No.10, pp.1223-1230, October 1989.

[9] Schmidt, G.S., and Mueller, T.J., "Analysis of Low Reynolds Number Separation Bubbles Using Semiempirical Methods", AIAA Journal, Vol.27, No.8, pp.993-1001, August 1989.

[10] Schlichting, H., "Boundary Layer Theory", McGraw Hill Series, 1960.

[11] White, F.M., "Fluid Mechanics", McGraw Hill Book Co., 1986.

[12] Jones, B.M., "Flight Experiments on the Boundary Layer", AIAA Journal, February 1981.

[13] Kiya, M., and Sasaki, K., "Structure of a Turbulent Separation Bubble", Journal of Fluid Mechanics, Vol.137, pp.83-113, 1983.

[14] Chandrsuda, C, and Bradshow, P., "Turbulence Structure of a Reattaching Mixing Layer", Journal of Fuid Mechanics, Vol.110, pp.171-194, 1981.

[15] Gai,S.L., and Sharma, S.D., "Pressure Distribution Behind a Rearward Facing Segmented Step", Experiments in Fluids, Vol.5, pp.154-158, 1987.

[16] de Jornette, F.R, and Woodson, S.H., "Numerical and Experimental Determination of Secondary Separation on Delta Wings in Subsonic Flow", Journal of Aircraft, Vol.22, No.7, pp.602, July 1987.

[17] Dianat, M., and Castro, I.P., " Fluctuating Surface Shear Stresses on Bluff Bodies", Journal of Wind Engineering and Industrial Aerodynamics, Vol.17, pp.133-146, 1984.

[18] Adatia, A., "The Effect of Turbulence and Shear on the Flow Around Three-Dimensional Square Cylinders", Ph.D Thesis, Aeronautical Engineering Department Quenn Mary Collage University of London, 1980.

[19] Cherry, J., Hillier, R., and Latour, M.E.M.P., "Unsteady Measurements in a Separated and Reattaching Flow", Journal of Fluid Mechanics, Vol.144, pp.13-46, 1984.

[20] Ruderich, R., and Fernholz, H.H., "An Experimental Investigation of a Turbulent Shear Flow with Separation, Reverse Flow and Reattachment", Journal of Fluid Mechanics, Vol.163, pp.283-322, 1986.

[21] Kegelman, J.T, and Mueller, T.J., "Experimental Studies of Spontaneous and Forced Transition on Axisymmetric Body", AIAA Journal, Vol.24, No.3, pp.397-403, March 1986.

[22] Merzkirch, W., "Flow Visualization", 2nd Addition, Academic Press, 1987.

[23] Merzkirch, W., "Flow Visualization", Academic Press, 1974.

[24] Sedney, R., and Kitchens, C.W.Jr., "Separation Ahead of Protuberances in Supersonic Turbulent Boundary Layers", AIAA Journal, Vol.15, pp.546-552, April 1977.

[25] Atlı, V., "Havacılıkta Kullanılan Bazı Eksenel Simetrik Cisimlerin Aerodinamik Karakteristiklerinin Teorik ve Deneysel Olarak İncelenmesi", Doktora Tezi, İTÜ, Aralık 1983.

[26] Atlı, V., "Subsonic Flow Over a Two-Dimensional Obstacle Immersed in a Turbulent Boundary Layer on a Flat Surface", Journal of Wind Engineering and Industrial Aerodynamics, Vol.31, pp.225-239, 1988.
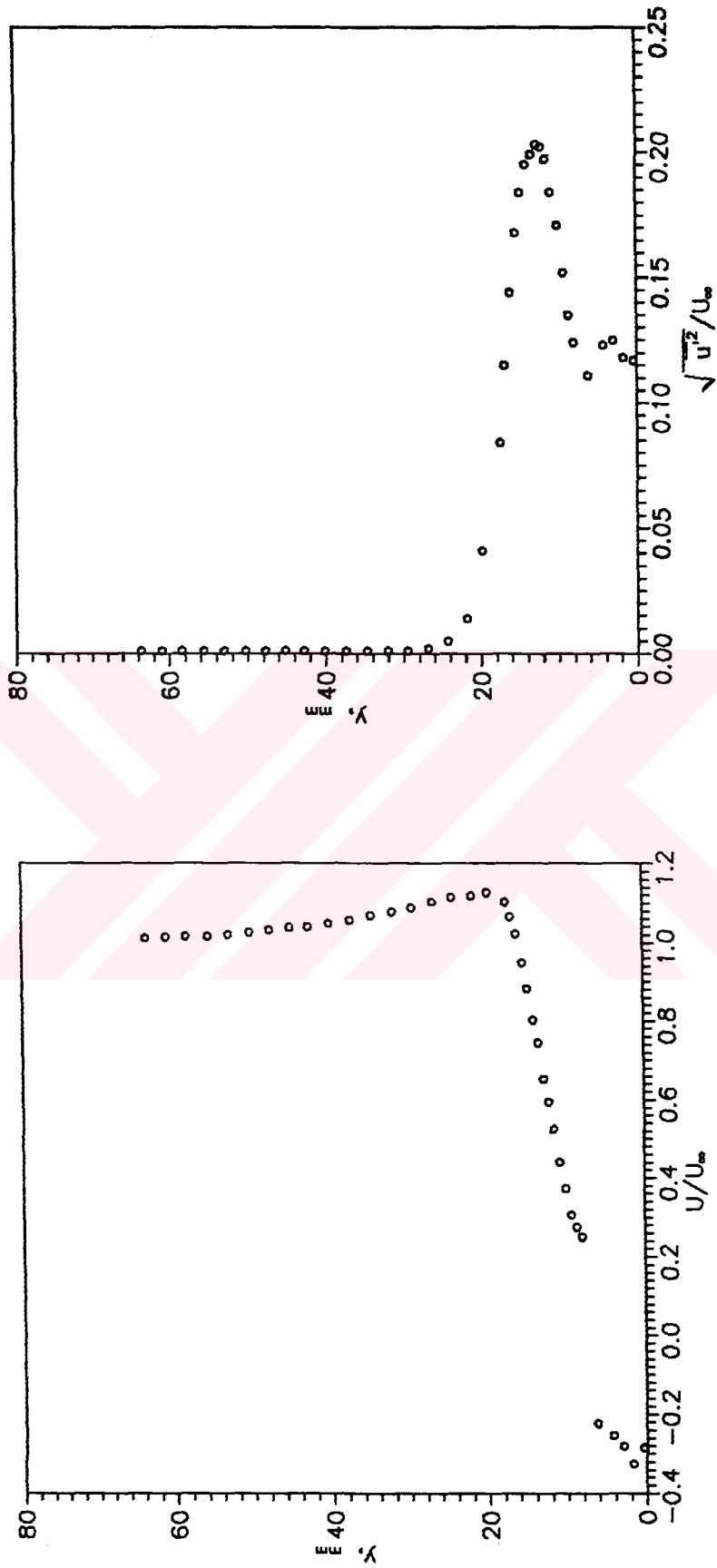
APPENDIX - A

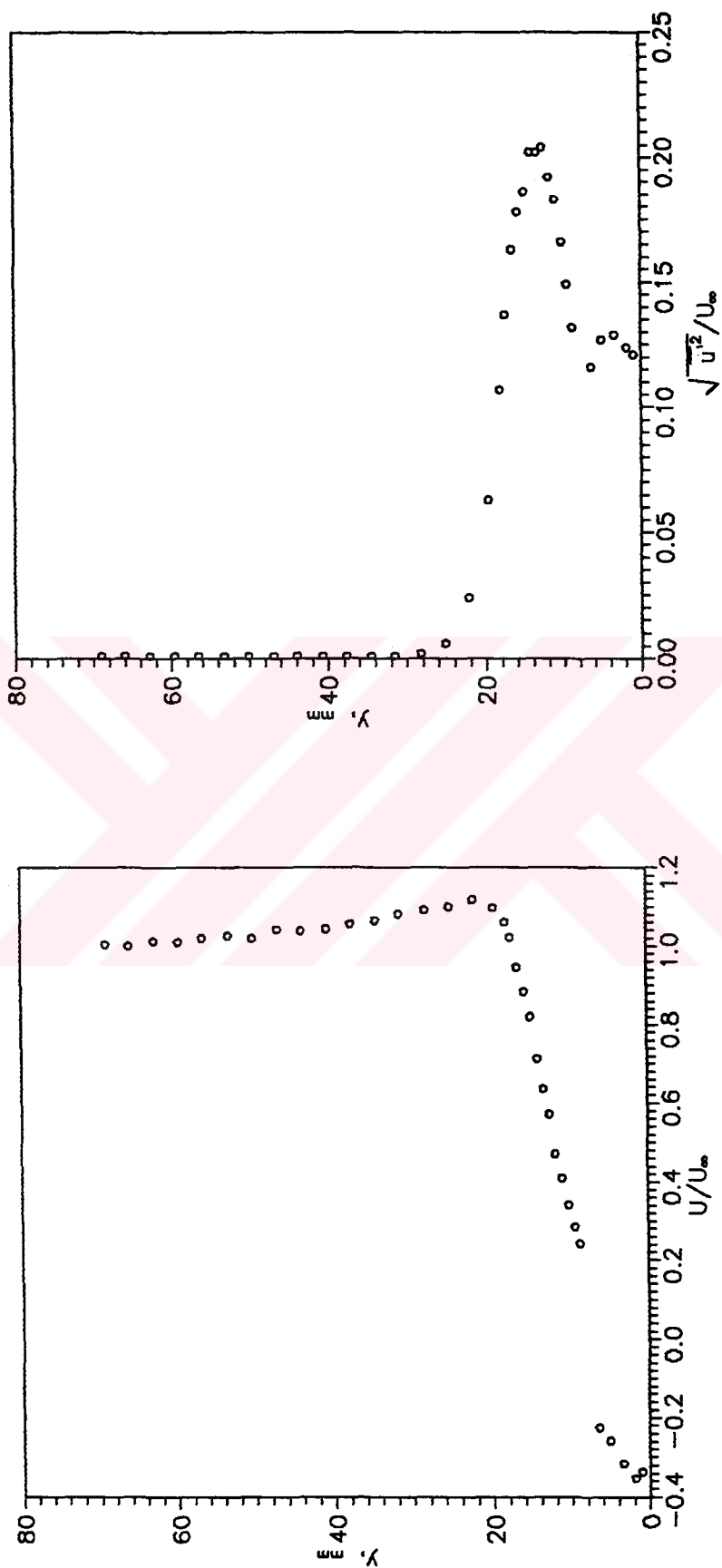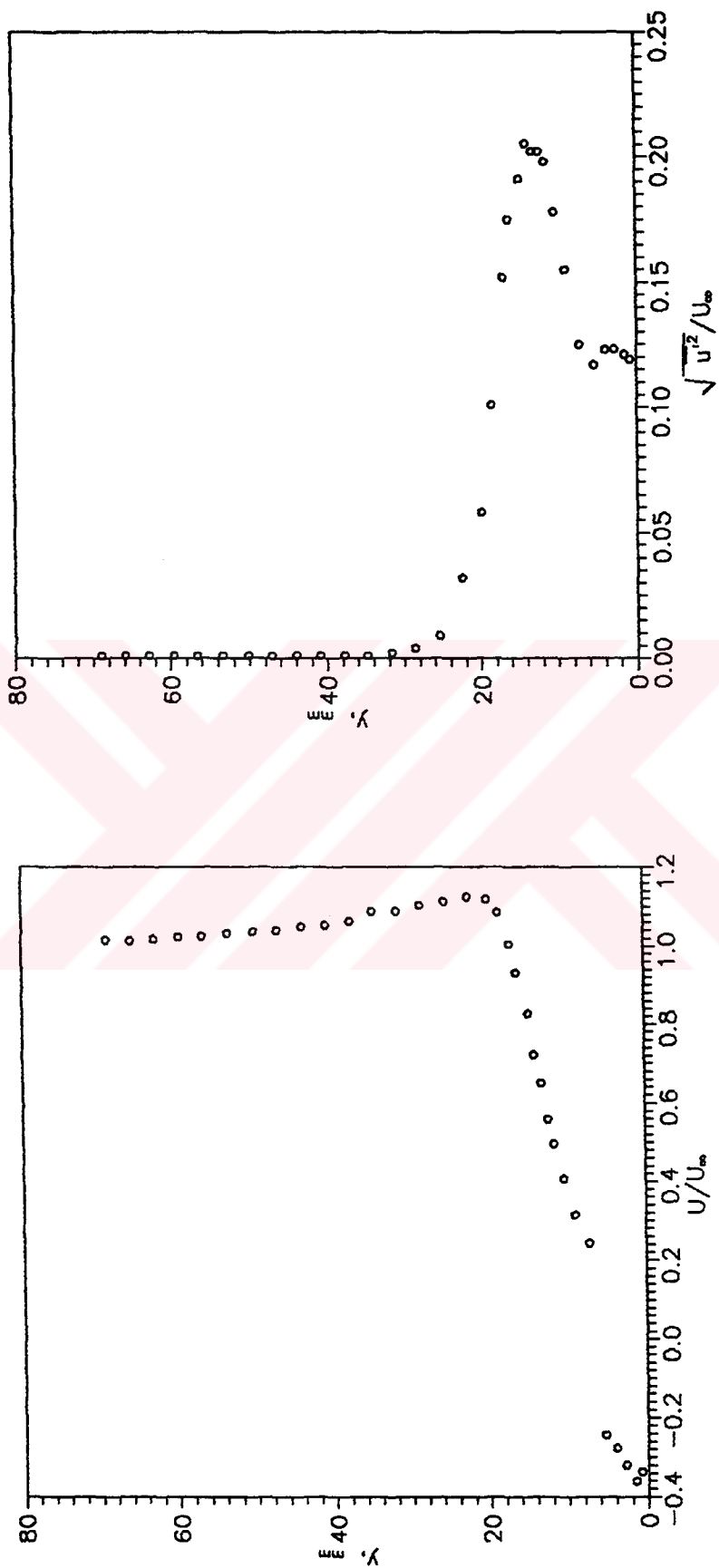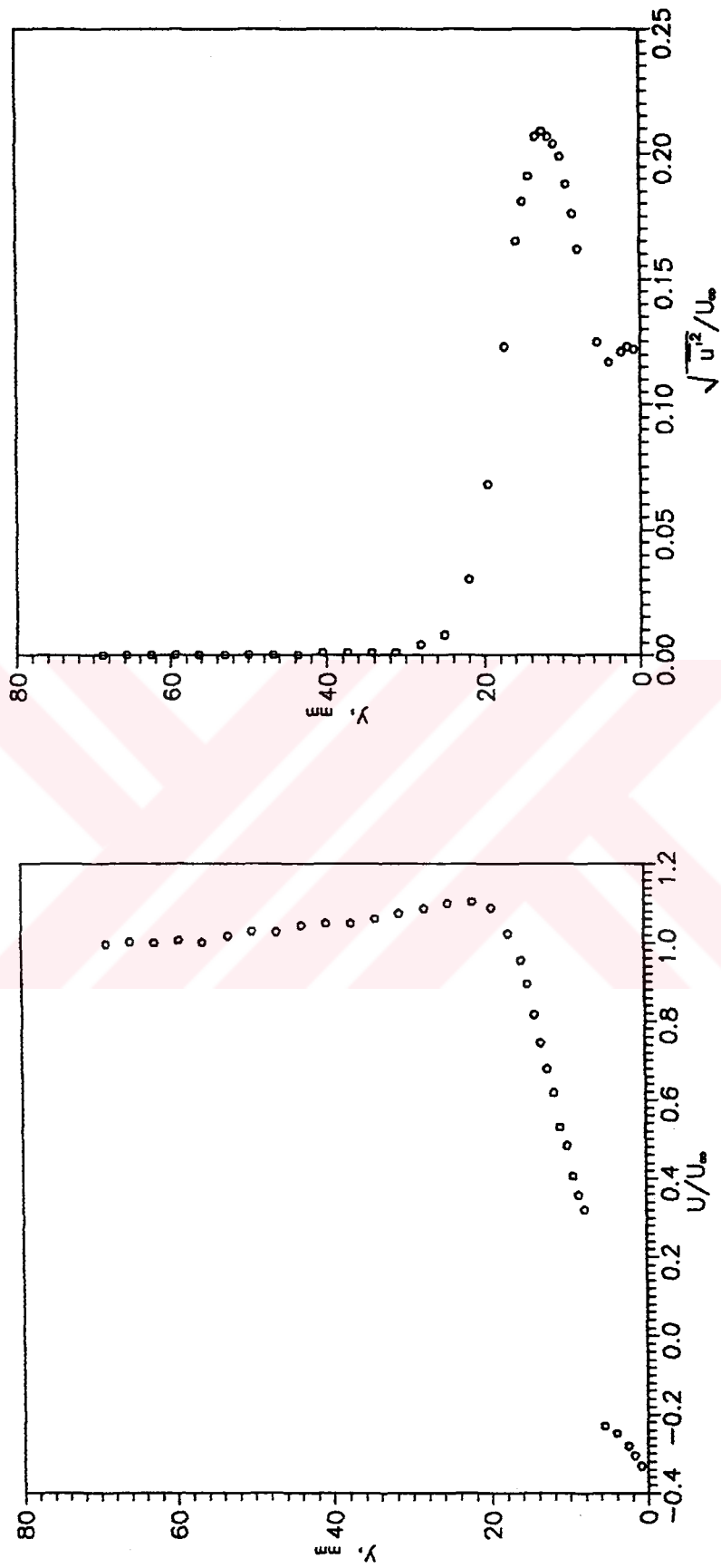## SAMPLES FOR HOT-WIRE MEASUREMENTS
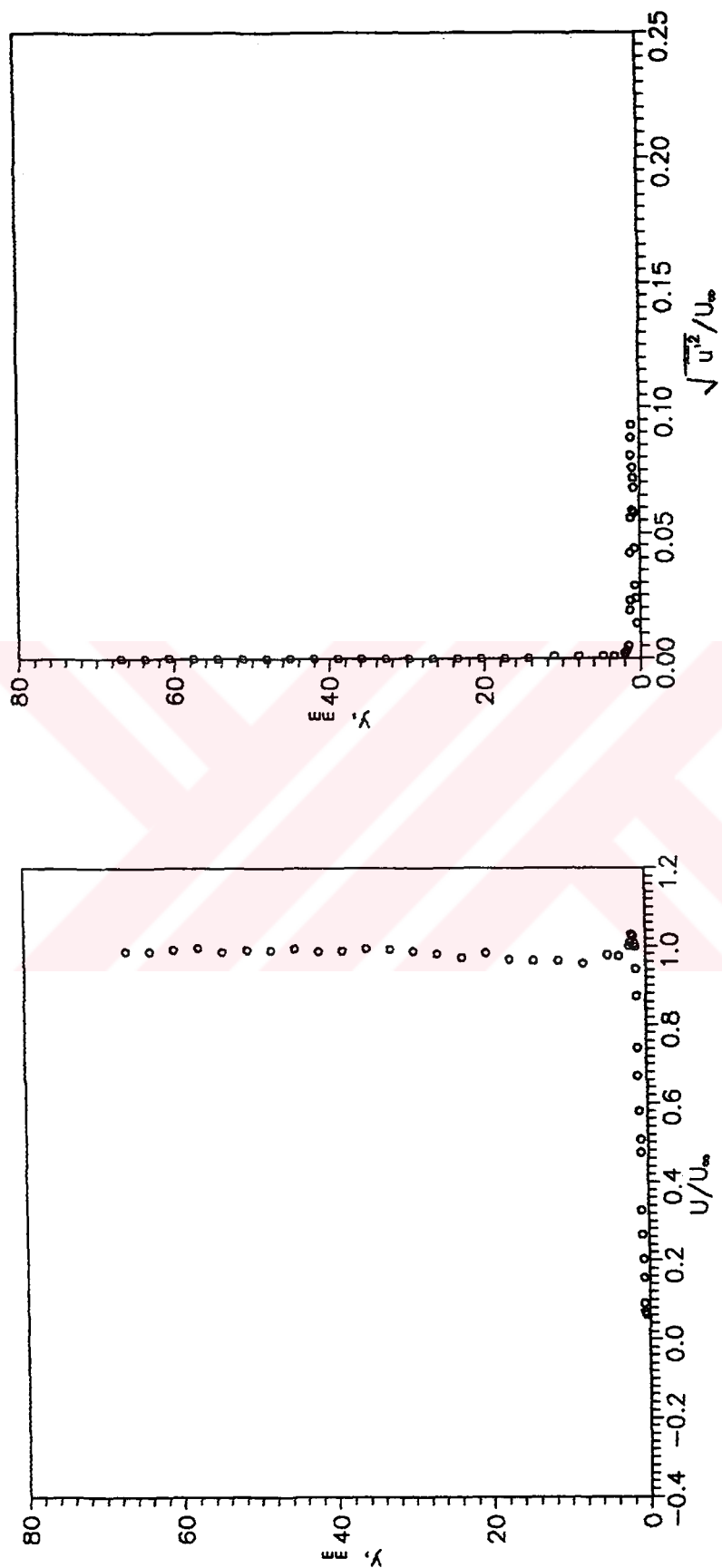
Figure A.1 a) Mean velocity profiles, b) Turbulence velocity profiles, at the station (x/d=0.0) on the model surface. $Re_d = 3.54 \times 10^4$.
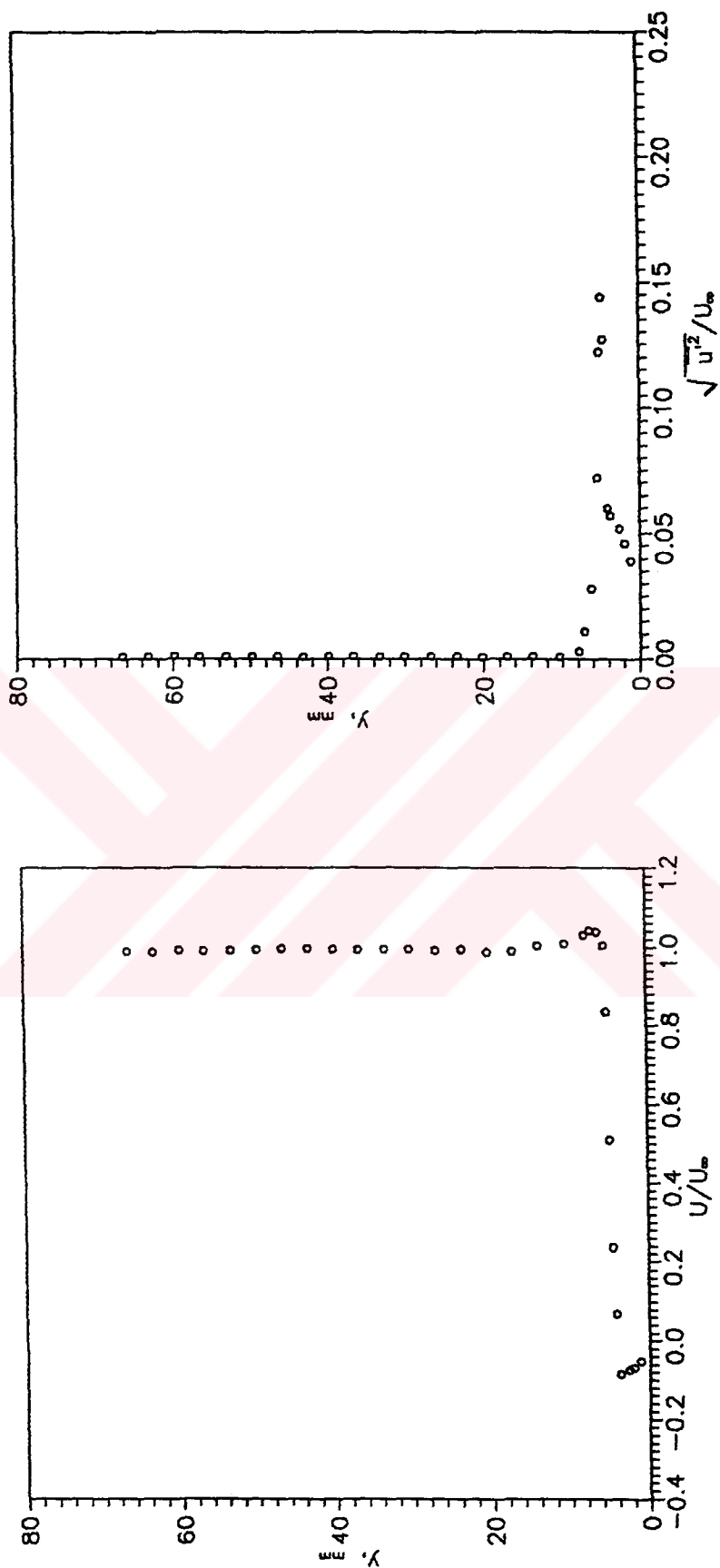
Figere A.2 a) Mean velocity profiles, b) Turbulence velocity profiles, at the station (x/d=0.1) on the model surface. Re_d=3.54x10⁴.
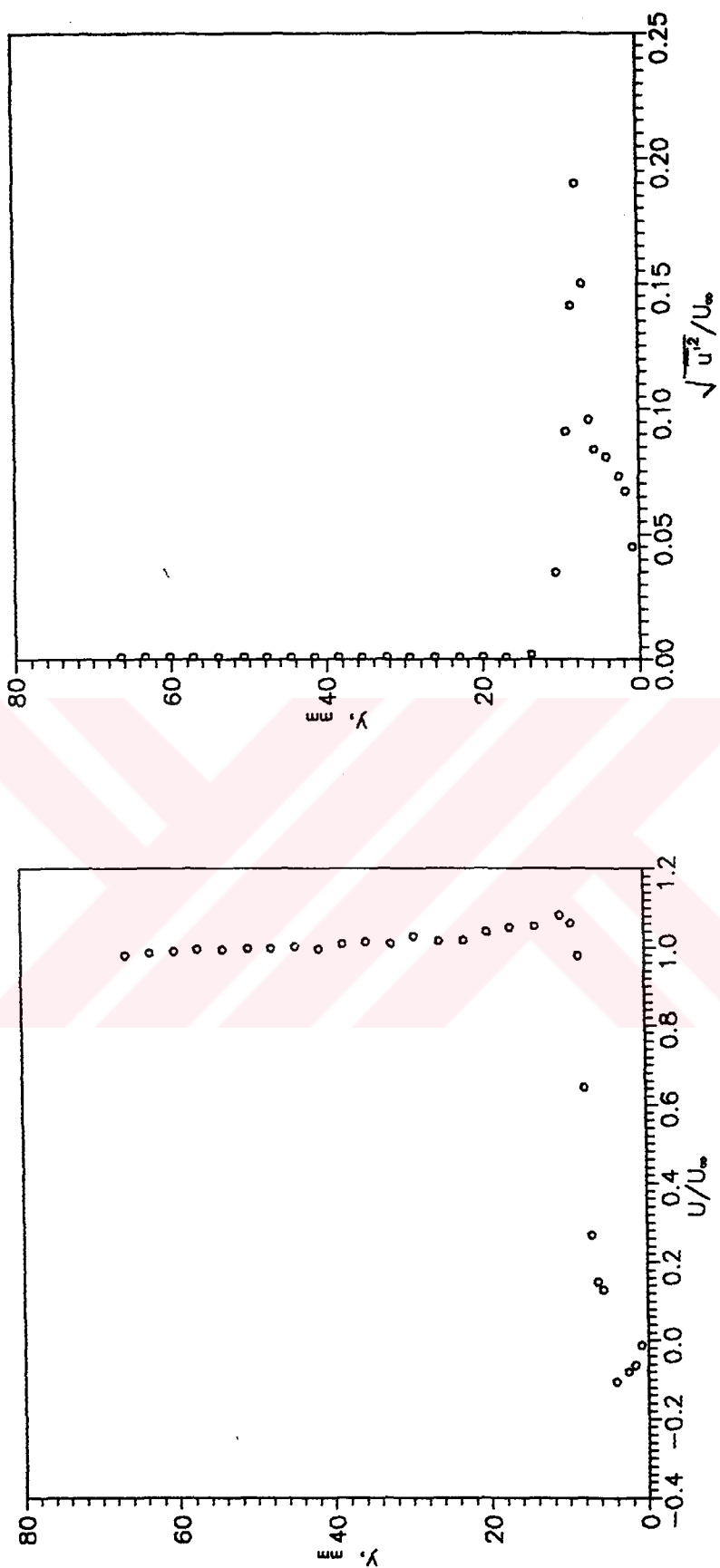
Figere A.3   a) Mean velocity profiles, b) Turbulence velocity profiles,
at the station (x/d=0.2) on the model surface.
Re_d=3.54x10
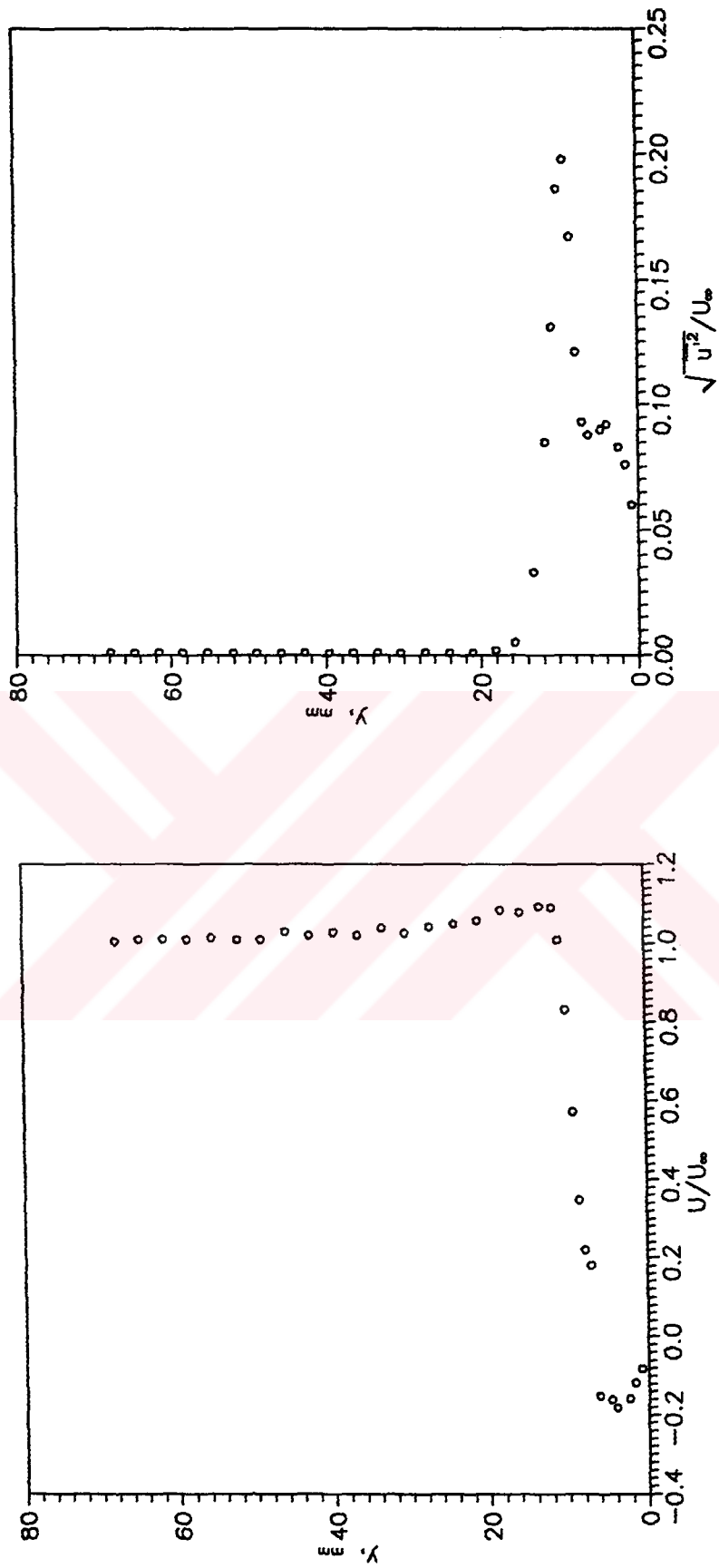
Figere A.4   a) Mean velocity profiles, b) Turbulence velocity profiles, at the station (x/d=0.3) on the model surface. $Re_d = 3.54 \times 10^4$.
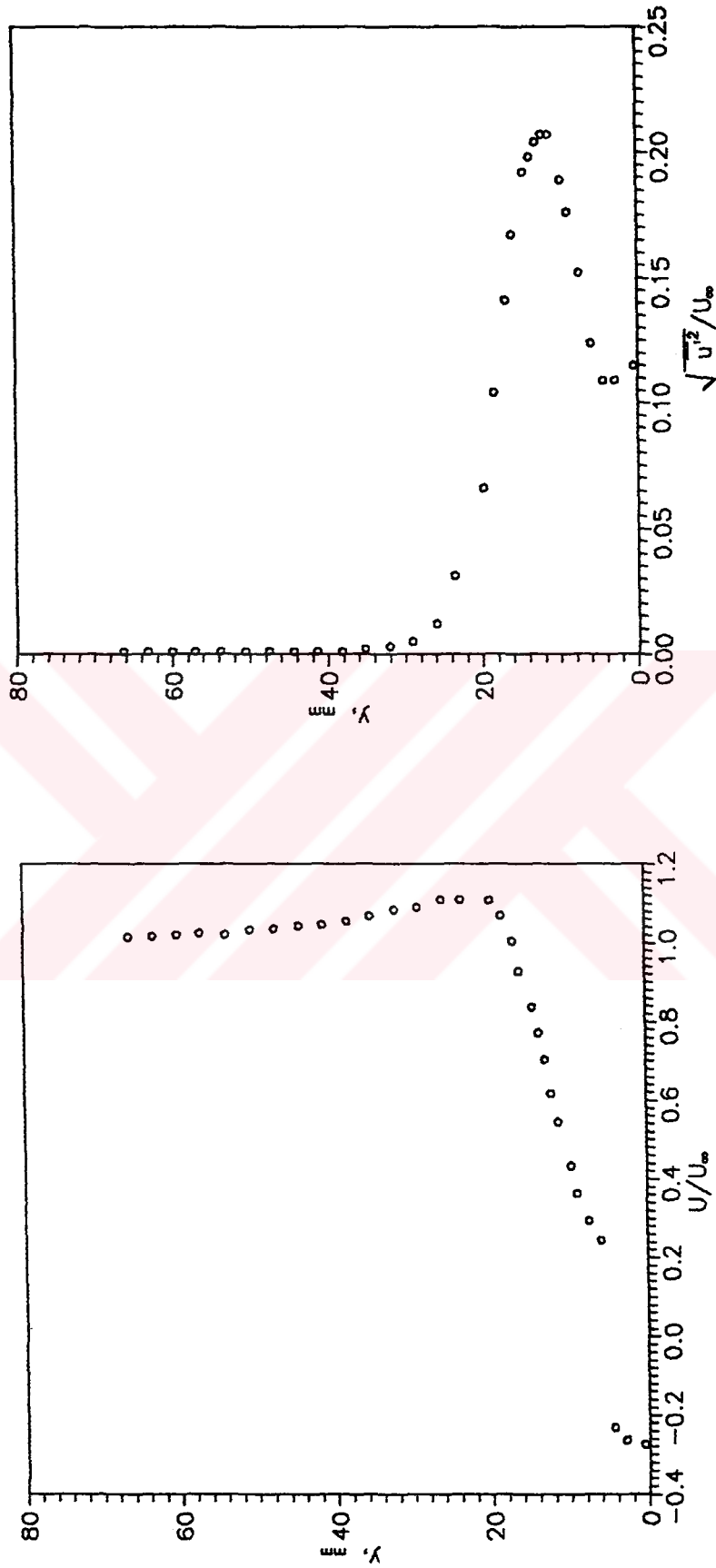
-78-
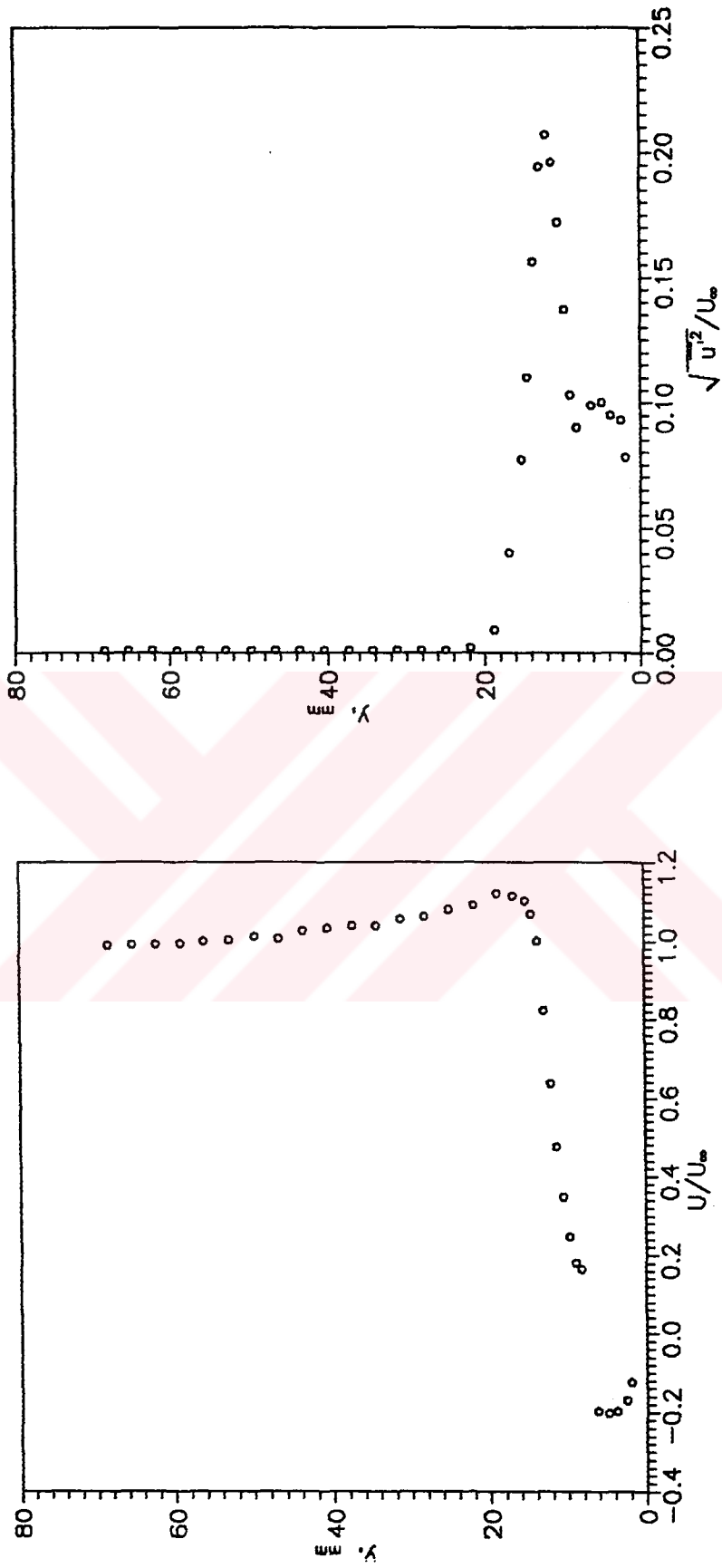
Figere A.5 a) Mean velocity profiles, b) Turbulence velocity profiles, at the station (x/d=0.4) on the model surface. $Re_d=3.54\times10^4$.
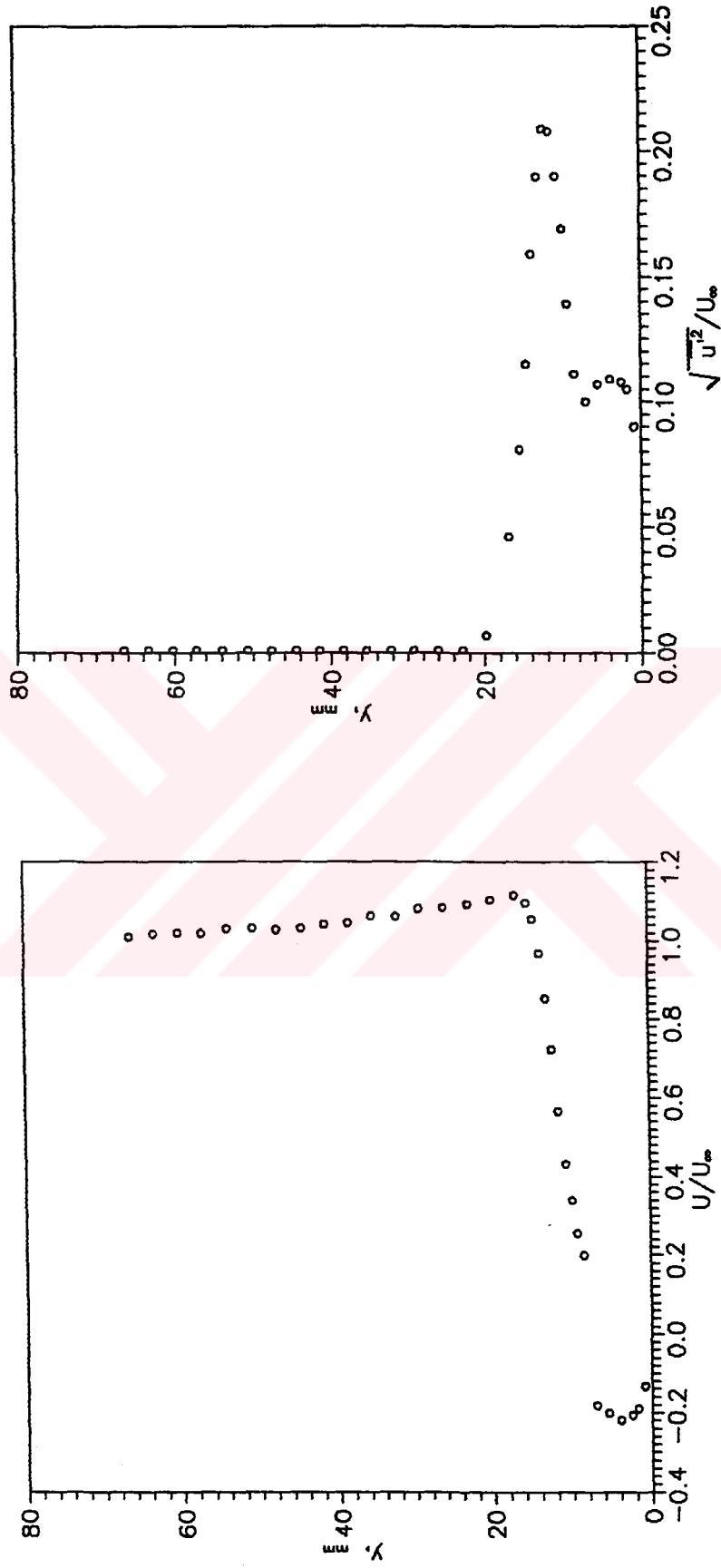
Figure A.6   a) Mean velocity profiles, b) Turbulence velocity profiles, at the station (x/d=0.5) on the model surface. $Re_d=3.54\times10^4$.
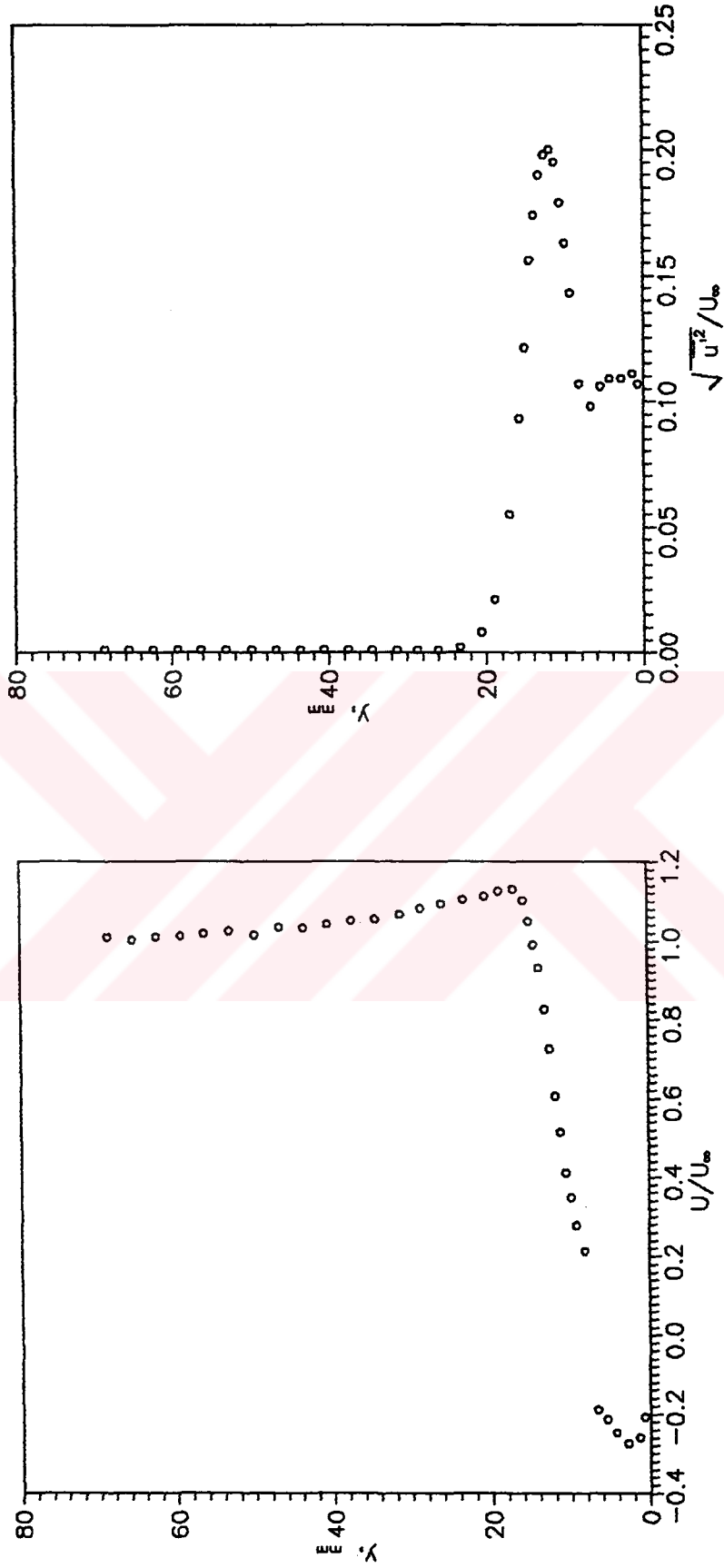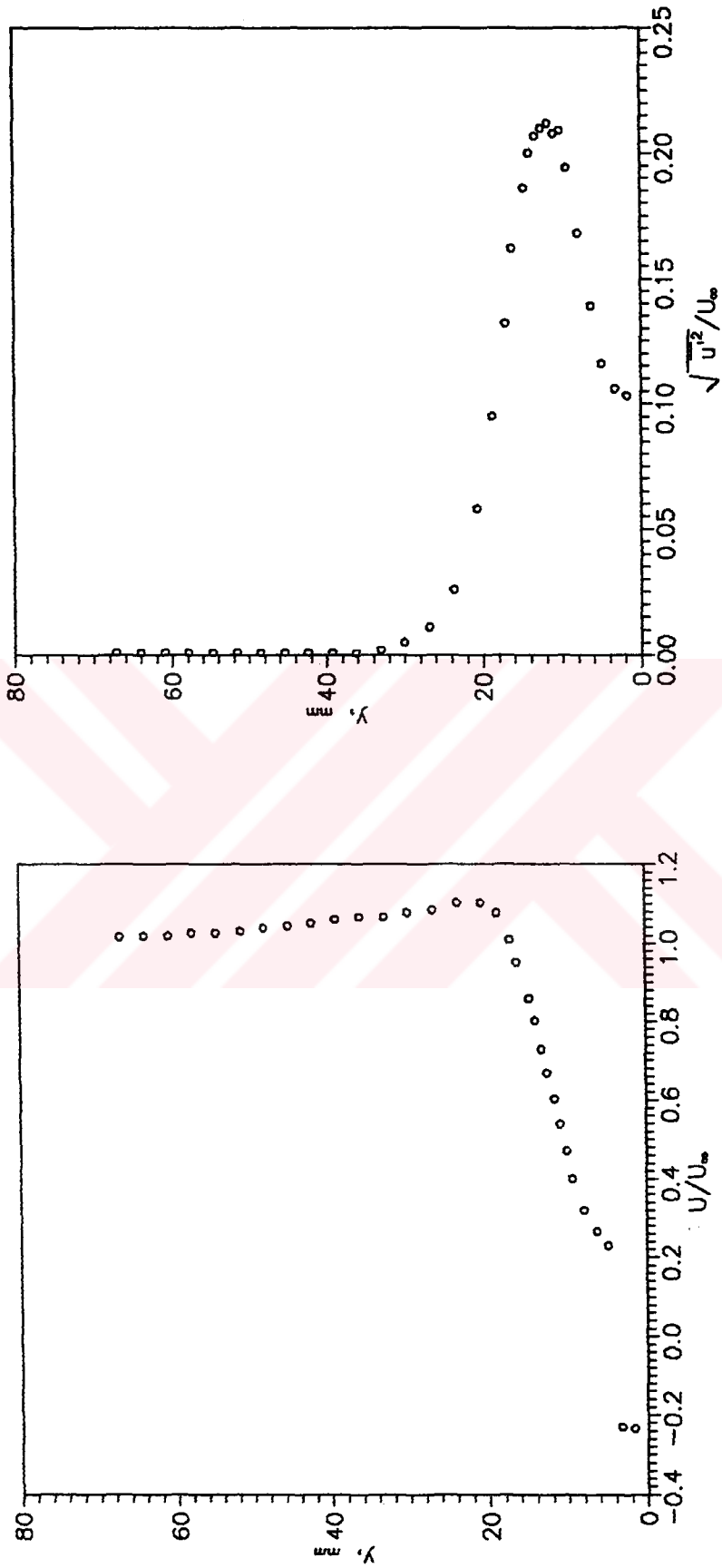
Figere A.7 a) Mean velocity profiles, b) Turbulence velocity profiles,
at the station (x/d=0.6) on the model surface.
$Re_d=3.54\times10^5$.
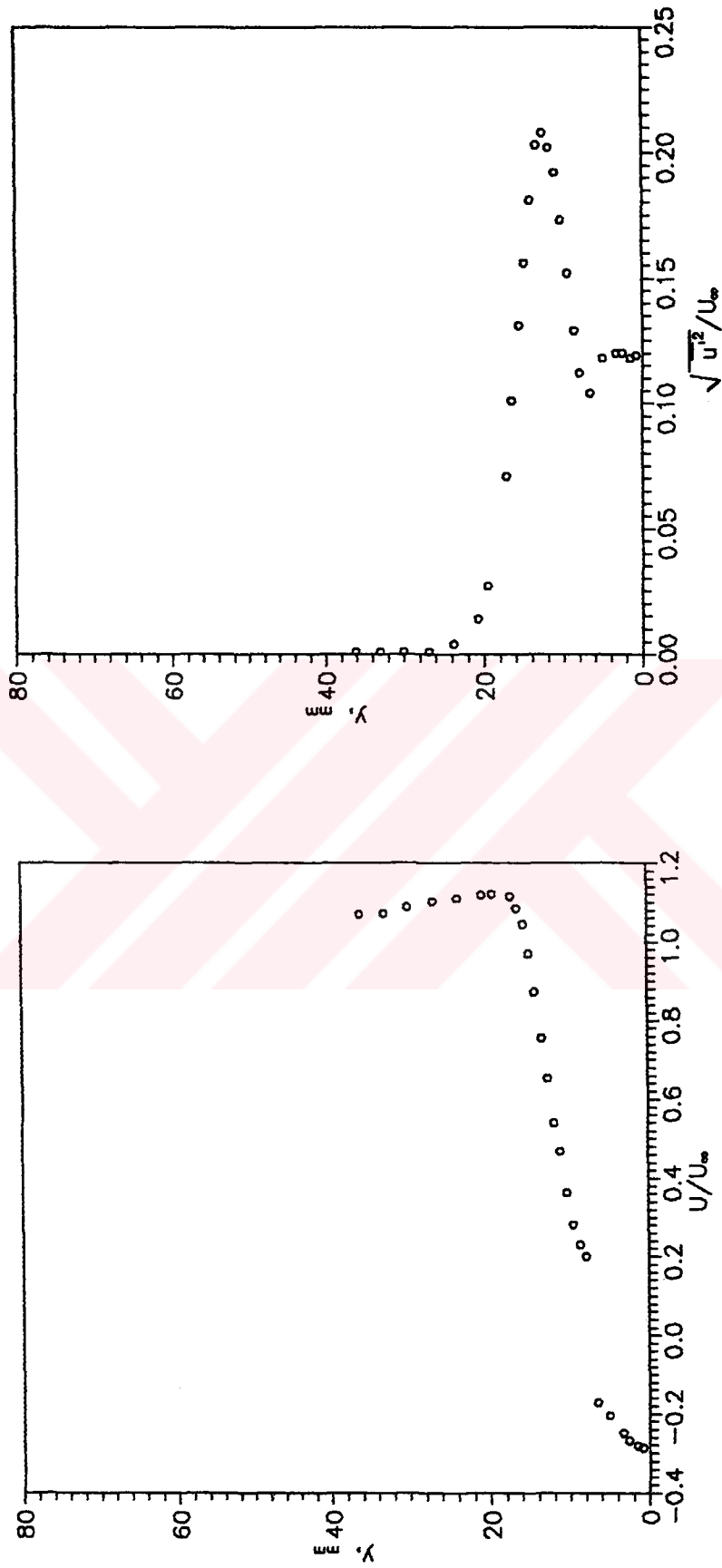
Figere A.8 a) Mean velocity profiles, b) Turbulence velocity profiles, at the station (x/d=0.7) on the model surface. $Re_d=3.54\times10^4$.

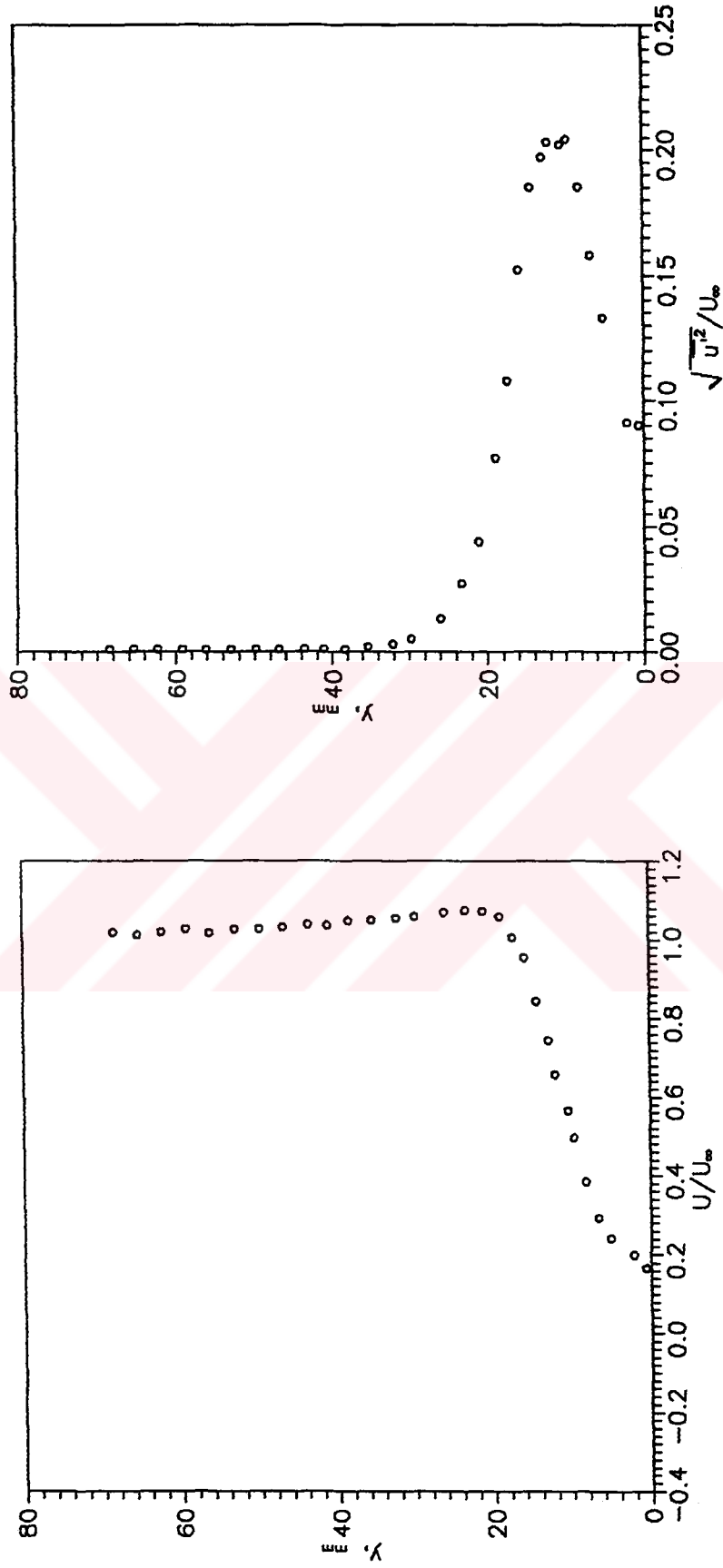Figere A.9   a) Mean velocity profiles, b) Turbulence velocity profiles,
at the station (x/d=0.8) on the model surface.
$Re_d=3.54\times10^4$.

Figure A.10 a) Mean velocity profiles, b) Turbulence velocity profiles, at the station (x/d=0.9) on the model surface, $Re_d=3.54\times10^5$
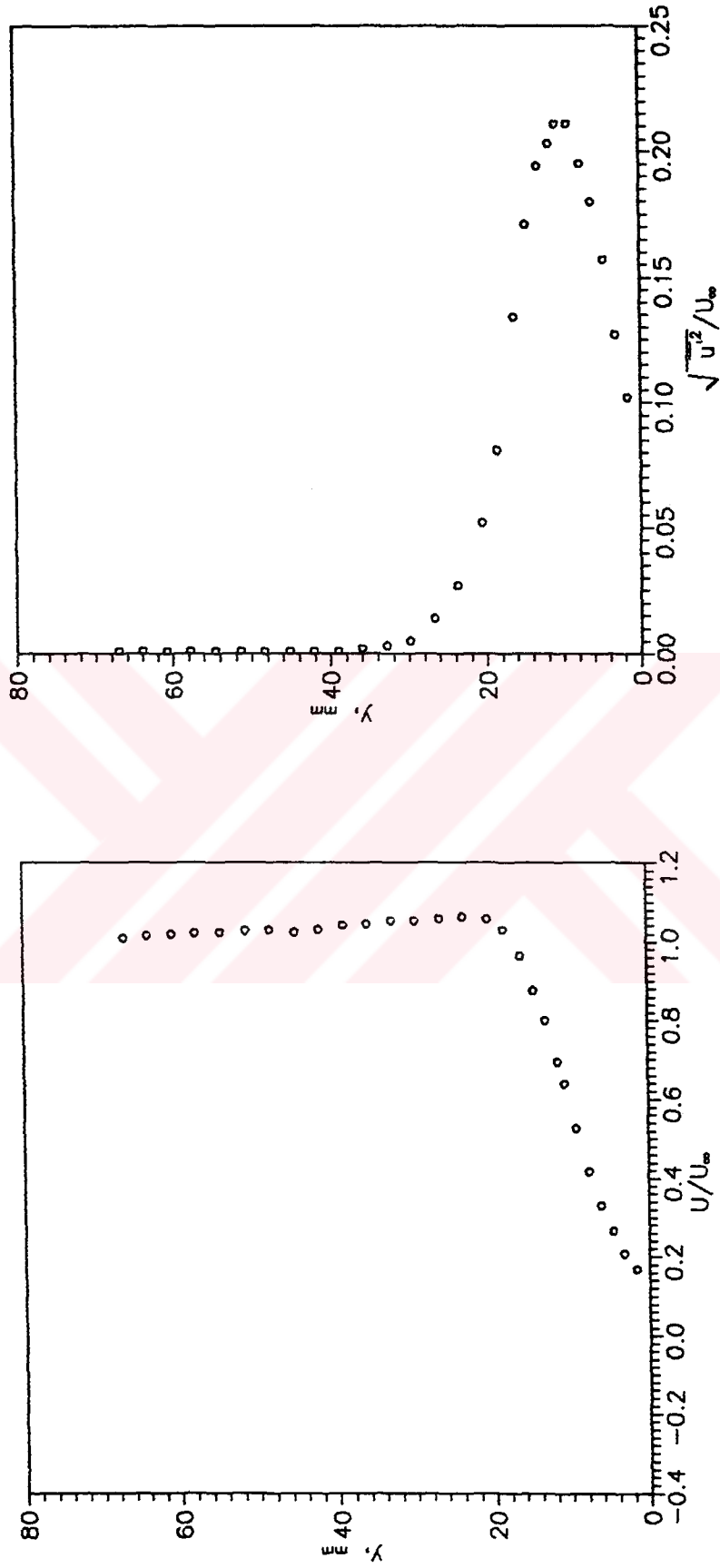
Figure A.11 a) Mean velocity profiles, b) Turbulence velocity profiles, at the station (x/d=1.0) on the model surface. $Re_d=3.54\times10^4$
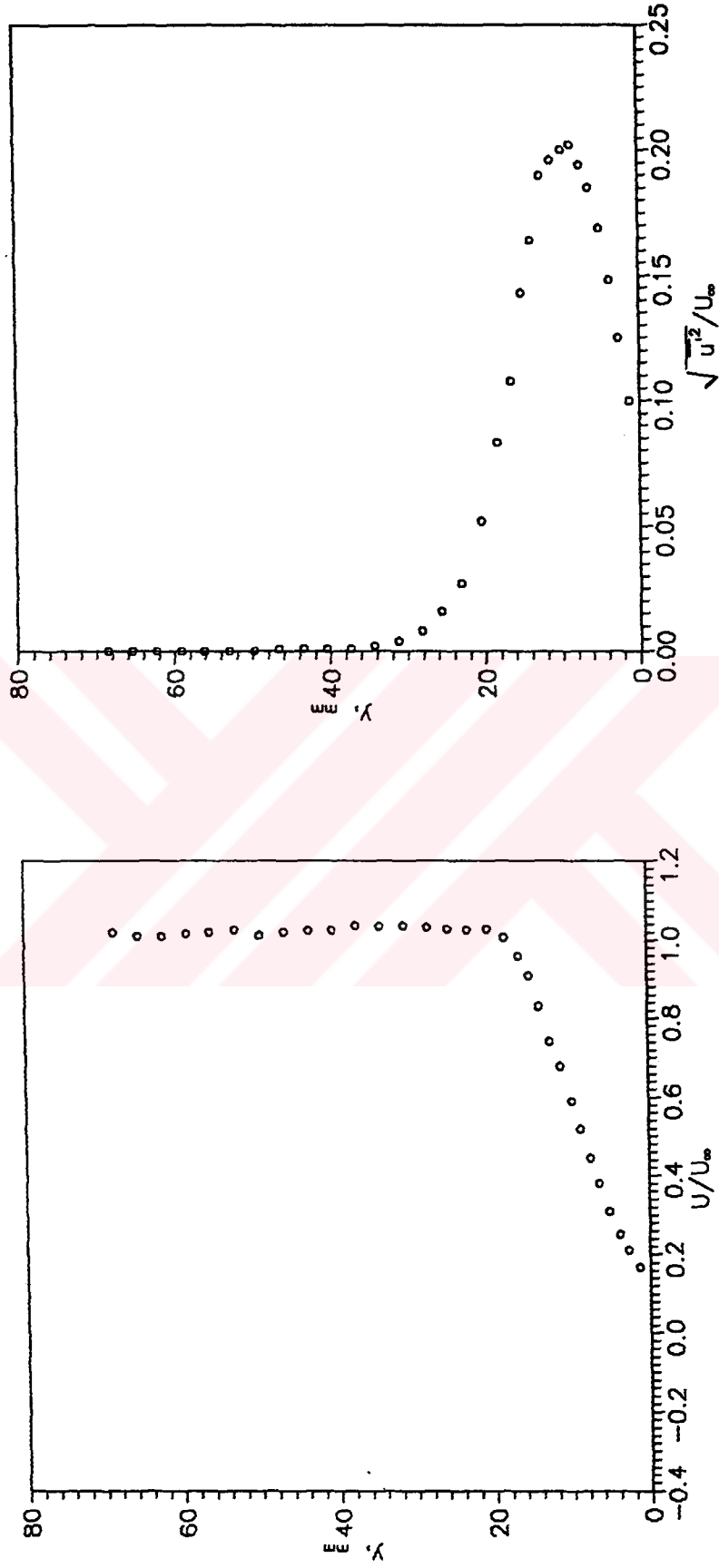
Figure A.12 a) Mean velocity profiles, b) Turbulence velocity profiles, at the station (x/d=1.1) on the model surface. $Re_d=3.54\times10^4$

Figure A.13 a) Mean velocity profiles, b) Turbulence velocity profiles,
at the station (x/d=1.2) on the model surface.
$Re_d=3.54\times10^5$
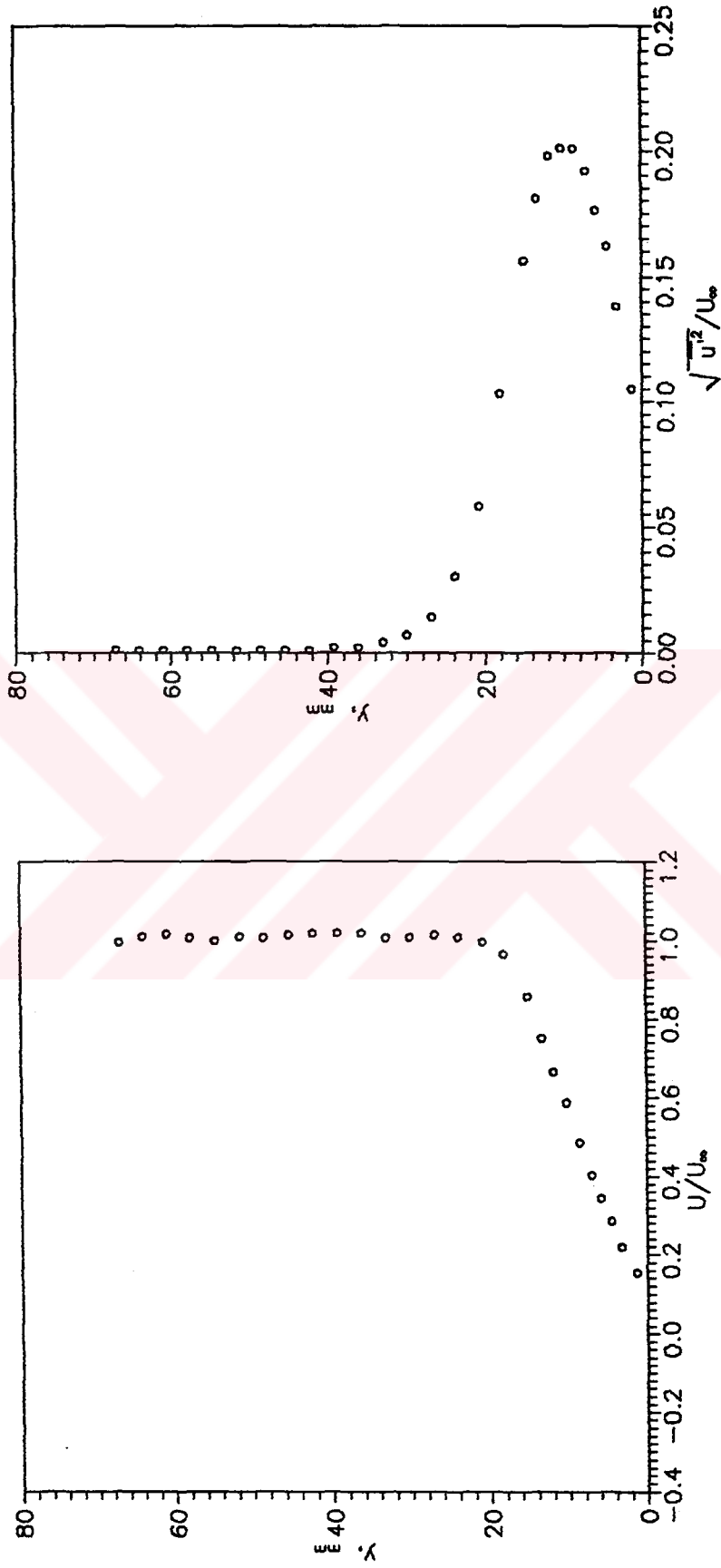
Figure A.14 a) Mean velocity profiles, b) Turbulence velocity profiles, at the station (x/d=1.3) on the model surface. $Re_d=3.54\times10^4$

Figure A.15 a) Mean velocity profiles, b) Turbulence velocity profiles. at the station (x/d=1.4) on the model surface. $Re_d=3.54\times10^4$
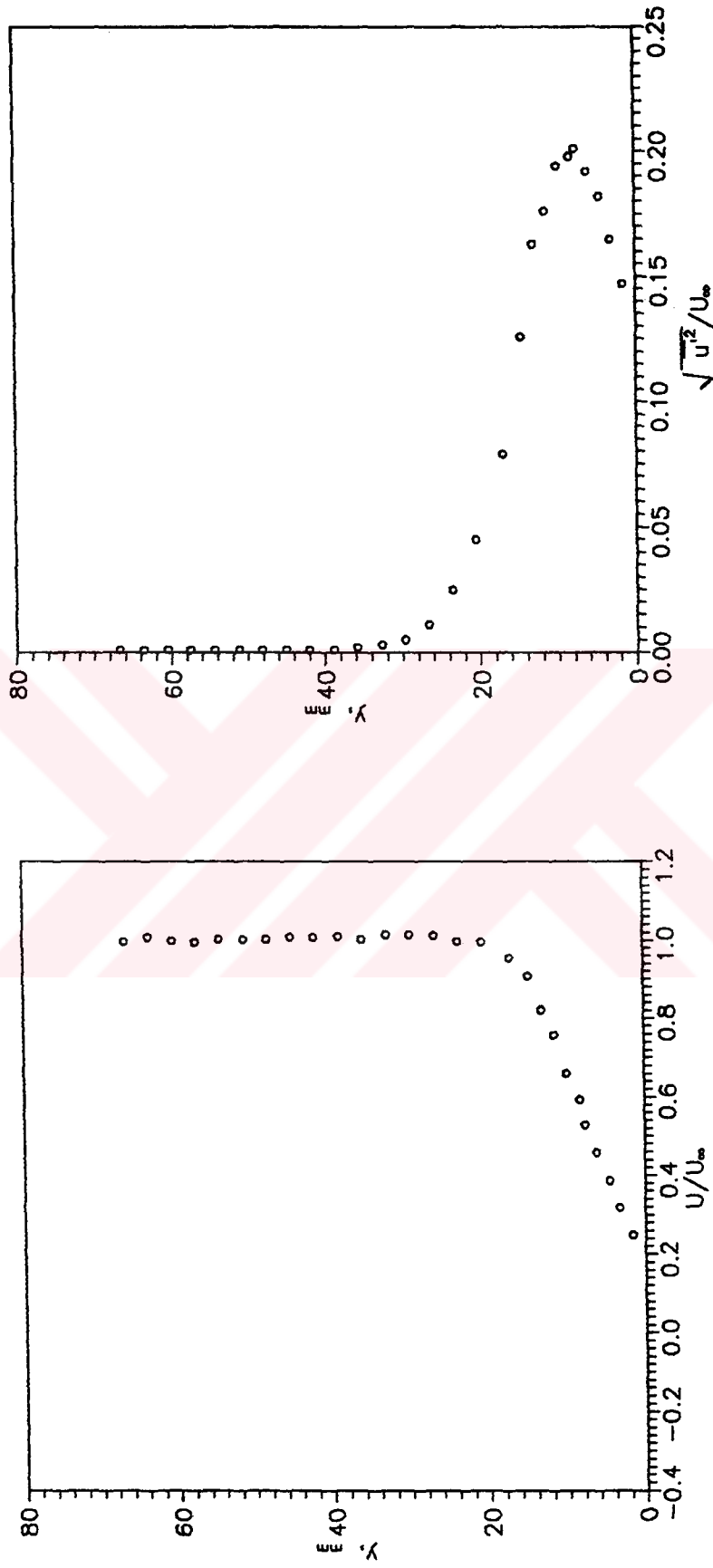
Figure A.16 a) Mean velocity profiles, b) Turbulence velocity profiles, at the station (x/d=1.5) on the model surface. $Re_d=3.54\times10^6$

Figure A.17 a) Mean velocity profiles, b) Turbulence velocity profiles, at the station (x/d=1.6) on the model surface. $Re_d=3.54 \times 10^4$
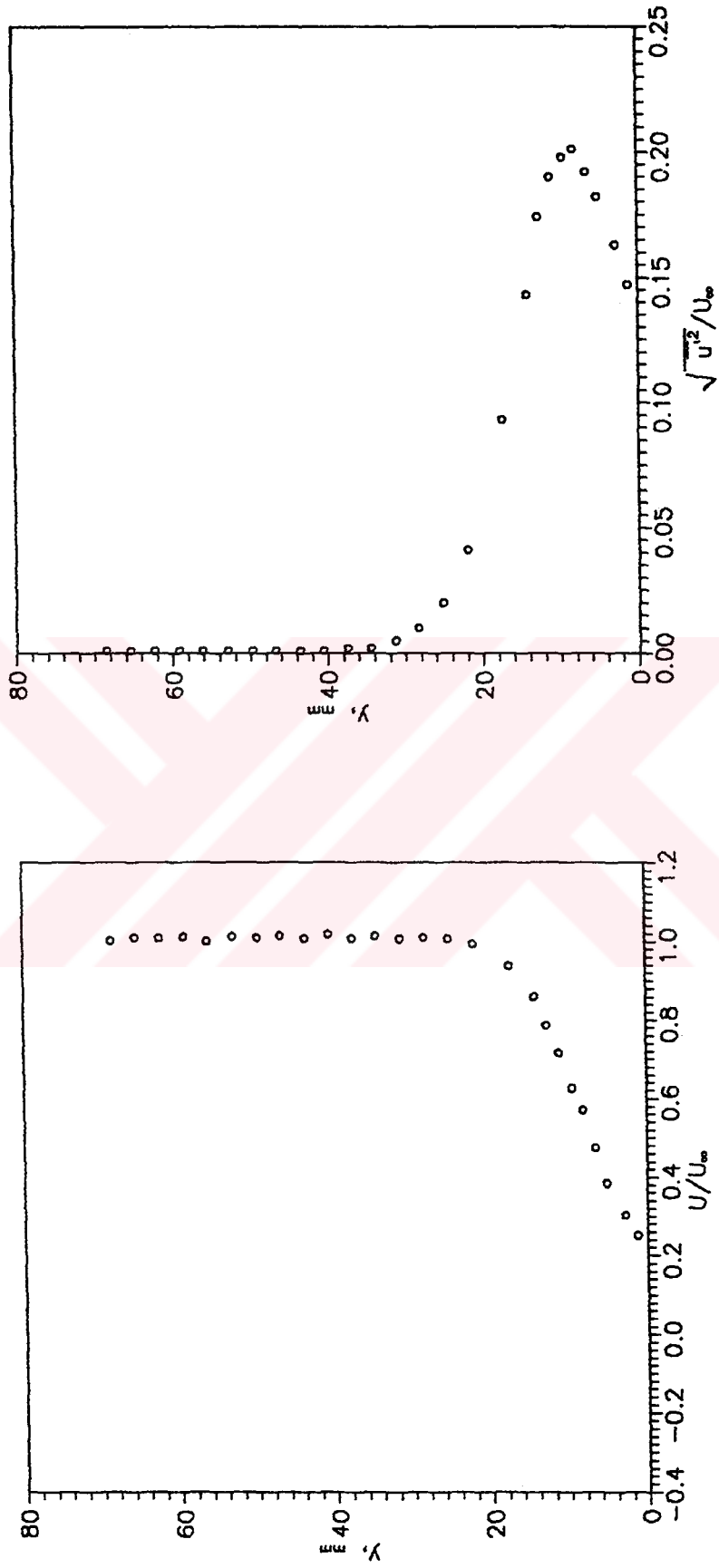
-16-

Figure A.18 a) Mean velocity profiles, b) Turbulence velocity profiles, at the station (x/d=1.7) on the model surface. $Re_d=3.54 \times 10^4$

Figure A.19 a) Mean velocity profiles, b) Turbulence velocity profiles, at the station (x/d=1.8) on the model surface. $Re_d=3.54 \times 10^4$

Figure A.20 a) Mean velocity profiles, b) Turbulence velocity profiles, at the station (x/d=1.9) on the model surface. $Re_d=3.54\times10^4$

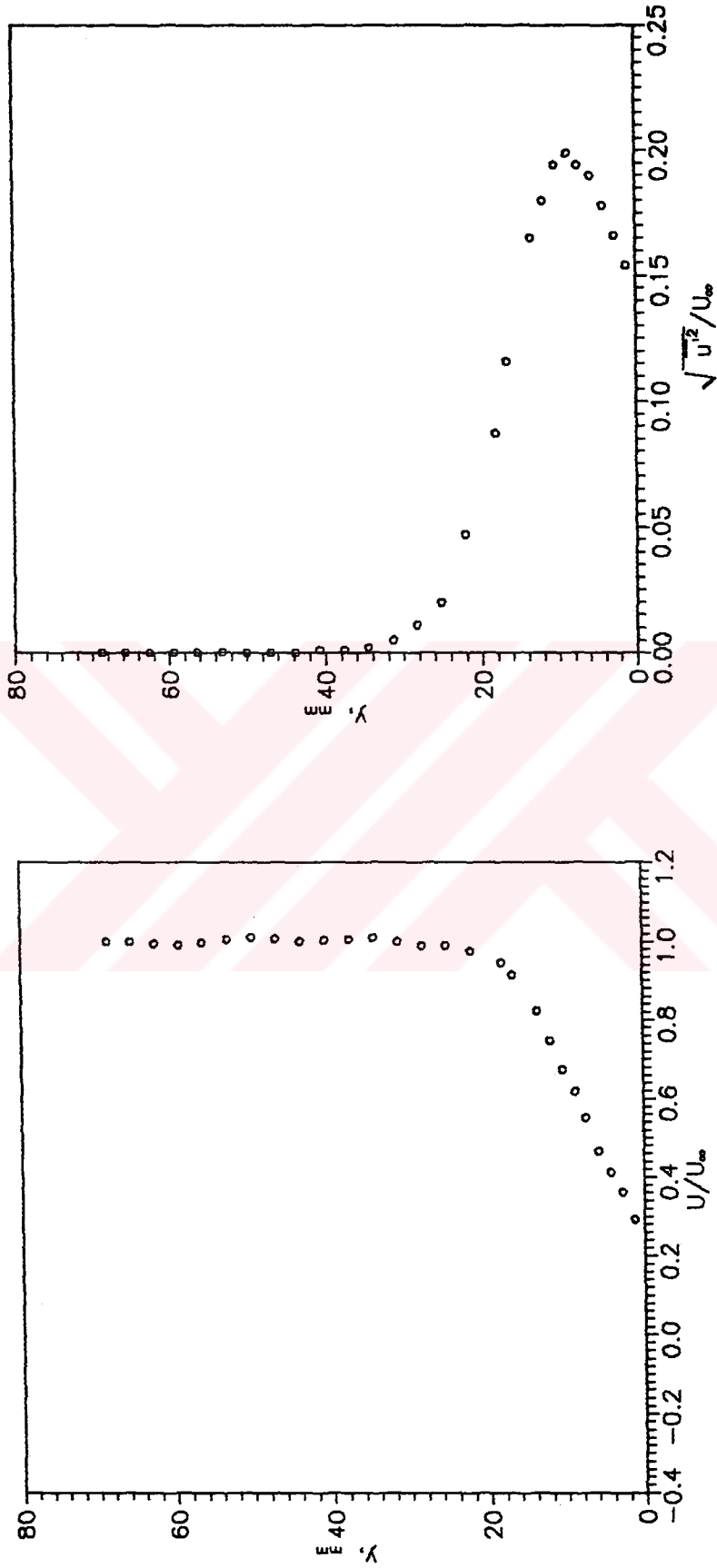Figure A.21 a) Mean velocity profiles, b) Turbulence velocity profiles, at the station (x/d=2.0) on the model surface. $Re_d=3.54\times10^4$
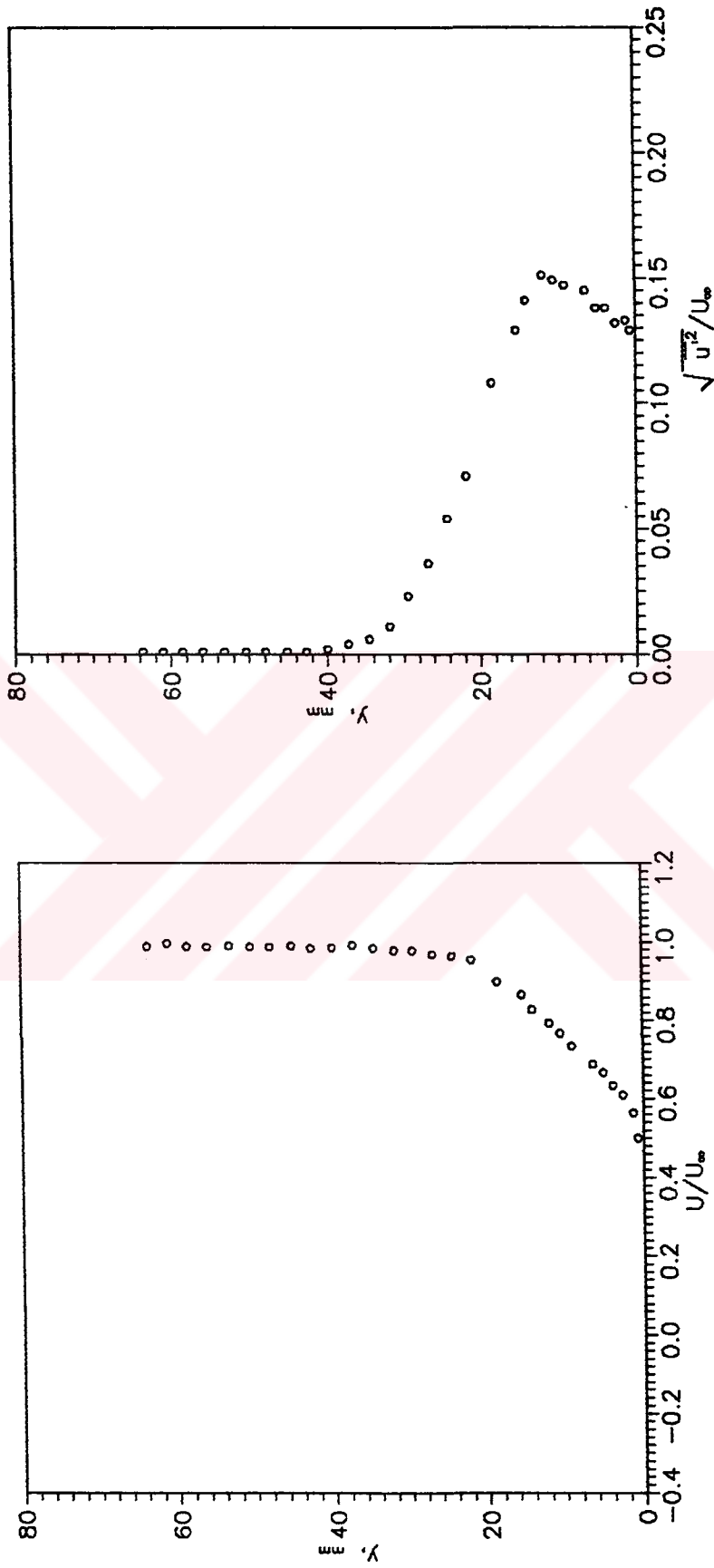
Figure A.22 a) Mean velocity profiles, b) Turbulence velocity profiles,
at the station (x/d=3.0) on the model surface.
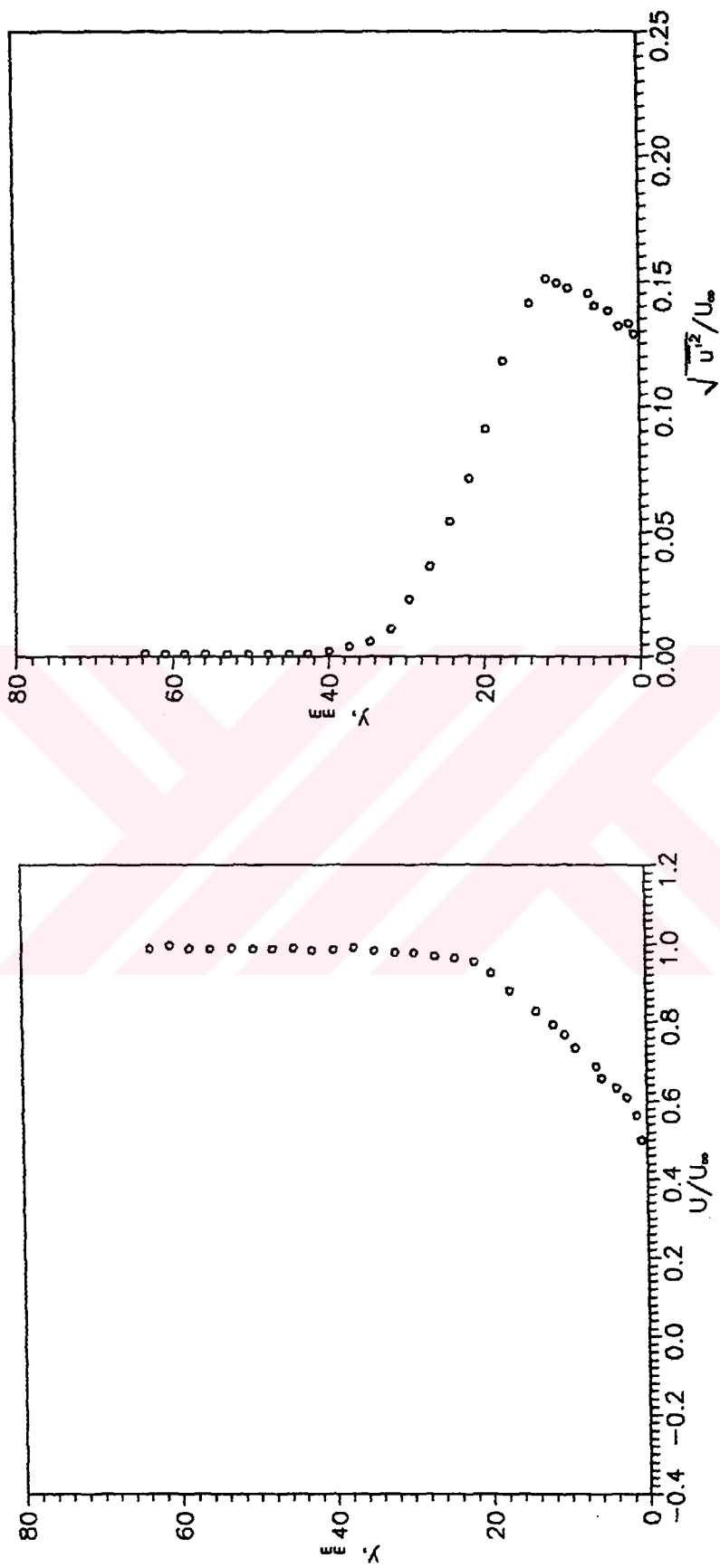$Re_d = 3.54 \times 10^4$

Figure A.23 a) Mean velocity profiles, b) Turbulence velocity profiles, at the station (x/d=4.0) on the model surface. $Re_d=3.54\times10^4$

CURRICULUM VITAE

Hayri Acar was born in Fethiye-TURKIYE in November 6, 1965. He has completed his Lycee education in Izmir Bornova Anadolu Lisesi. In 1985 he entered the Faculty of Aeronautics and Astronautics of ITU as an undergraduate student and in 1989 graduated with a degree of Bachelor of Science in Aeronautical Engineering. In the same year he has enrolled to M.S. program of the Institute of Science and Technology of ITU and has been employed by the Faculty of Aeronautics and Astronautics as a Research Assistant. He is expected to fulfil all the requirements for an M.S. Degree in Aeronautical Engineering by the end of the June 1991.